Environment Canada | Environnement Canada

National Hydrology Research Institute

~~NHRI PAPER NO. 11~~

IWD SCIENTIFIC SERIES NO. 114

Morphology, Hydrology and Hydrochemistry of Karst in Permafrost Terrain near Great Bear Lake, Northwest Territories

R. O. van Everdingen

HRI

NATIONAL HYDROLOGY RESEARCH INSTITUTE
INLAND WATERS DIRECTORATE
CALGARY, ALBERTA, 1981

Introduction

Large areas in northern Canada are underlain by water-soluble bedrock strata such as limestone and dolomite. Bird (1963, p. 16), in describing the occurrence and morphology of limestone terrain in northern Canada, stated: "Karst features are rare. They are believed to occur in northern Alberta and may exist locally south of Great Bear Lake." Brandon (1963, p. 176) postulated that ". . .in regions of continuous permafrost, ground water infiltration can only occur in karst rocks where solution channel flow is possible." Brandon (1965) further indicated that two formations of particular significance in this respect are the Lower Devonian Bear Rock Formation and the Upper Cambrian Saline River Formation because they contain solution channels in brecciated dolomite and limestone and in salt and gypsum, respectively.

The presence of karst in northern Alberta has since been confirmed. It was described in some detail by Ozoray (1977), who indicated that this is an active karst, the development of which is related to underground removal of evaporites (salt and/or gypsum) by moving groundwater. The northern Alberta karst extends northward into the Northwest Territories to the vicinity of Great Slave Lake (Douglas and Norris, 1974), through the zone of scattered permafrost and into the zone of widespread discontinuous permafrost (Brown, 1978).

The most accentuated karst terrain yet reported from higher latitudes in the zone of widespread discontinuous permafrost is the Nahanni North Karst, north of the South Nahanni River, N.W.T., first described by Ford and Brook in 1973. Then the Nahanni North Karst was the most complex subarctic karst landscape known in North America. It is developed entirely in carbonate rocks. Hydrologic observations made in the area in 1972 and 1973 were described by Brook (1977).

Karst development in an even more northerly area, the Colville Hills west and northwest of Smith Arm (Great Bear Lake), was indicated by Aitken and Cook (1969) and by Cook and Aitken (1971). The existence of a very large sinkhole near Vermilion Creek, about 40 km southeast of Norman Wells, was mentioned by Ford and Quinlan (1973).

During hydrogeological reconnaissance in June 1975, it was found that karst development is widespread in the Franklin Mountains, Great Bear Plain and Colville Hills, from Great Bear River at least as far north as 67°N (van Everdingen, 1976, 1978b). This karst terrain extends into the zone of continuous permafrost.

As pointed out by Ozoray (1977), the presence of active karst can present hazards to mining as well as to various types of surface development, through flooding and through subsidence or collapse of the ground surface. In addition to such geotechnical hazards, the presence of karst is likely to aggravate potential environmental problems. Groundwater in karst areas is generally extremely vulnerable to contamination from surface sources. When compared with non-karst areas, the lack of chemical and physico-chemical attenuation mechanisms and the usually more rapid subsurface transport of contaminants may lead to accelerated contamination of surface waters at relatively distant discharge areas. These considerations have prompted a more detailed study of the morphology, hydrology and hydrochemistry of a portion of the karst terrain covered by parts of NTS map sheets 96C, 96E, 96F and 96K (Fig. 1) between 1975 and 1978, the results of which are presented in this report.

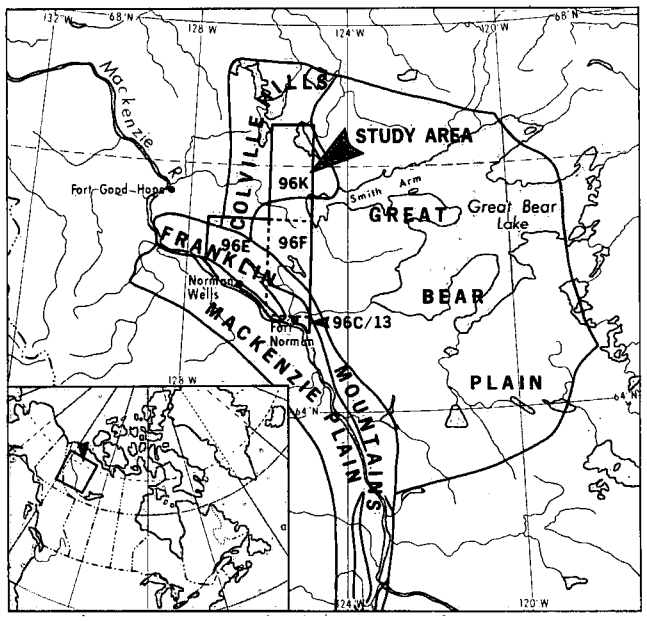

Figure 1. Index map showing location of study area with respect to regional physiography.

PHYSIOGRAPHY

The study area comprises parts of four physiographic subdivisions: Great Bear Plain, Colville Hills, Franklin Mountains and Mackenzie Plain (Fig. 1, after Bostock, 1967). Great Bear Plain, part of the Northern Interior Plains, is a region of low relief with elevations ranging from about 100 to about 525 m, which contains numerous swamps, ponds and small lakes poorly linked by sluggish streams. The Colville Hills consist of widely separated ridges of various trends with elevations of up to 725 m; the Franklin Mountains have maximum elevations of up to 1075 m in the study area. Elevations in the Mackenzie Plain, between the Franklin and Mackenzie mountains, range from about 100 to about 350 m. The area is only sparsely populated and information on the climate and hydrology is limited.

Meteorological observations are available from stations at Fort Norman, Norman Wells and Fort Good Hope for periods of various durations. These indicate that the climate is subarctic, with long cold winters (average of 240 days with frost) and short cool summers. Mean annual temperatures range from -6°C to -8°C, with extremes from +35°C to -56°C. Annual precipitation is quite variable at Norman Wells, ranging from 193 to 490 mm with a long-term mean of 335 mm, of which between 55% and 60% normally falls as rain during the period from May to October (data from Burns, 1973, 1974). Annual lake evaporation is of the order of 250 mm.

The study area forms part of the Mackenzie River drainage basin. Streamflow measurements are available from Water Survey of Canada gauging stations on the Mackenzie River at Fort Norman and Norman Wells, on Whitefish River near its mouth, and on Bosworth and Seepage creeks, both in the vicinity of Norman Wells. Information on other streams and on soil moisture and groundwater levels is essentially nonexistent except in the immediate vicinity of the Mackenzie Highway and pipeline corridor.

Most of the area is situated in the zone of discontinuous permafrost. Although permafrost is widespread, it is lacking beneath lakes, larger ponds and the active channels of many streams. It tends to be absent locally beneath well-drained south-facing slopes and in eskers or dune ridges, etc. The northernmost portion of the area falls within the zone of continuous permafrost. Measured thicknesses of perennially frozen ground range from 45 to 76 m around Norman Wells to more than 115 m east of the Franklin Mountains (Brown, 1978).

Norman Wells was the main point of access to the area. Travel in the area for the purpose of this study was primarily by helicopter. Overland travel is affected by terrain conditions which are determined mainly by the character of glacial and postglacial deposits and by the occurrence and distribution of permafrost and ground ice.

CHAPTER 2

Geology

BACKGROUND

A description of the geology along the Mackenzie River and along some of the other major rivers in the area was published by Hume (1954). Cambrian stratigraphy was described by Aitken *et al.* (1973), and Ordovician and Silurian stratigraphy, by Norford and Macqueen (1975). A geological map covering the Colville Lake area and part of the Coppermine area was published by Cook and Aitken (1971). Preliminary geological maps for the Fort Norman (NTS 96C), Norman Wells (NTS 96E) and Mahony Lake (NTS 96F) map areas are available in Geological Survey of Canada open files.

BEDROCK STRATIGRAPHY

Cambrian – Mount Cap and Saline River Formations

The Mount Cap Formation consists of grey, green and red shales with interbedded glauconitic sandstone and siltstone. The top of the formation is marked by brown-weathering, thin-bedded to laminated dolomite (Cook and Aitken, 1971; Aitken *et al.*, 1973). Outcrops of the Mount Cap Formation are rare in the study area.

The Saline River Formation overlies the Mount Cap Formation conformably. In the Imperial Vermilion Ridge No. 1 well (NTS 96E), it consists of a lower unit of 848 m of salt and anhydrite overlain by a succession of 171 m of red and green shale and mudstone, dolomite, and white and pink gypsum (Aitken *et al.*, 1973). The measured thickness of the lower unit may reflect tectonic thickening.

It should be pointed out here that the calcium sulphate evaporites commonly occur as anhydrite in the deep subsurface and as gypsum in outcrops and at shallow depth. They will be referred to as gypsum in the rest of this report.

The Saline River Formation outcrops locally in the Franklin Mountains. A maximum thickness of 162 m was quoted for the recessive, poorly exposed upper unit in a section in the Norman Range by Aitken *et al.* (1973); sulphur-isotope analyses published by van Everdingen and Krouse (1977b) indicated that at least 30 m of Lower Devonian Bear Rock Formation may be present in the lower portion of the measured section, unconformably overlain by the Saline River Formation as a result of local thrusting.

Figure 2 shows the regional distribution and isopachs for the Saline River Formation (N.C. Meyer-Drees, personal communication, 1980).

Cambro-Ordovician – Franklin Mountain Formation

A detailed description of the Franklin Mountain Formation was given by Norford and Macqueen (1975), who recognized three mappable units in outcrops of the formation which can commonly also be distinguished in the subsurface.

The lower *cyclic unit* consists of several types of dolomite arranged in repetitive sequences, indicative of cyclic deposition; the dolomites weather to a pale yellowish-orange. The unit ranges in thickness from 45 to 137 m. Its basal part is interbedded with red and green mudstone characteristic of the upper part of the Saline River Formation.

The middle *rhythmic unit*, consisting of rhythmic alternations of two types of dolomite, overlies the cyclic unit conformably. Weathering accentuates the differences between the two types of dolomite in outcrops; the rhythms may be more difficult to recognize in the Northern Interior Plains and they are generally not apparent in continuous cores from this region. The thickness of the rhythmic unit ranges from 150 to 490 m.

The upper *cherty unit* is a distinctive, finely to coarsely crystalline, thick-bedded dolomite that overlies the rhythmic unit in the Franklin Mountains and Northern Interior Plains. It was named the cherty unit by Norford and Macqueen (1975) to reflect the presence of white chert and drusy quartz, silicified oolites and large silicified stromatolites. The thickness of the cherty unit is extremely variable, ranging from 0 to about 300 m, because of several erosion periods that may have affected the unit locally.

According to Norford and Macqueen (1975), the boundary between Cambrian and Ordovician may lie either within the rhythmic unit or between the rhythmic and cherty units.

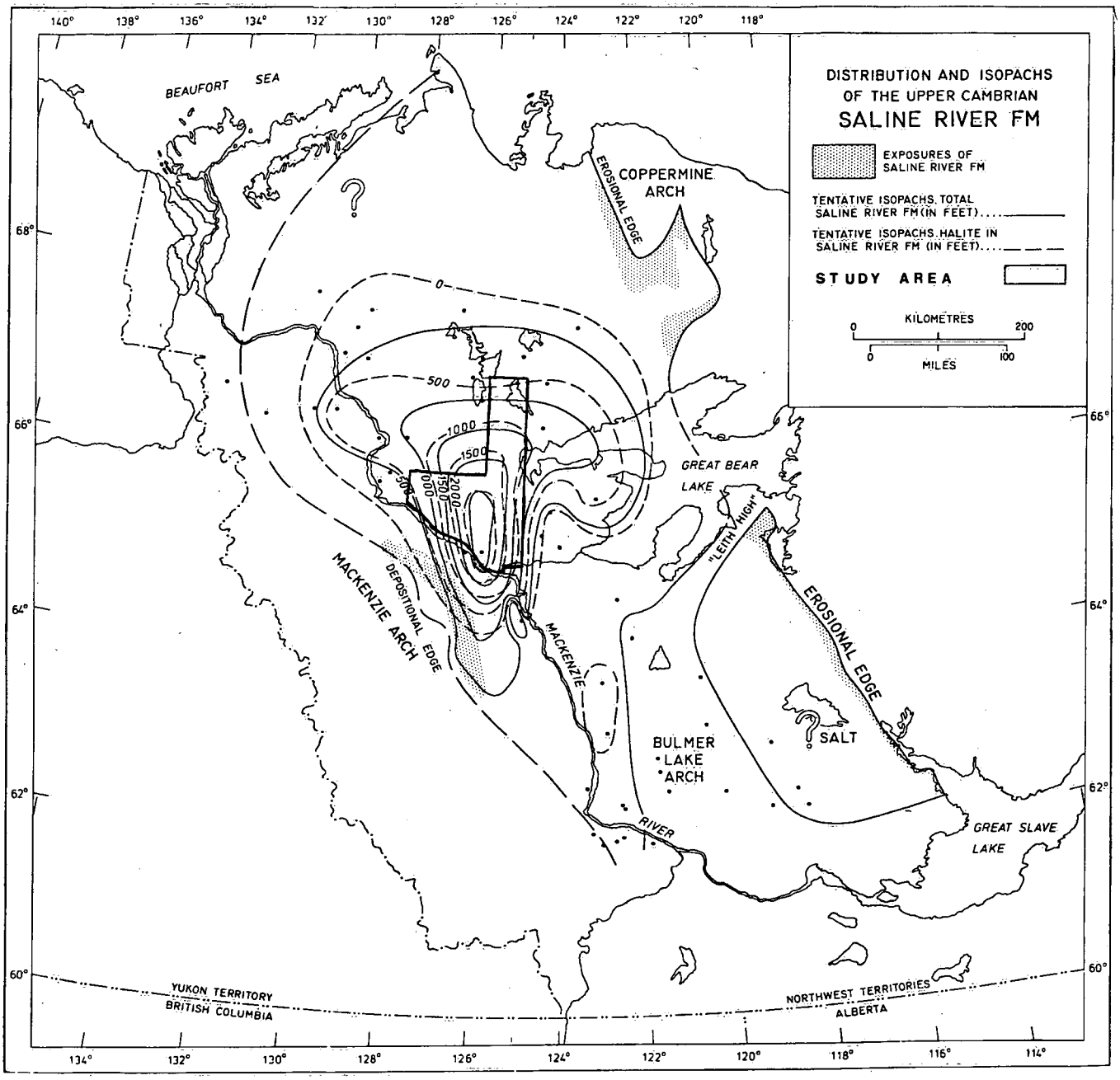

Figure 2. Distribution and isopachs of Saline River Formation evaporites.

Ordovician-Silurian – Mount Kindle Formation

The Mount Kindle Formation overlies the various units of the Franklin Mountain Formation disconformably; it is separated from either Devonian or Cretaceous formations by pre-Devonian and Cretaceous unconformities. It consists of brownish, medium to dark grey, finely crystalline, thin- to thick-bedded dolomites with horizons of abundant nodules of light grey to white chert and with a silicified fauna (corals, brachiopods and cephalopods) of Late Ordovician and Early Silurian age. Vuggy pores may contain solid hydrocarbons. During this study abundant fluorite crystals were found in vugs in outcrops of the upper part of the Mount Kindle Formation in one of the depressions north of Mahony Lake (No. 110 in Fig. 7). Cook and Aitken (1971) indicated the occurrence of "areas of sinkholes" in the outcrop areas of the Franklin Mountain and Mount Kindle formations west of Smith Arm (Great Bear Lake).

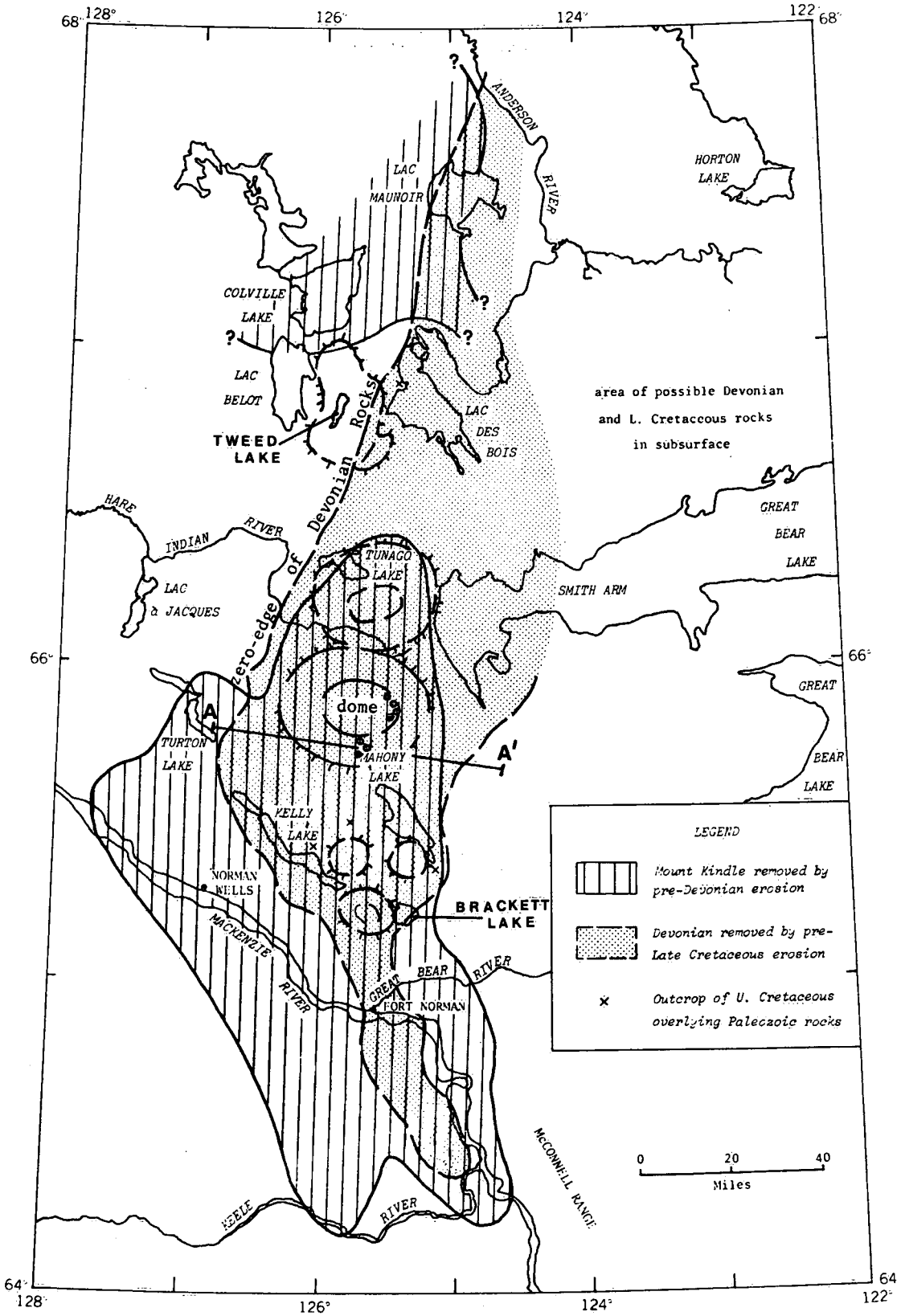

Figure 3. The Keele Arch and the Mahony Lake dome (after Cook, 1975, Fig. 41.1). Black dots indicate outcrops of Mount Kindle Formation around the dome. Location of other domes from Haimila (1975, Fig. 12.1).

The variations in thickness of the Mount Kindle Formation, from 42 to about 270 m, appear to be the result of pre-Devonian erosion. Outcrops of the Mount Kindle Formation are widespread in the Franklin Mountains. There are fewer outcrops in the portions of the study area in the Colville Hills and Great Bear Plain where the Mount Kindle Formation appears to occur as isolated erosional remnants.

In his description of the Keele Arch, Cook (1975) indicated the approximate extent of the area of removal of the Mount Kindle Formation by pre-Devonian erosion (Fig. 3). Haimila (1975) discussed the possible occurrence of several large dome-like features along the Keele Arch between Great Bear River and Colville Lake, which he named from north to south: "Tweed Lake Dome," "Tunago Lake Dome," "Mahony Lake Dome" and "Brackett Lake Dome." During the present study, several outcrops of the Mount Kindle Formation were discovered in sinkholes around the central part of the Mahony Lake dome (black dots in Fig. 3; locations marked "K" in Fig. 7). These outcrops are located in narrow bands on the northeast and southwest flanks of the dome, at elevations as much as 75 m *lower* than the stratigraphically older cherty unit of the Franklin Mountain Formation exposed on the central part of the dome.

A possible explanation for the unusual spatial relationship between the Franklin Mountain and Mount Kindle formations at the Mahony Lake dome could be that the present isolated areas of Mount Kindle strata have been protected during subsequent erosion intervals as a result of gradual subsidence (starting shortly after deposition) caused by subsurface removal of evaporites from the Upper Cambrian Saline River Formation. This suggestion is illustrated in a schematic cross section over the Mahony Lake dome presented in Figure 4. Subsurface data to assess this suggestion and its implications further have not yet become available.

Lower Devonian – Bear Rock Formation

The Bear Rock Formation overlies the Mount Kindle and older formations unconformably. It is exposed in both the Franklin Mountains and the Colville Hills. The area from which the Bear Rock Formation and younger Devonian formations were removed by pre-Late Cretaceous erosion is indicated in Figure 3 (after Cook, 1975). Measured thickness of the Bear Rock Formation ranges up to about 240 m.

The Bear Rock Formation consists of laminated to thick-bedded, pale brown, finely crystalline dolomites; thick-bedded pale-grey weathering limestones; and white gypsum. Thick sequences of carbonate solution breccia occur widely. Postglacial or postglacially rejuvenated sinkholes and associated subterranean drainage indicate that subsurface solution of gypsum is actively occurring. Evidence of similar activity during the Cretaceous is provided by the Cretaceous sandstone fillings of fossil sinkholes (Cook and Aitken, 1971).

A.E.H. Pedder (quoted by Cook and Aitken, 1971) and A.W. Norris (personal communication, 1978) have suggested a Late Lower Devonian to Early Middle Devonian age for the Bear Rock Formation.

Middle and Upper Devonian

The Middle and Upper Devonian formations are of limited significance for the present study. They occur in both the Franklin Mountains and Colville Hills. The following summary description is based on the work of Cook and Aitken (1971).

The Hume Formation conformably overlies the Bear Rock Formation. It consists of fossiliferous, brown, thin- to medium-bedded limestone, with beds and partings of brown shale. Its thickness is estimated at between 105 and 135 m

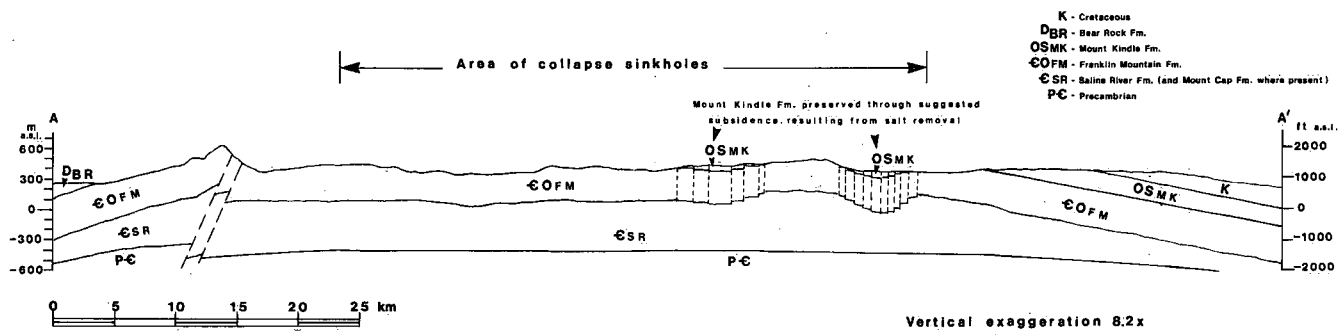

Figure 4. Schematic cross section through the Mahony Lake dome (see Fig. 3 for location).

in the study area. Sinkholes resulting from the removal of gypsum from the underlying Bear Rock Formation by subsurface solution occur in both the Hume Formation and the overlying Hare Indian Formation in the Norman Wells map area (NTS 96E).

The Hare Indian Formation overlies the Hume conformably. It consists of greenish grey, grey and brown shales, minor siltstone, and beds of fossiliferous limestone. It can be up to 215 m thick.

The Ramparts Formation consists of medium-bedded, brown, partly argillaceous limestone (0-90 m thick), overlain by thick-bedded, massive, pale brown limestone with large globular stromatoporoids (0-15 m thick), which in turn may be overlain by up to 15 m of dark argillaceous and bituminous limestone and calcareous shale.

The Canol and Imperial formations occur within the study area only along the southwest flank of the Franklin Mountains. The Canol Formation consists of up to 535 m of black, siliceous and bituminous shales. The Imperial Formation is composed of a sequence of shale, sandstone and minor limestone, ranging in thickness from 130 to 215 m.

Cretaceous

Cretaceous strata are of limited extent in the study area. Where present, they overlie a profound regional unconformity that truncates progressively older formations from west to east. The Cretaceous is of little significance to the present study because of the almost complete absence of karst features from areas with a Cretaceous cover.

UNCONSOLIDATED DEPOSITS

The study area was extensively glaciated during the Pleistocene Epoch, and as a consequence, glacial deposits cover most of Great Bear Plain as well as much of the Colville Hills and the bordering slopes of the Franklin Mountains. Glacial and postglacial deposits in the area have most recently been described by Hughes *et al.* (1973). The following summary is based on their work.

Till plains and rolling to hummocky moraine constitute most of the glacial cover of the area. Glaciolacustrine plains form a belt of varying width along the Mackenzie River; many small areas of glaciolacustrine sediments occur in or adjacent to areas of rolling and hummocky moraine. Glaciofluvial deposits (deltas, outwash plains, kames and eskers) occupy only a small percentage of the area. Alluvial flood plains and alluvial terraces are associated with the major streams and many of the larger tributaries.

Organic deposits locally overlie any of the above. They are most common on till plains, especially those developed over Cretaceous shale. They also occur in depressions in rolling or hummocky moraine and they are widespread on the glaciolacustrine deposits.

For a more detailed description of the deposits as well as of their associated landforms and the types and amounts of ground ice to be expected, the reader is referred to Hughes *et al.* (1973).

Karst

INTRODUCTION

In this report the term "karst" is used to indicate a region characterized by the presence of soluble rocks at or below the land surface that have been modified by solutional erosion (after Paloc, 1975). The conditions required for the development of karst can be summarized as follows (modified after Thornbury, 1954):

(1) strata of soluble rock (carbonates, gypsum, halite or others) should be present at or some distance below the surface;
(2) the soluble rock should be jointed and preferably have a low mass permeability;
(3) there should be well-developed valleys adjoining the uplands that are underlain by the soluble jointed bedrock; and
(4) at least moderate amounts of precipitation should be available for infiltration.

In terms of its position relative to the land surface, karst can be *naked* (with solution-affected rocks widely exposed); *covered* (with a cover of solution residue or other unconsolidated deposits); *buried* (fossil or palaeokarst, unconformably overlain by unaffected younger bedrock strata) or *subjacent* (or subterranean, with active solution phenomena centred in strata at some depth below less soluble or nonsoluble overlying bedrock).

The different processes that may be involved in karst development are (after Jennings, 1971; Wigley *et al.*, 1973):

(a) solution of soluble bedrock by moving water;
(b) precipitation of dissolved minerals from moving water;
(c) piping of unconsolidated sediments into underlying solution cavities or joints enlarged by solution;
(d) subsidence of unconsolidated sediments into solution depressions in the underlying soluble bedrock;
(e) collapse of bedrock and unconsolidated sediments into an underlying solution cavity (shallow collapse);
(f) collapse of bedrock and unconsolidated sediments into a breccia "funnel" resulting from progressive upward stoping over a solution cavity at greater depth (deep-seated collapse).

Processes (c) and (d) are generally related to covered karst; process (e) can be related to either covered or subjacent karst; and process (f) occurs only in relation to subjacent karst.

The majority of the karst areas of the world owe their development to solution of limestone and, to a considerably smaller degree, dolomite. Although the carbonates (calcite and dolomite) involved in these karst developments are more soluble in cold water than in warm water, the most extensive karsts are found in relatively warm climates where vegetation growth and bacterial action are more vigorous, leading to sustained CO_2 saturation in infiltrating water and hence to more efficient dissolution of the carbonates.

An additional factor that may slow down karst development in carbonate rocks at higher latitudes is the occurrence of temperatures below freezing. Jennings (1971, p. 184) stated: "In cold climates where water on the surface and in soil and rock is frozen most or all of the year in association with... permafrost, karst development is also inhibited." He took this one step further when he added: "In the permafrost zone underground karst development stops...." Although this may be true on a small scale, karst development is nevertheless taking place in various areas in the permafrost zone. At least one of these, the Nahanni North Karst described by Ford and Brook (1973), occurs entirely in carbonate rocks.

The effect of water temperature is of much smaller significance and the relative concentration of biogenic CO_2 is of no significance in the case of karst development in hypersoluble rocks (evaporites, like gypsum and halite, with solubilities several orders of magnitude higher than calcite). Both gypsum and halite are low-permeability rocks that tend to concentrate available water exclusively in solution channels and along other available discontinuities. Relatively small amounts of water can, therefore, initiate and continue the development of karst in these rock types.

The terminology used to describe characteristic morphological features of karst terrain is extensive, and in some cases different terms are used locally to describe similar features. Only general terms that describe features identified during the present study are discussed in the following paragraphs.

Two terms will be used to indicate small-scale features: (1) *clints* (*lapiés* or *karren*), for the etched, pitted, grooved or fluted rock surface of exposed soluble rocks and (2) *kamenitzas*, for the oval or circular solution pits in the walls of joints in soluble rock.

Most of the medium-scale karst features will be grouped under the general term *sinkholes*, which indicates solution-related depressions varying in depth from less than 1 m to more than 40 m and in area from a few square metres to several hundred square metres. They are often funnel-shaped; variations include dish-shaped and cylindrical, vertical-walled sinkholes. Accumulation of sediments in a sinkhole will flatten its cross section; the resulting shallow sediment-filled depression is sometimes called a *solution pan*. Following the scheme suggested by Jennings (1971), five different types of sinkholes may be distinguished on the basis of the process most directly involved in their formation.

Solution sinkholes are formed by solution from the land surface down, along pre-existing fractures or joints; they are mostly funnel-shaped.

Collapse sinkholes are formed by shallow collapse of unconsolidated sediments and/or bedrock strata into an underlying solution cavity. They can be funnel- or bowl-shaped, especially in areas with a thick cover of unconsolidated sediments or they can initially be vertical-walled. In the latter case their cross section commonly changes to funnel or bowl shape with time. They often have a larger depth-to-width ratio than most solution sinkholes.

Subjacent karst collapse sinkholes are formed by deep-seated collapse of bedrock and unconsolidated sediments into a breccia "funnel" resulting from progressive upward stoping over a solution cavity at greater depth. They can also initially be vertical-walled and commonly degrade into gentler shapes with time.

Subsidence sinkholes result from gradual subsidence and piping of unconsolidated material into underlying solution openings. More or less continuous small-scale removal of material creates a funnel shape; sudden movements may temporarily lead to a more cylindrical shape.

Alluvial stream sinkholes may be formed in alluvial sediments where a stream sinks into underlying karst. This is similar to the formation of subsidence sinkholes, with additional mechanical action, provided by running water, accelerating the downward transport of the alluvium.

The coalescing of a number of sinkholes will lead to *compound sinkhole depressions*, called *uvalas* by some authors; others reserve the latter term for large depressions resulting from the collapse of the roof over an underground karst stream.

The largest surface features found in karst terrain are *poljes*. These are typically elongated basins with a flat floor and relatively steep enclosing walls. Although the term as originally defined implies formation through solution of downfolded or faulted limestone strata (Thornbury, 1954), others have distinguished *solutional*, *tectonic* and *glacio-karstic poljes* (Ford and Quinlan, 1973).

Integrated surface drainage is usually widely spaced, disrupted or absent in karst areas; flow in most surface streams is intermittent. A larger percentage of the annual precipitation enters the groundwater system and a smaller percentage is available for evaporation than in non-karst areas. The regime of large rivers that drain karst areas usually shows the effects of the large storage capacity of the karst, which are higher base flows that are sustained longer than in non-karst areas with similar topography and climate.

Streams that lose their water underground are called *sinking streams*. The loss of water may occur over a certain distance along the streambed (the *sink range*) or at observable *sinks* or *swallow holes* in sinkholes and poljes. The continuation of the valley of a sinking stream beyond its sink range or swallow hole is called a *dry valley*; such a dry valley may be re-occupied by the stream during periods of high runoff.

Water bodies that form in sediment-clogged sinkholes are called *sinkhole ponds*. Larger water bodies formed in poljes whenever swallow holes are unable to carry inflow away fast enough are known as *karst lakes*. Many sinkhole ponds and karst lakes are intermittent; a few of them may persist during a sequence of years with above-average precipitation. Others may show large fluctuations in their water levels without ever draining completely.

Large springs in karst areas in many cases discharge water derived from identifiable sinking streams. Such springs are called *rises* or *resurgences*. They are usually perennial and may be artesian in character.

In the following sections, the distribution of karst features in the study area is outlined and a discussion of their morphology and of the processes probably responsible for their development is presented.

DISTRIBUTION OF KARST FEATURES

Karst features that could be identified in air photographs have been mapped for most of the area covered by

the northwest quarter of NTS 96C/13, the east half of NTS 96E, and the west half of NTS 96F and NTS 96K (Figs. 5 to 8, in pocket). Other features were mapped from field observations.

Clints (or karren) were only found locally in areas where exposed gypsum beds are not brecciated. These include portions of Mount Richard (No. 79 in Fig. 6) and the MacKay Range (20 to 25 km south of Fort Norman). Well-developed kamenitzas, with diameters ranging from less than 1 cm to as much as 10 cm, were found in Mount Kindle dolomites in exposures around the Mahony Lake dome.

Sinkholes have developed in many places in the Franklin Mountains and the Colville Hills where Paleozoic formations ranging from the Upper Cambrian Saline River Formation to the Upper Devonian Canol Formation are exposed. The majority of the sinkholes are located in areas where the Franklin Mountain and Mount Kindle formations crop out. Comparison of Figures 5 to 8 with Figure 3 shows that major concentrations of sinkholes and larger depressions are centred on the domes identified by Haimila (1975). So far no sinkholes have been found in areas where Cretaceous formations are present in NTS map areas 96C/13, 96E and 96K. A few sinkholes occur in possible Cretaceous areas in NTS map area 96F west of Mahony Lake.

The number of sinkholes identified in each individual map area is: 16 in Figure 5, 317 in Figure 6, 636 in Figure 7, and 418 in Figure 8 — a total of 1387. It is reasonably certain that the actual number of sinkholes in the study area is larger than this, since small sinkholes may have escaped detection because of the scale of the available air photographs, whereas other sinkholes may not have been recognized because they were full of water when photographed.

Compound sinkhole depressions and poljes have also been found in all four NTS map areas (2 in Fig. 5, 10 in Fig. 6, 14 in Fig. 7, and 1 in Fig. 8). Not included in these numbers are intermittent sinkhole ponds and karst lakes that were identified during this study (5 in Fig. 5, 19 in Fig. 6, 20 in Fig. 7, and 12 in Fig. 8); these are usually formed in compound sinkhole depressions or poljes. All these large karst features of course contain one or more sinks or swallow holes; some of the poljes have numerous collapse sinkholes in their floors.

Springs in the area have been mapped in the field, with the occurrence of small or large icings identified on air photographs used as a guide. Some of the 63 springs and spring areas marked in Figures 5 to 8 (4 in Fig. 5, 33 in Fig. 6, 14 in Fig. 7, and 12 in Fig. 8) as well as some of the sinking streams in the area will be discussed in Chapter 4.

Solution caves may exist in the study area, but their presence has not been positively established during this study. Only two minor dry valleys have been identified.

MORPHOLOGY OF SINKHOLES AND LARGER KARST DEPRESSIONS

A small number of sinkholes in the study area show the funnel shape characteristic of mature solution sinkholes that have little or no sediment fill. Most of these were found in gypsum exposures of the Bear Rock Formation (on Bear Rock, on the Norman Range, and on and around Mount Richard); a few are situated in areas with relatively thick unconsolidated deposits. Their single swallow hole is normally situated at the apex of the funnel. Since their drainage areas are very limited in size, stream erosion has little effect on their shape.

A considerably larger number of sinkholes have the flat saucer or shallow bowl shape of a solution pan shown, for example, by sinkhole No. 95 (Figs. 7 and 9). As shown in Figure 9B, the grass- and sedge-covered floor of such sinkholes may contain several swallow holes. The swallow holes are not necessarily situated at the centre of the sinkhole; in a number of cases, including sinkhole No. 95, swallow holes were found near the edge of the sinkhole floor.

Concentric zonation of vegetation, from a bare centre, through successive zones of sedges, grasses, willows and sometimes poplar, to the edge of the black spruce forest or muskeg, characterizes many of these sinkholes (e.g. No. 95 in Fig. 9B). The location of individual sinkholes can often be recognized on air photographs or during airborne reconnaissance because of the presence around the sinkholes of trees (poplar, white or black spruce) that are considerably taller than those in the surrounding forest and muskeg areas. The presence of the taller trees reflects the better drainage conditions existing in the vicinity of the sinkholes, which may also have promoted the local absence of permafrost.

Most of the sinkholes observed have a relatively irregular outline and cross section, with bedrock exposed along part or all of their periphery and/or in their swallow hole(s). Some sinkholes, like those in group No. 86 in Figure 7, are of considerable size. The air photograph in Figure 10 shows the four sinkholes of this group as well as a number of smaller ones of similar character in the same area. Sinkholes Nos. 86A, 86B and 86C are situated on a straight line with

Figure 9. Aerial views of sinkhole No. 95 (Fig. 7). *A* – Flooded, May 9, 1976; *B* – Drained, June 22, 1976.

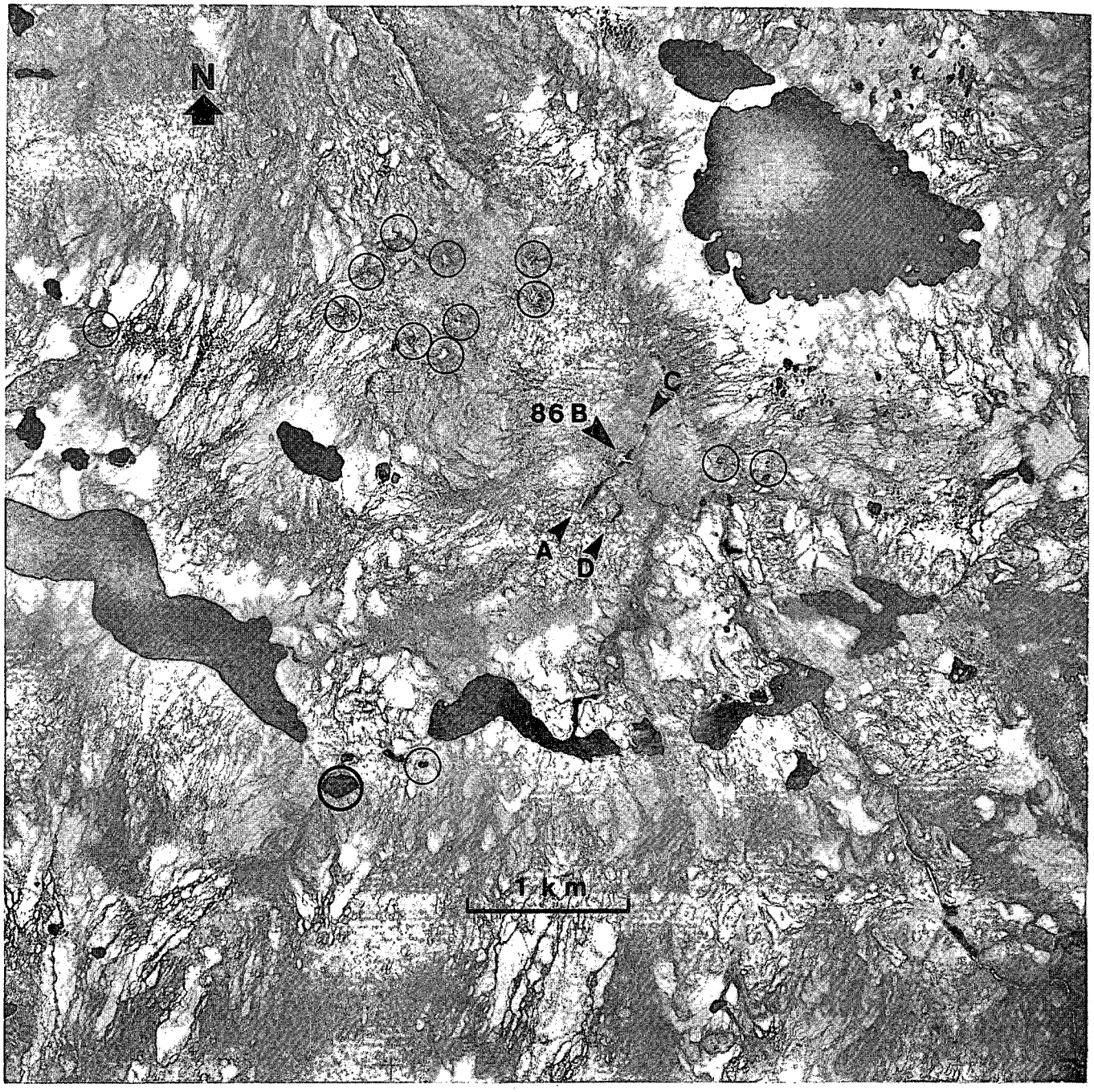

Figure 10. Air photograph showing sinkholes in group No. 86 (Fig. 7) with the "Disappearing River" flowing into sinkhole No. 86B, June 18, 1950 (air photograph A12603-40). Approximate dimensions of sinkholes: *A* – 195 × 50 m; *B* – 100 × 30 m and 18 m deep; *C* – 40 × 15 m; *D* – 85 × 25 m. Black circles mark other sinkholes.

a southwest to northeast direction, which is parallel to one of the joint directions prevailing in this area.

Sinkhole No. 86B is the primary sink of a large sinking stream (Fig. 11) that has provisionally been called the "Disappearing River." The upper portion of the sinkhole walls, consisting of bedrock, is vertical; rubble slopes form the lower portion of the walls. A large cone of rocky debris has been formed below the point where the Disappearing River cascades into the sinkhole. Its swallow hole is located near the northeast end of the sinkhole.

A dry valley meanders from the northwest side of sinkhole No. 86B to the northeast end of sinkhole No. 86A (Fig. 10 and the right-hand side of Fig. 11). The existence of this dry valley in combination with the relative dimensions of sinkholes Nos. 86A, 86B and 86C (Fig. 10) as well as differences in the degree of weathering of their bedrock

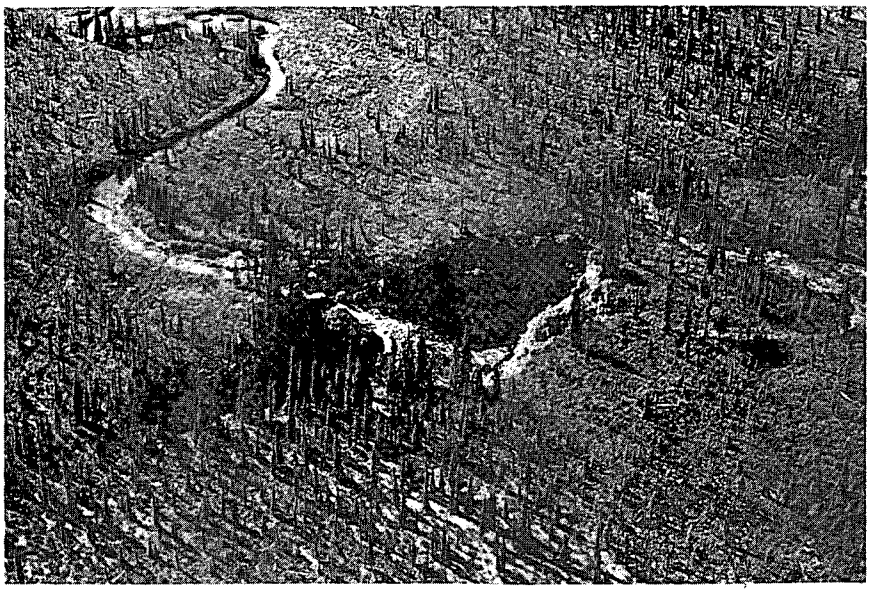

Figure 11. Aerial view of "Disappearing River" flowing into sinkhole No. 86B, June 30, 1975 (looking south).

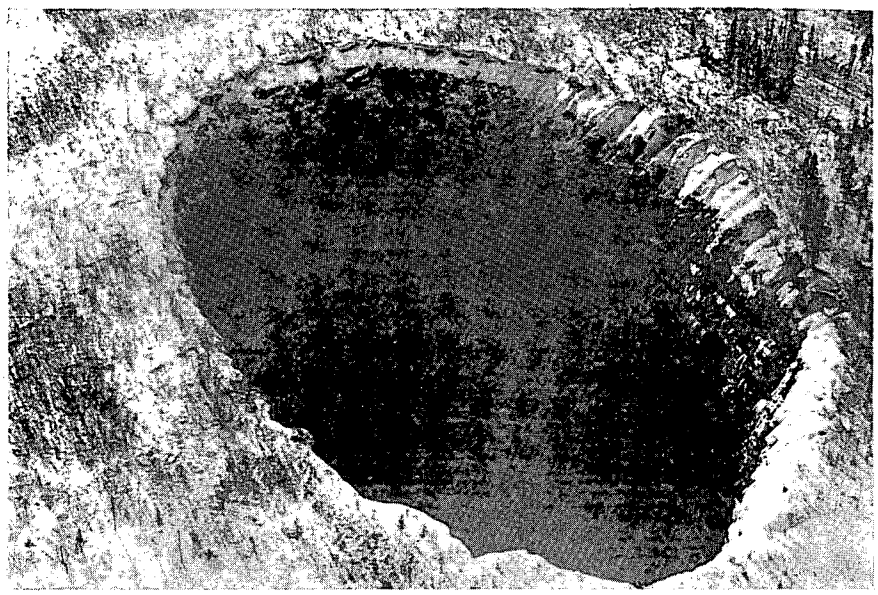

Figure 12. The large collapse sinkhole near Vermilion Creek (No. 175 in Fig. 6); approximate dimensions are 60 × 120 m and 40 m deep.

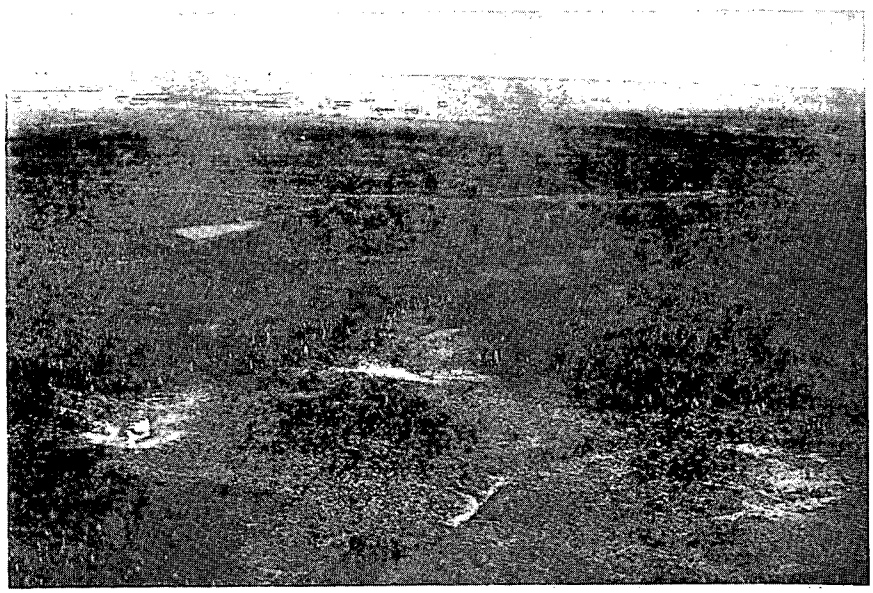

Figure 13. Aerial view of depression No. 111 (Fig. 7), showing individual sinkholes (width of grass-covered area is approximately 500 m).

exposures led to the conclusion that sinkhole No. 86A is the oldest in the group and sinkhole No. 86C, the youngest. Fresh rockfalls observed in these and a few other sinkholes indicate that development of the sinkholes is continuing.

The most impressive single sinkhole in the study area is No. 175 in Figure 6. An aerial view of this sinkhole, which was described as "semi-stupendous" by J.F. Quinlan (Ford and Quinlan, 1973, p. 107), is shown in Figure 12. It is located in slightly sloping ground on the lower southwest slope of the Norman Range, approximately 375 m west of Vermilion Creek. Its walls, rising vertically about 40 m above the surface of a "lake" of unknown depth, consist almost entirely of shales of the Upper Devonian Canol

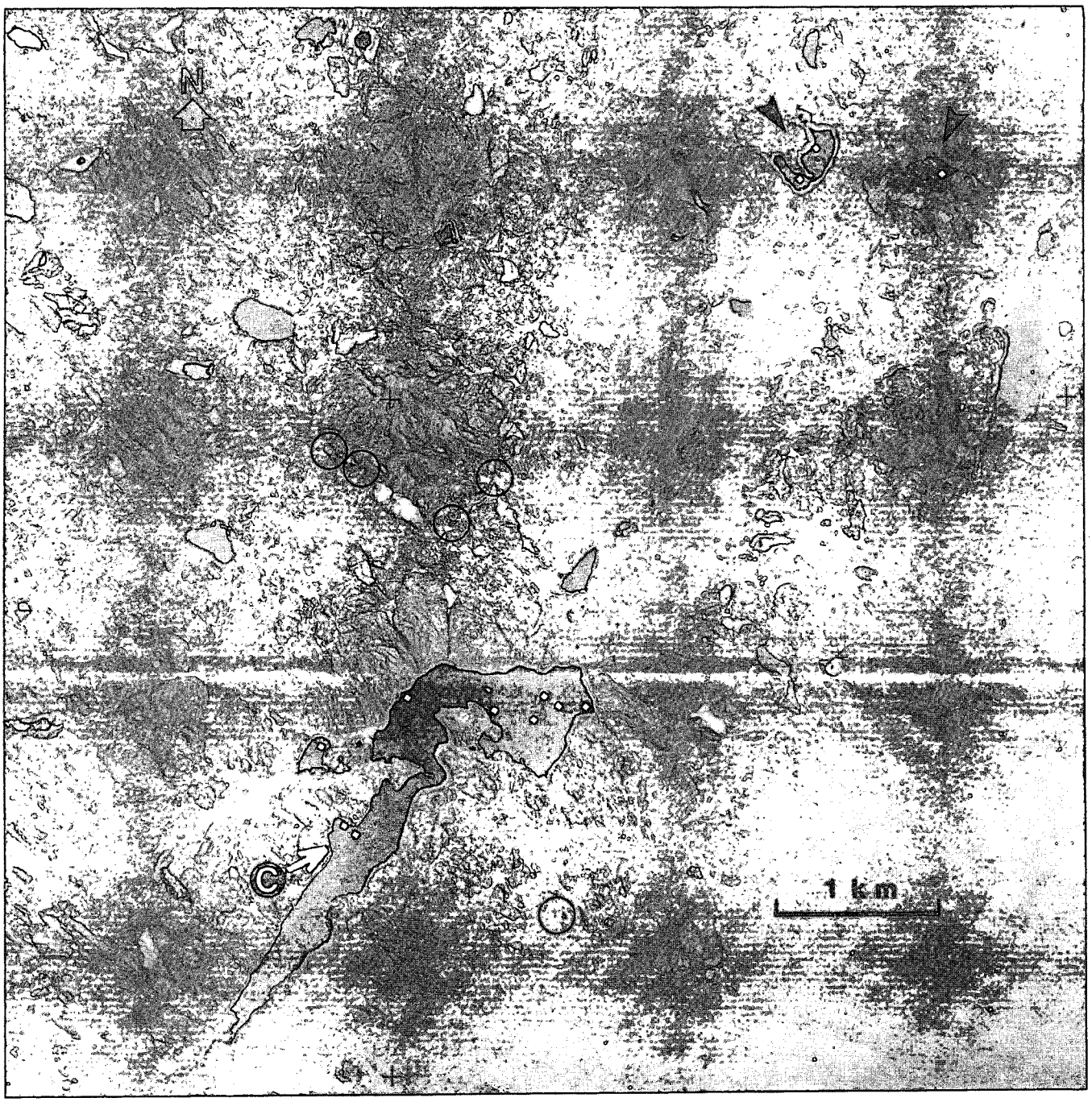

Figure 14. Air photograph showing depression No. 142 (Fig. 8) flooded, June 18, 1950 (air photograph A12601-101). Black arrows indicate smaller depressions; white arrow indicates camera location; white squares mark swallow holes in flooded depressions; black circles mark other sinkholes in the vicinity of depression No. 142.

Formation with a thin cover of unconsolidated material. The level of the "lake" seems to be only a few metres above the level of Vermilion Creek. Three smaller sinkholes of similar character are located between 500 and 1250 m east of Vermilion Creek, on an almost straight east-west line through No. 175.

Larger karst depressions found in the study area range in area from a fraction of a square kilometre to several square kilometres. Some, like No. 111 in Figure 7, have a roughly rectangular to square outline as shown in Figure 13; others, like No. 141 in Figure 6, are more irregular in shape. The largest ones, which have tentatively been designated as poljes (e.g., No. 110 in Fig. 7 and No. 142 in Fig. 8), are distinctly elongated in outline.

Several swallow holes are usually present in the more or less level floor of these large karst features. Five can be recognized in No. 111 in Figure 13; fossiliferous Mount Kindle dolomite is exposed in all of these.

One of the largest karst depressions identified in the study area, No. 142, is shown flooded on the air photograph in Figure 14, taken on June 18, 1950, and almost completely drained in the aerial view taken on June 21, 1976 (Fig. 15). The depression is shown as a lake in the first edition of NTS map 96K, which was produced using the 1950 air photographs. A low ridge divides this depression into a northeast and southwest portion. The northeast portion receives its inflow from a number of minor streams; a stream from the southwest provides the bulk of the inflow to the southwest portion.

The locations of individual sinks or swallow holes in depression No. 142 and in two smaller karst depressions are indicated in Figure 14. The prime sink for the stream from the southwest is a sinkhole located at the base of a steep rock wall below the more or less continuous exposures of the Franklin Mountain Formation that form the northwest boundary of this part of the depression. A second sink, which becomes active after water in the depression has reached a somewhat higher level, consists of a small cavern in bedrock a short distance southwest of the prime sink. At least six sinks were identified in the northeast portion of the depression; three of these have bedrock exposed in them. Unconsolidated materials of mixed glacial, fluvial and lacustrine origin cover the bedrock (cherty dolomite of the Franklin Mountain Formation) with a blanket (2 to 5 m thick) in this depression.

The vegetation in depression No. 142 (Fig. 14) shows a zonation similar to that described for sinkhole No. 95 (Fig. 9B) except for the absence of poplar.

The largest karst depression identified during this study is No. 110 in Figure 7. An air photograph of the area (Fig. 16) shows the full extent of the depression. It is strongly elongated in outline and slightly curved; its length is about 5.5 km and its maximum width is slightly less than 700 m.

The northwestern portion of depression No. 110 contains three large swallow holes (or sinkholes?), marked in Figure 16 by black circles. Vegetation patterns indicate that small areas around these are probably flooded every

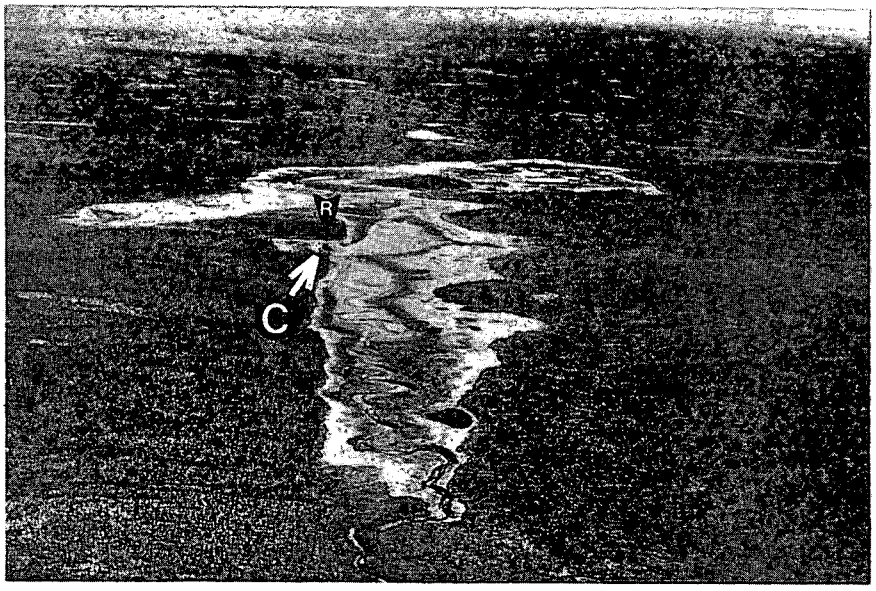

Figure 15. Aerial view of drained depression No. 142 from the southwest, on June 21, 1976. Arrow marked *C* indicates camera location and direction of view; arrow marked *R* indicates recorder location.

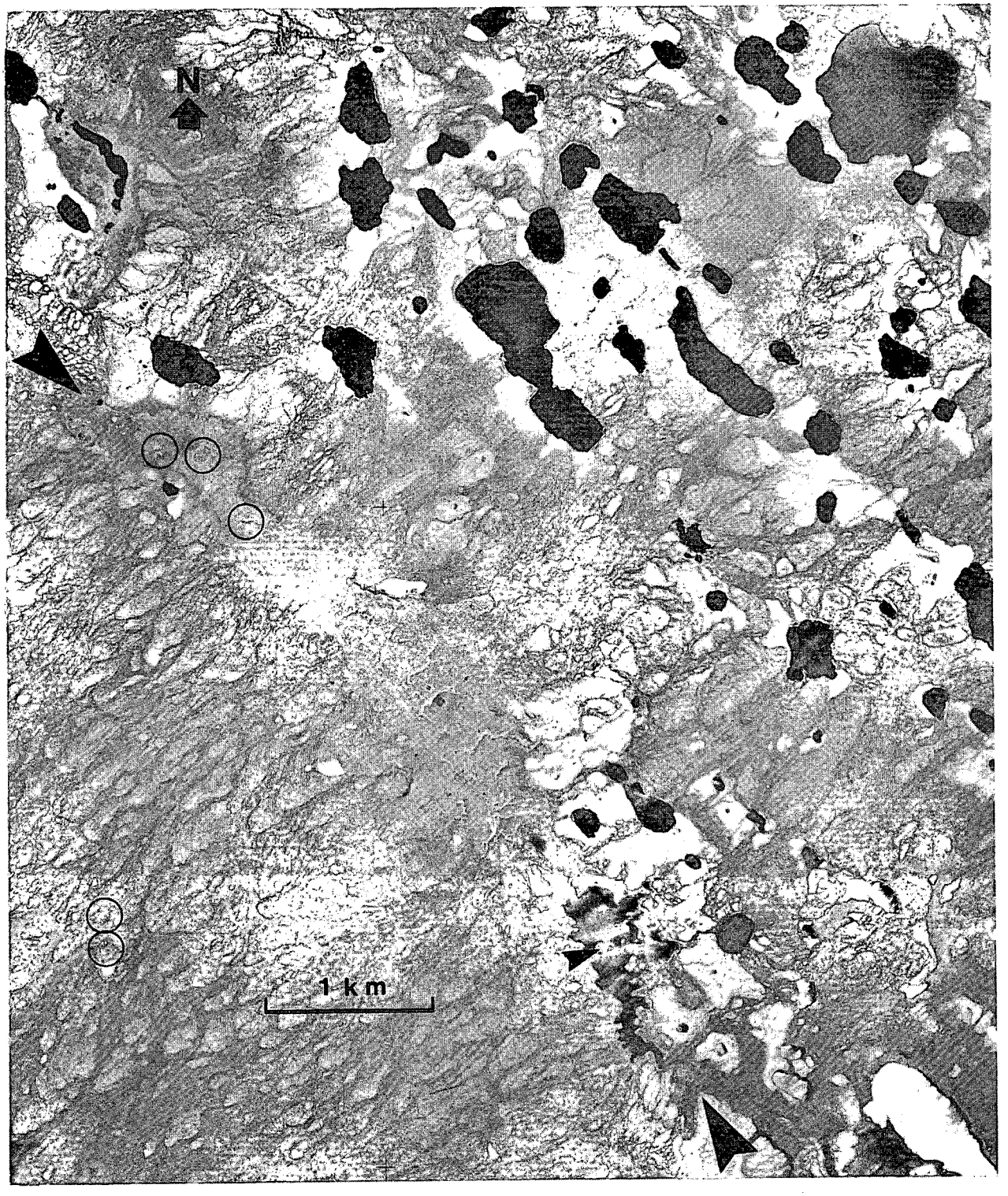

Figure 16. Air photograph showing depression No. 110 (Fig. 7), extending between the two large arrows. Southeastern portion of depression flooded; small arrow indicates location of cameras. Central portion of depression shows numerous sinkholes. Black circles in northwestern portion of the depression indicate three large swallow holes; those near the southwest corner of the photograph indicate sinkholes (air photograph A12609-359, June 18, 1950).

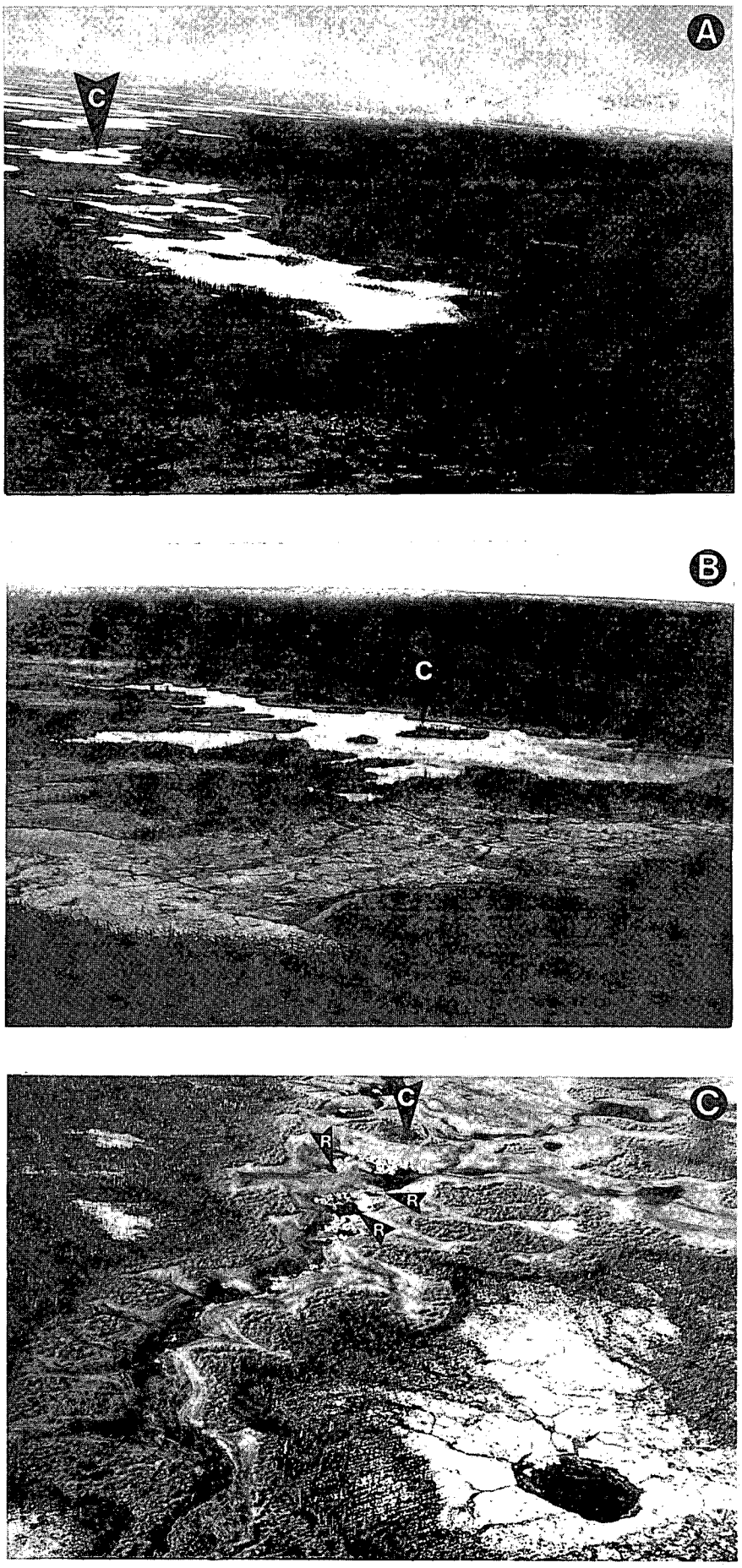

Figure 17. Aerial views of depression No. 110. *A* – Widespread flooding in central and southeastern portions on June 30, 1975 (viewed from northwest). *B* – Flooded southeastern portion, from the north, on June 30, 1975. *C* – Drained southeastern portion, from the southeast, on September 10, 1975. Arrows marked *C* indicate camera location; arrows marked *R* indicate locations of pressure recorders.

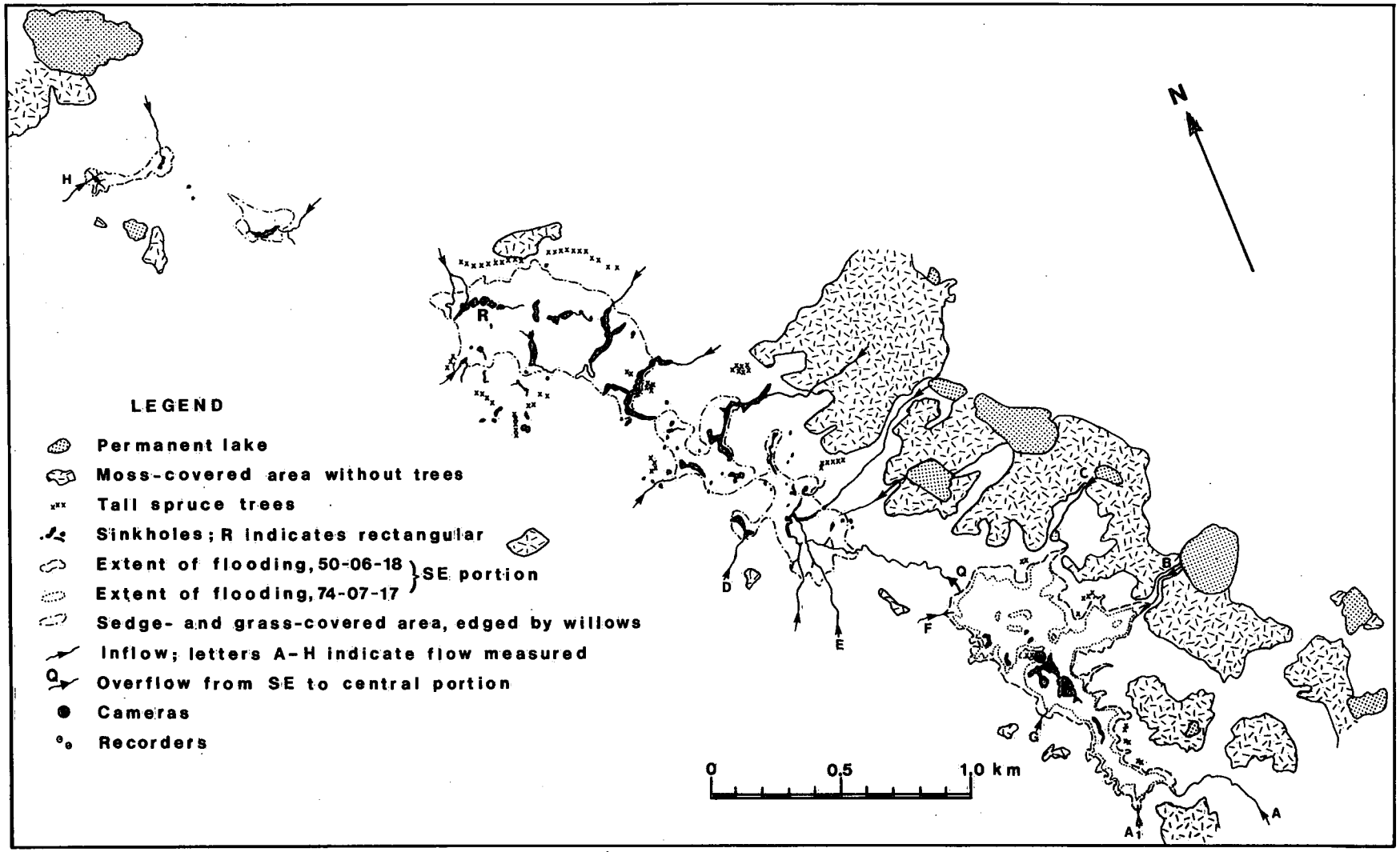

Figure 18. Detailed map of depression No. 110.

year for a short period during the snowmelt. The central portion of the depression shows a large number of partly interconnected swallow holes and sinkholes; vegetation patterns indicate that most of this area is flooded for some time in at least some years (as on June 30, 1975, Fig. 17A). The southeastern portion of the depression was covered by water when the air photograph (Fig. 16) was taken on June 18, 1950; it is shown as a lake in the first edition of NTS map 96F. This part of the depression was flooded when first seen by the author on June 30, 1975 (Fig. 17B); it was dry and bedrock was exposed in the swallow holes when next observed on September 10, 1975 (Fig. 17C).

The swallow holes and sinkholes in this and other large karst depressions are in character similar to the individual sinkholes discussed earlier. Many have vertical or near vertical bedrock walls with low talus slopes along the base. The original bedding of the bedrock is well preserved in the walls of some of the holes; in others, the bedrock presents a chaotic jumble of large blocks and smaller fragments. The bottoms of the swallow holes and sinkholes that have bedrock exposed in their walls often contain a pile of bedrock rubble.

Although most of the swallow holes and sinkholes in the large karst depressions are irregular or even spidery in outline, some have almost perfectly square or rectangular outlines with the sides parallel to the prevailing direction of jointing in the bedrock. Examples are presented by three of the five sinkholes arranged in a curved row near the north end of the central portion of depression No. 110 (marked "R" in Fig. 18). The central hole is 19.5 m long, 17.3 m wide and 12.7 m deep in bedrock. Very few of the holes show the cylindrical shape exhibited by the Vermilion Creek sinkhole (No. 175 in Fig. 12).

Bedrock exposed in depression No. 110 consists of fossiliferous Mount Kindle Formation dolomite. Unconsolidated material of mixed origin (glacial, fluvial, lacustrine) forms a blanket approximately 6 m thick on the bedrock over much of this depression.

PROCESSES INVOLVED IN KARST DEVELOPMENT

Direct evidence of solution of bedrock is limited in the study area. The clints and sinkholes found on and around Mount Richard (No. 79 in Fig. 6) clearly result from the solution of gypsum; kamenitzas found in joint walls in dolomites of the Mount Kindle Formation in depression No. 110 were also formed by solution. Some of the shallow saucer-shaped sinkholes like No. 95 (Fig. 9) may be the result of subsidence caused by lowering of the underlying bedrock surface through solution of carbonates or they may be sediment-filled collapse features.

Collapse has been suggested earlier as the cause of sinkhole formation in the study area. In their description of the large Vermilion Creek sinkhole (Fig. 12), Ford and Quinlan (1973, p. 107) stated: "This is the largest and best-formed example of a collapse sinkhole that is known to us in Canada. Indeed, we do not know of any more shapely example in the Western Hemisphere." They argued that the vertical shale walls of the sinkhole indicate that this is "covered" karst (*subjacent* karst as defined earlier) and that it is a collapse sinkhole which is relatively young. Three potential collapse targets were suggested by Ford and Quinlan: (i) a cave in limestone of the Middle Devonian Hare Indian Formation, about 150 m below the surface; (ii) a cave in gypsum of the Lower Devonian Bear Rock Formation, about 300 m below the surface or (iii) a cave in salt of the Upper Cambrian Saline River Formation, about 1100 m below the surface. Ford and Quinlan (1973) also mentioned the existence of collapse sinkholes in an area underlain by the Bear Rock Formation around Lac Belot northeast of the study area.

The vertical bedrock walls and the high depth-to-width ratios of many of the sinkholes in the study area indicate that collapse is the most probable immediate cause of their formation. This tentative conclusion is supported by a number of observations illustrated in Figure 19.

In many of the swallow holes and sinkholes in depression No. 110, large sections of bedrock can be seen to have *subsided en bloc* over appreciable vertical distances (Fig. 19A). In some cases the downward displacement was accompanied by considerable tilt. Bedrock walls in some of the sinkholes display *arching fractures* (Fig. 19B) of the type that develops in unsupported or inadequately supported bedrock strata over a large subsurface opening. Low wide cavities found at the base of the bedrock walls in a number of sinkholes exhibit the rubble floor and irregular, slightly arched roof (Fig. 19C) that often occur in caves as a result of *stoping*.

Over most of the study area more than one formation is present in which solution cavities could be formed that would lead to eventual collapse of overlying strata. Brandon (1965) indicated the significance of both the Saline River Formation and the Bear Rock Formation in this respect. Ford and Quinlan (1973) added Middle Devonian limestone (Hare Indian Formation) as a third possibility. Little evidence of solution, however, has been found in areas where the latter is exposed.

Sinkholes of the solution type were only found where either the Bear Rock or the Saline River Formation is exposed; a number of collapse sinkholes were identified in areas where the Bear Rock Formation is overlain by Middle Devonian strata. The largest concentrations of collapse

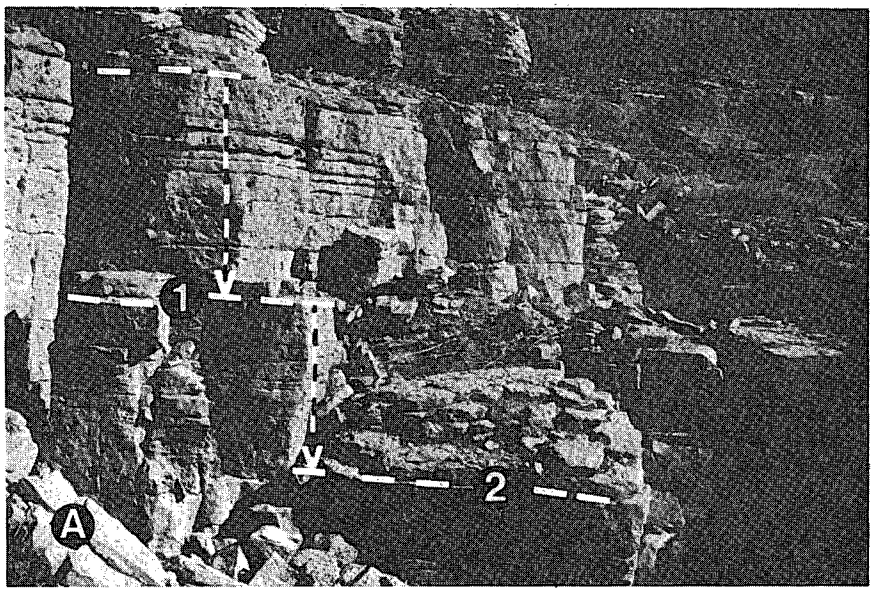

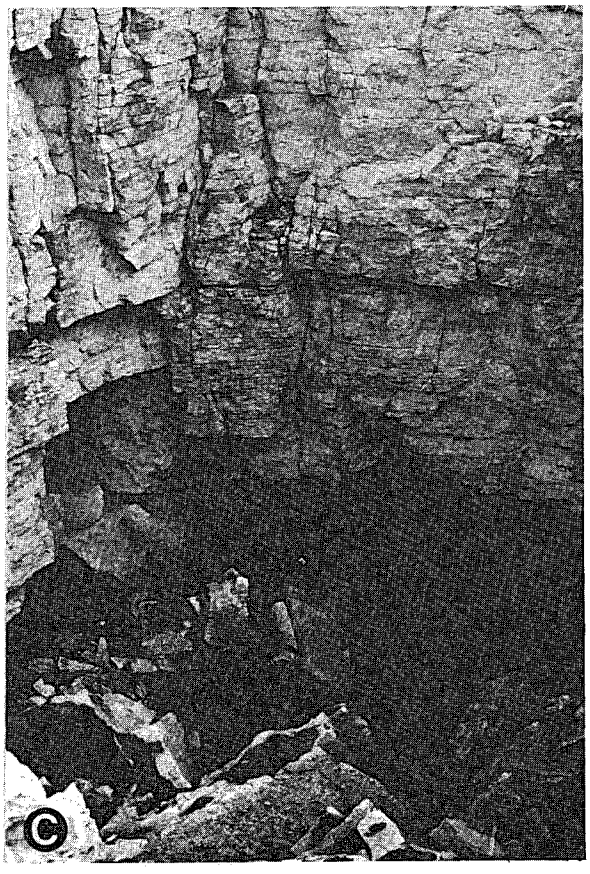

Figure 19. Indications of sinkhole formation through collapse, from depression No. 110 (Fig. 7). *A* – Downward displacement of bedrock blocks (block 1 dropped 2.8 m, block 2 dropped 5.0 m). Note kamenitzas in walls of joints. *B* – Arching fractures (height of rock wall at right-hand edge of photograph is approximately 9 m). *C* – Stoping (depth of hole from top edge of photograph is approximately 7.5 m).

sinkholes occur where the Mount Kindle and Franklin Mountain formations are exposed (e.g. around the Mahony Lake dome). It is not likely that solution of the low-solubility dolomites of these formations could have led to the widespread collapse features observed in these areas. The evaporite beds of the underlying Saline River Formation are the most probable solution focus there.

The absence of identifiable solution caves in the study area is a direct consequence of the collapse nature of the karst. The solution portion of the system, where solution caves may be formed, is not only unexposed but also located at considerable depth below the surface. Small caverns at shallow depth, like the secondary sink in the southwest portion of depression No. 142 and the cavern shown in Figure 19C, all indicate formation by stoping (part of the collapse process). Less competent rocks like gypsum and halite are, moreover, not likely to support major solution cave systems at depths greater than 500 m; any cavities formed by dissolution tend to be closed through plastic deformation or viscous flow of the evaporite, followed by subsidence and/or collapse of overlying, more competent strata.

The rate of development of karst may generally be expected to be slower in relatively low-lying areas (e.g. the Mahony Lake dome) than in areas with higher elevations and more pronounced relief, such as the Norman Range. This does not necessarily apply, however, in the case of a subjacent karst developing in hypersoluble rocks like gypsum and salt.

Development of collapse features at the ground surface as a result of solution of salt in the subsurface has been described for other parts of Canada by a number of authors. One such feature, Crater Lake about 26 km south of Yorkton, Saskatchewan, was investigated in detail by Christiansen (1971) and by Gendzwill and Hajnal (1971). They concluded that the almost perfectly circular depression with a diameter of 244 m is the surface expression of a breccia chimney above a solution cavity formed in Prairie Evaporite salt beds, more than 900 m below the surface, through removal of approximately 38 m of salt. Christiansen and Gendzwill (1973) described a second, similar depression (Howe Lake, about 76 km northwest of Yorkton, Saskatchewan) with a diameter of about 270 m and a water depth of 24 m, which contains at least 138 m of recent sediments. The Prairie Evaporite Formation in the Howe Lake area lies approximately 975 m below the surface.

Terzaghi (1970) described gradual subsidence of an area 300 m in diameter, followed by catastrophic formation of a surface depression 152 m across and 7.6 m deep above a solution-mining cavity in one of the salt beds of the Salina Formation at a depth of approximately 265 m near Windsor, Ontario.

The probable collapse process in solution mining areas was outlined in some detail by Nieto-Pescetto and Hendron (1977) on the basis of drill hole information and well performance data from the Windsor-Detroit area. Successive collapses of unsupported roof rock (stoping) above a developing solution cavity lead to formation of an upward growing, conical to cylindrical chimney in strata overlying the cavity. The collapsed material forms a growing debris cone on the floor of the cavity. When the height of the debris pile exceeds the height of the solution cavity (often equal to the thickness of the salt bed), debris starts accumulating inside the chimney. As the chimney continues to extend upwards by stoping the distance between the top of the chimney and the top of the debris decreases because of the volume increase (bulking) of the collapse debris relative to the original rock. When the distance between the top of the chimney and the debris becomes zero, the debris starts supporting the rock at the top of the chimney and the stoping process is interrupted, at least temporarily. It may be reactivated by further solution at depth.

If stoping is not interrupted and the chimney approaches the surface, a subsidence or collapse sinkhole will eventually form. The larger the horizontal extent of the solution cavity at the start of the collapse process and the closer the cavity to the surface, the higher the probability that a sinkhole will be formed. Larger blocks may fall into a larger solution cavity without breaking up, and the debris is less likely to reach the top of the chimney before the chimney reaches the surface.

Methods to relate the size of a collapse sinkhole or larger depression to the size of the subjacent solution cavity responsible for the collapse have not been developed.

Nieto-Pescetto and Hendron (1977) used purely geometric calculations, without concern for any rock-mechanics implications, to determine limiting dimensions for propagation of cylindrical collapse chimneys exactly to the ground surface. Their calculations require that the depth below surface and the thickness of the salt layer be known. They assume that the complete thickness of the salt bed is removed from a circular area and that a cylindrical chimney is formed, which will result in a circular sinkhole with the same radius as the chimney. These assumptions may be valid for cavities developed during solution mining. These calculations should not be applied to sinkholes in the study area (e.g., the Mahony Lake dome sinkholes or the Vermilion Creek sinkhole), even if the depth and the thickness of the Saline River salt were known in detail, because it is unlikely that the assumptions are

warranted in the case of natural subsurface solution of bedded salt.

Karst processes have been active in the study area at least as long ago as the Cretaceous; Cretaceous sandstone infilling of fossil sinkholes in the Bear Rock Formation in the Lac Belot area was described by Cook and Aitken (1971). Active solution of Saline River and Bear Rock Formation evaporites may well have commenced shortly after their deposition and continued, with interruptions, until the present, in a manner similar to the solution history described by Holter (1969) for the Prairie Evaporite Formation in Saskatchewan. Holter listed Late Devonian, post Mississippian to pre-Jurassic, and post Jurassic solution periods in addition to the evidence for Late Pleistocene to Recent solution presented by Christiansen (1967, 1971).

Karst development in the study area may temporarily have been slowed down or stopped during the Pleistocene glaciation. It was probably reactivated relatively promptly and easily after retreat of the ice. Because of its collapse nature it would not have required initiation of sinkholes by solution from the surface down, but only that a few collapse "funnels" would have reached the surface from below to permit high-rate subsurface drainage to become re-established. The almost complete absence of dry valleys is likely a reflection of this; subsurface drainage into collapse sinkholes should have been reactivated before post-glacial fluvial erosion developed an entrenched integrated drainage system.

The presence of permafrost, which could delay or impede redevelopment of a solution karst, has little influence on the revival and further development of a subjacent (collapse) karst. Widespread permafrost might in effect enhance its development, actually promoting concentration of recharge in a relatively small number of sinks.

Torn vegetation mats, tilted shrubs and fallen trees observed in the sinkholes in depression No. 110 and elsewhere in the study area indicate that the collapse process is active. This would seem to indicate that subsurface solution of evaporite beds is continuing, even though a large proportion of the groundwater circulation appears at present to take place through brecciated zones in the rock strata overlying the evaporites (see Chapter 5).

Some of the saucer-shaped sinkholes and small karst depressions with one or more swallow holes, draining somewhat larger areas, may be flooded for short periods ranging from a few days to a few weeks, starting during the snowmelt. An example of this is presented by sinkhole No. 95 (Fig. 9), with a drainage area of about 1 km^2. Even though this sinkhole contains at least five swallow holes, inflow rates during a rapid snowmelt will exceed the rate at which the swallow holes can take the water. Other examples of this type are sinkholes Nos. 167 and 180 in Figure 7. The vegetation pattern in depression No. 111 (Fig. 13), with a drainage area of the order of 5 km^2, indicates that the areas directly around its swallow holes are flooded for a short time in most years; minor flooding was observed there on May 9, 1976.

An example of a large sinkhole with an extensive drainage area (about 65 km^2) of low relief is No. 86B (Figs. 10 and 11). Observations in early May 1976 indicated that the inflow rate during the snowmelt was high enough to raise the water level in the sinkhole by at least 5 m. There was also evidence that at some time during that period the sinkhole was filled completely, with water overflowing through the normally abandoned dry valley into the larger and presumably older sinkhole No. 86A; some overflow was also directed into the smaller and presumably younger sinkhole No. 86C. In early May 1976, sinkhole No. 86D received only minor inflow from local snowmelt. The sequential development of sinkholes Nos. 86A, 86B and 86C, which is presumed to have progressed from southwest to northeast, likely reflects the direction of subsurface drainage.

The large karst depression No. 142 (Figs. 8, 14 and 15) can receive inflow from a number of minor streams. The southwest portion of the depression, however, receives the bulk of its input from a single stream from the southwest. Swallow holes in both portions are situated in such a way that a gradual increase in water level will activate progressively higher swallow holes; this tends to limit the rise in water level. The most extensive flooding observed here is shown in Figure 14 (June 18, 1950); flooding to a slightly smaller extent was observed in June and early July of 1975. When the depression is drained (Fig. 15), the stream from the southwest meanders down the length of the southwest portion of the depression and flows directly into its prime sink (below the arrow marked "R" in Fig. 15). Small ponds usually persist in both portions of the depression until freeze-up.

The hydrology of the largest karst depression in the study area (No. 110 in Fig. 7; Figs. 16, 17 and 18) is complex. Separate streams flow into the three individual sinkholes in the northwestern portion of this depression (Fig. 18). As indicated earlier, small areas around these sinkholes are covered by water for some time every spring; a larger area may be flooded occasionally. No flooding is apparent in Figure 16 (June 18, 1950); a small pond was observed over each of the sinkholes on June 30, 1975.

The central portion of the depression receives inflow from at least 12 small streams. Some of these flow only during and immediately after the snowmelt; the others flow throughout the frost-free season. During the summer most of these streams sink into their gravel and boulder beds somewhere in the depression before they can reach one of the numerous visible sinkholes. The air photograph (Fig. 16) of June 18, 1950, shows no flooding in the central portion of the depression; most of the area was, however, covered by water on June 30, 1975 (Fig. 17A). A number of sinkholes are situated just outside the grass- and sedge-covered area along the southwest and northeast borders of the central portion of the depression (Fig. 18). These receive local inflow only after heavy rain and during snowmelt, and ponding has not been observed in any of them.

The southeastern portion of depression No. 110 is fed by two sizeable streams (marked A and B in Fig. 18) and at least four small ones, all of which carry runoff throughout the frost-free season. A number of minor streams discharge into this portion of the depression only during and immediately after the snowmelt. Once the snowmelt gets underway, the combined inflow rates from the large drainage area of this portion of the depression will exceed the rate at which the sinkholes (or swallow holes) can convey the water into the subsurface. The southeastern portion of the depression is shown flooded on the air photograph (Fig. 16) of June 18, 1950. It was also flooded when first observed during this study on June 30, 1975 (Figs. 17A and B), and it was completely drained and bedrock exposed in the swallow holes on September 10, 1975 (Fig. 17C). The nonvegetated area extending down the centre of this part of the depression represents the area of extended annual flooding; the sedge- and grass-covered zone is inundated every year, but for a considerably shorter period of time; high water may inundate the zone of willow bushes in some years. The edge of the black spruce forest and muskeg represents the limit of flooding during extreme high water over the past 40 or 50 years (the approximate age of the trees).

When rising water in the southeastern portion of depression No. 110 starts covering the grassy zone, overflow to the central portion will take place through the channel marked "Q" in Figure 18. Flow was observed in this channel on June 30, 1975, when it discharged into the flooded central portion of the depression. On June 18 and 22, 1976, and on June 7 and 23, 1977, water in the over-

CHAPTER 4

Karst Hydrology in Permafrost Terrain

BACKGROUND

The presence of permafrost usually exerts a restrictive influence on the rate at which water can infiltrate into and percolate through soil to recharge groundwater flow systems, because the hydraulic conductivity of frozen soil is often several orders of magnitude lower than that of the same soil in an unfrozen condition. Under permafrost conditions, infiltration through joints and solution openings in exposed bedrock must therefore account for a major proportion of groundwater recharge. Brandon (1965) has stressed the hydrogeologic significance of the Saline River and Bear Rock formations as local aquifers. The presence of collapse sinkholes and zones of brecciated rock in formations overlying the Saline River and Bear Rock formations will be shown to be of similar importance for the existence of active groundwater flow systems in the study area.

Incidental hydrologic observations have been made on a number of sinkholes throughout the study; inflow measurements and water-level recordings have been obtained for depressions No. 110 and No. 142. Locations of a number of springs and associated icings were earlier described by Hughes *et al.* (1973); combined discharge rates have been determined for some of these during this study. The results of the hydrologic observations are presented in the following sections.

CORRECTIONS TO DRAINAGE PATTERNS

Some parts of the drainage patterns shown on NTS map sheets 96F and 96K with scale 1:250 000 have been found to be incorrect during fieldwork in the area. The necessary corrections have been incorporated in Figures 7 and 8.

The major correction concerns drainage near the northwest corner of NTS 96F. As indicated in Figure 7 and shown by Figure 11, sinkhole No. 86B is the sink for a significant stream draining a number of lakes and ponds located to the southwest, south and southeast of the sinkhole group No. 86.

Correction was also required at depression No. 110 (Fig. 7), the southeastern portion of which is shown on the topographic map as a permanent lake; it was found to be an intermittent karst lake, drying up sometime in late summer or early fall in most years. The same applies to lake No. 167 (Fig. 7); the lake in depression No. 142 and two small lakes northeast of it (Fig. 8); a small lake shown immediately northeast of sinkhole No. 173 (Fig. 6); and several others marked on Figures 5 to 8. A number of small- and medium-sized lakes in the study area show a significant reduction in water-covered area in most years as a result of a drop of several metres in their water levels; some of these are likely to go dry at some stage during an extended period of below average precipitation.

In several places, NTS 96F and NTS 96K show surface drainage connections where divides were found to exist (e.g., the small streams shown draining depression No. 142 and the two small karst lakes northeast of it); these have also been corrected in Figures 7 and 8.

INTERPRETATION OF AERIAL OBSERVATIONS

Hydrologic Significance of Karst Features

The hydrologic significance of sinkholes and larger karst depressions is determined by a combination of factors including their size, the extent of their drainage areas and their topographic setting. The actual hydrologic performance of karst features depends on climatic conditions (temperature regime, amount and seasonal distribution of precipitation, etc.). The variety of hydrologic significance will be discussed in this section on the basis of a number of examples.

Many small sinkholes have drainage areas covering less than one tenth of a square kilometre. Inflow rates into these can be as high as 5 L/s during the peak of the snowmelt, but they do not lead to ponding of water in these sinkholes. Therefore, the "lakes" found in the bottom of some deep sinkholes with small drainage areas, for example in the Vermilion Creek sinkhole (No. 175 in Fig. 6; Fig. 12), do not represent ponding of excess inflow but they show in their lake levels the local subpermafrost water table.

flow channel sank into the bedrock exposed in the bottom of the channel, about 200 m upstream from the nearest sinkhole in the central portion of the depression that was not inundated on these dates. Water levels in the southeastern portion of the depression therefore do not represent groundwater levels in the depression as a whole and no evidence has been found that lower-lying parts of the depression are flooded because of a rise in the level of a "karst water table," as suggested by Brook (1977) for the Nahanni North Karst. All flooding that occurs in depression No. 110 is the result of excess inflow contributed by surface streams.

The observations on the relationship between water levels in the various portions of depression No. 110 show that its floor does not act as a single water-controlling level; it was earlier established that the floor is not a solution plane either. For these reasons it has to be concluded that this is not a polje in the classical sense. It could, however, be designated as a *subjacent karst polje* or a *collapse karst polje*.

Extent of Flooding, 1973–1977

After the initial observations of flooding in some of the karst depressions during 1975, all LANDSAT (Land Satellite) imagery available for the area for the year 1975 was checked to determine whether the occurrence of flooding could be detected on standard black and white prints of MSS band 7 images (scale 1:1 000 000). It was found that due to the presence of snow and ice, images recorded before the end of May or after the end of September are generally of little use for this purpose. Some of the images recorded between late May and early October were unusable because of cloud cover. The remaining images revealed that the occurrence and recession of flooding could be detected, even for relatively small depressions (van Everdingen, 1976).

Composites of the usable LANDSAT images for 1975 are presented in Figure 20 (A to H). As the LANDSAT satellites operate on an 18-day cycle and considerable overlap exists between images on adjoining tracks, intervals for images from a single satellite could vary from 17 to 19 days. The nine-day intervals between image dates for the period from June 9 until July 16 were possible because both LANDSAT 1 and 2 were operational at the time. The larger gaps in coverage in the period between July 16 and September 17 are the result of extensive cloud cover over the area.

The depressions for which changes in the extent of water cover could be detected on the original imagery are: No. 140 on NTS 96E (Fig. 6); Nos. 110, 111 and 180 on NTS 96F (Fig. 7); and Nos. 142, 181 and 182 on NTS 96K (Fig. 8). Five of these are indicated on the composites of Figure 20 by arrows numbered from 1 to 5.

In Figure 20, No. 1 indicates the intermittent lake No. 180 situated in a depression between two perennial lakes. It persisted from June 9 to July 16 and was gone by August 20.

In Figure 20, No. 2 is the large depression No. 110. All three portions of the depression were flooded on June 9; flooding in the northwestern portion was receding by June 27 and gone by July 7; flooding in the central portion was receding by July 7 and gone by July 16; flooding in the southeastern portion was still noticeable on July 16, but it was gone by August 20.

In Figure 20, No. 3 is the depression No. 142. It was completely flooded on June 9; this remained with little change until July 7. By July 16 the flooded area had been split into two portions; these were gradually reduced in size, but two small "ponds" still persisted by September 17.

In Figure 20, No. 4 is the elongated depression No. 181. It was flooded over its full length on June 9; this persisted with little change until July 16. Flooding receded from the northern portion of the depression by August 20; only a small "pond" remained in the southern portion by August 29.

In Figure 20, No. 5 is another elongated depression, No. 182. It was completely flooded on June 9; the depression remained filled, with only minor changes in the extent of the water-covered area until September 17.

At a later stage during this study, all usable LANDSAT imagery for the same area for the period 1973 to 1977 inclusive was checked for evidence of the occurrence and recession of flooding in the depressions numbered 1 to 4 in Figure 20. The observations are listed in Table 1. They indicate that depressions Nos. 180, 110 and 142 (Nos. 1 to 3 in Table 1) were flooded and subsequently drained every year, whereas depression No. 181 (No. 4 in Table 1) appears to have been flooded and subsequently drained in 1973, 1975 and 1977, but not in 1974 and 1976.

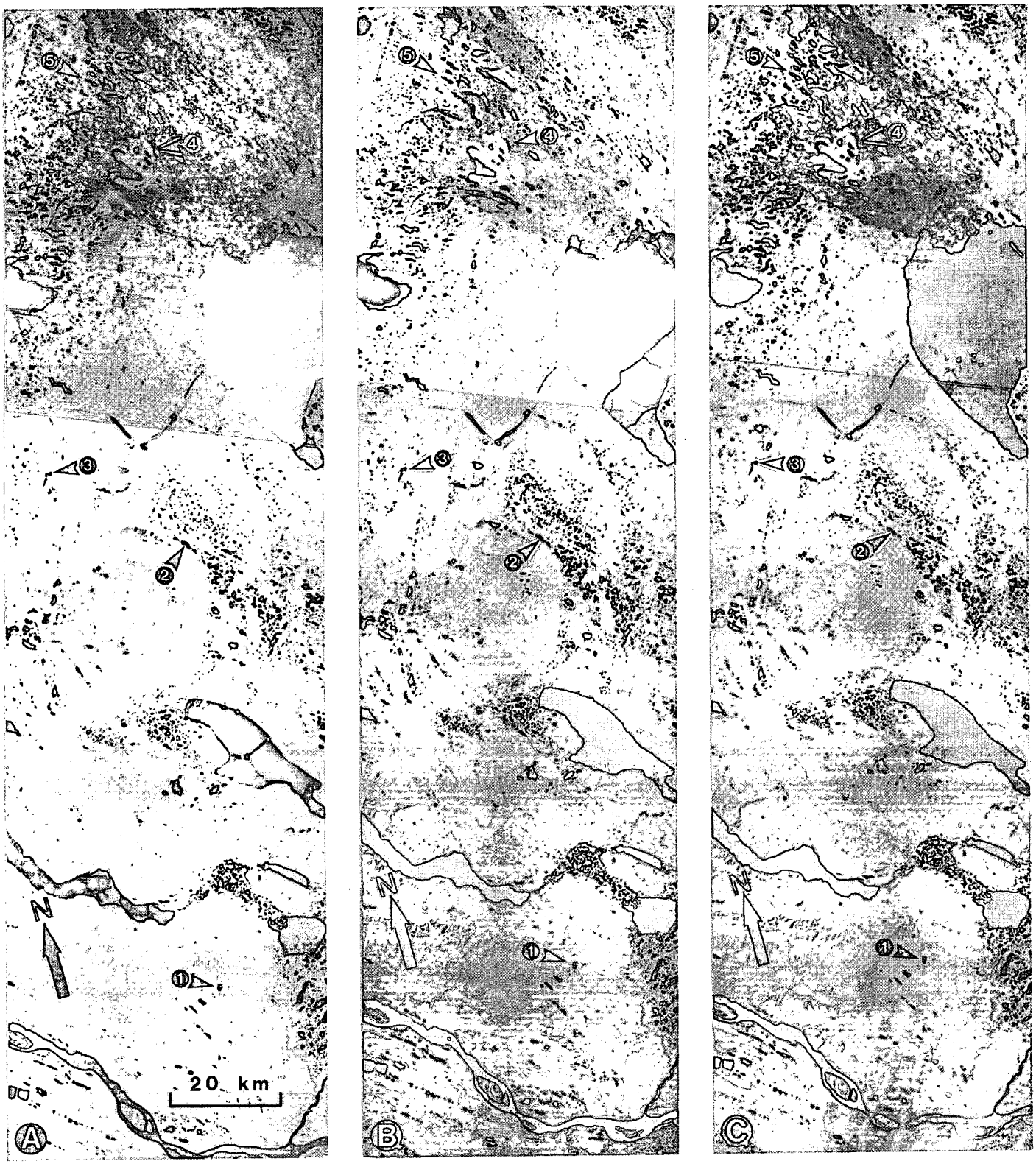

Figure 20. LANDSAT imagery showing occurrence and recession of flooding in five depressions (*1* – No. 180; *2* – No. 110; *3* – No. 142; *4* – No. 181; *5* – No. 182) during 1975: *A* – June 9; *B* – June 18; *C* – June 27; *D* – July 7; *E* – July 16; *F* – August 20; *G* – August 29; *H* – September 17.

Environment Canada Environnement Canada

National Hydrology Research Institute

NHRI PAPER NO. 11
IWD SCIENTIFIC SERIES NO. 114

Morphology, Hydrology and Hydrochemistry of Karst in Permafrost Terrain near Great Bear Lake, Northwest Territories

R. O. van Everdingen

NHRI

NATIONAL HYDROLOGY RESEARCH INSTITUTE
INLAND WATERS DIRECTORATE
CALGARY, ALBERTA, 1981

Contents

	Page
ABSTRACT	vii
RÉSUMÉ	vii
ACKNOWLEDGMENTS	ix
1. INTRODUCTION	1
Physiography	2
2. GEOLOGY	3
Background	3
Bedrock stratigraphy	3
Cambrian – Mount Cap and Saline River formations	3
Cambro-Ordovician – Franklin Mountain Formation	3
Ordovician-Silurian – Mount Kindle Formation	4
Lower Devonian – Bear Rock Formation	6
Middle and Upper Devonian	6
Cretaceous	7
Unconsolidated deposits	7
3. KARST	8
Introduction	8
Distribution of karst features	9
Morphology of sinkholes and larger karst depressions	10
Processes involved in karst development	19
4. KARST HYDROLOGY IN PERMAFROST TERRAIN	23
Background	23
Corrections to drainage patterns	23
Interpretation of aerial observations	23
Hydrologic significance of karst features	23
Extent of flooding, 1973–1977	25
Water-level measurements, 1976–1978	29
Pressure recording, 1976–1977	29
Time-lapse photography, 1977–1978	33
Streamflow measurements, 1976–1978	36
Climatic and hydrologic summaries, 1973–1978	37
5. HYDROCHEMISTRY	39
Background	39
Major-ion composition	39
Deuterium and oxygen-18 abundances	43
Tritium levels	46
Sulphur-34 abundances	48
6. POTENTIAL GEOTECHNICAL AND ENVIRONMENTAL HAZARDS IN THE STUDY AREA	50
Foundation hazards	50
Flooding	50
Contamination of groundwater	50

Contents (Cont.)

Page

7. CONCLUSIONS 51

REFERENCES 52

Tables

1. Observations on flooding, 1973–1977, from LANDSAT imagery 29
2. Streamflow measurements, 1976–1978 36
3. Climatic and hydrologic summaries, 1973–1978 38
4a. Chemical analyses of recharge samples 40
4b. Chemical analyses of samples from springs and spring-fed lakes 40
5a. $\delta\ ^{18}O$, δD and tritium levels in precipitation samples 43
5b. $\delta\ ^{18}O$, δD and tritium levels in recharge samples 44
5c. $\delta\ ^{18}O$, δD, $\delta\ ^{34}S$ and tritium levels in samples from springs and spring-fed lakes 44

Illustrations

Figure 1. Index map showing location of study area with respect to regional physiography 1
Figure 2. Distribution and isopachs of Saline River Formation evaporites 4
Figure 3. The Keele Arch and the Mahony Lake dome 5
Figure 4. Schematic cross section through the Mahony Lake dome 6
Figure 5. Karst features, northwest portion of NTS map sheet 96C/13 . . . . . (In pocket)
Figure 6. Karst features, NTS map sheet 96E . . . . . (In pocket)
Figure 7. Karst features, NTS map sheet 96F . . . . . (In pocket)
Figure 8. Karst features, NTS map sheet 96K . . . . . (In pocket)
Figure 9. Aerial views of sinkhole No. 95: (a) flooded, May 9, 1976; (b) drained, June 22, 1976 11
Figure 10. Air photograph showing sinkholes in group No. 86 and the "Disappearing River," June 18, 1950 12
Figure 11. Aerial view of "Disappearing River" flowing into sinkhole No. 86B, June 30, 1975 13
Figure 12. Large collapse sinkhole near Vermilion Creek 13
Figure 13. Aerial view of depression No. 111, showing individual sinkholes 13
Figure 14. Air photograph showing depression No. 142 flooded, June 18, 1950 14
Figure 15. Aerial view of drained depression No. 142, June 21, 1976 15
Figure 16. Air photograph of depression No. 110, showing the southeastern portion flooded, June 18, 1950 16

Illustrations (Cont.)

Page

Figure 17. Aerial views of depression No. 110: (a) widespread flooding in the central and southeastern portions on June 30, 1975; (b) flooded southeastern portion on June 30, 1975; (c) drained southeastern portion on September 10, 1975 17
Figure 18. Detailed map of depression No. 110 18
Figure 19. Indications of sinkhole formation through collapse, from depression No. 110: (a) downward displacement of beds; (b) arching fractures; (c) stoping. 20
Figure 20. LANDSAT imagery showing occurrence and recession of flooding in five depressions (Nos. 180, 110, 142, 181 and 182) during 1975 on June 9, June 18, June 27, July 7, July 16, August 20, August 29 and September 17 26
Figure 21. Pressure recorder installed in sinkhole in southeastern portion of depression No. 110, May 9, 1976 30
Figure 22. Daily mean temperatures and daily precipitation at Norman Wells Airport for 1976, and water level in the southeastern portion of depression No. 110, recorded by pressure recorders 31
Figure 23. Daily mean temperatures and daily precipitation at Norman Wells Airport for 1977, and water levels in the southeastern portion of depression No. 110 (from time-lapse photography and pressure recording) and in depression No. 142 (from pressure recording) 32
Figure 24. Time-lapse camera installed on island in southeastern portion of depression No. 110, March 29, 1977 34
Figure 25. Example of time-lapse photography, depression No. 110, September 13, 1977. 34
Figure 26. Daily mean temperatures and daily precipitation at Norman Wells Airport for 1978, and water levels in the southeastern portion of depression No. 110 and in depression No. 142 (from time-lapse photography) 35
Figure 27. Semilog plots showing major-ion analyses for samples of karst recharge and discharge from the areas of Bear Rock, Vermilion Creek and Mount Richard 41
Figure 28. Semilog plots showing major-ion analyses for samples of karst recharge and discharge from the Mahony Lake–Hare Indian River area: (a) recharge entering sinkhole No. 86B; (b) recharge entering depression No. 110; (c) recharge entering depression No. 142 and sinkhole No. 49; (d) discharge from "Grizzly" springs, a spring in lake No. 2 and a spring just below lake No. 2; (e) lake No. 1 near "Grizzly" springs and outflow from lakes Nos. 1 and 2 42
Figure 29. Plot of δD vs. $\delta\ ^{18}$O for samples of precipitation 45
Figure 30. Plot of δD vs. $\delta\ ^{18}$O for samples of karst recharge and discharge 46
Figure 31. Tritium levels in samples of precipitation, karst recharge and karst discharge for the period 1975–1978 compared with extrapolated tritium levels for precipitation in the central Mackenzie Valley for the period 1961–1975 47
Figure 32. Plot of δT vs. δD and $\delta\ ^{18}$O for three snowstorms at Norman Wells. 48

Abstract

Collapse karst is widespread in the Franklin Mountains, Colville Hills and Great Bear Plain between Great Bear River and 67°N. Collapse features in the area are interpreted as being the result of subsurface solution of evaporites from the Upper Cambrian Saline River Formation and the Lower Devonian Bear Rock Formation; they appear to be concentrated on and around a number of small "domes" on the Keele Arch. Integrated surface drainage is limited or lacking over portions of the karst area. Hydrologic measurements (rates of inflow into sinkholes; water levels in seasonally flooded depressions; discharge from springs) indicate that subsurface runoff may be as high as 40 mm per year or about 15% of the annual precipitation and that rainfall rates as low as 6 mm per day can initiate recharge to the karst-water system. Results of deuterium and oxygen-18 analyses show that snowmelt provides a major portion of the recharge; tritium levels in discharge from springs indicate that residence times in the karst-water system are relatively short.

Seasonal flooding of karst depressions may cause problems for future engineering developments in the region; the tendency of the karst to collapse presents a special geotechnical hazard in addition to the problems related to the widespread occurrence of ice-rich permafrost. The karst-water system is extremely vulnerable to contamination from the surface because of the close spacing of high-rate recharge points and the unfiltered nature of the recharge. Once a contaminant has entered the karst-water system, rapid subsurface transport will make containment, recovery and cleanup after an accidental spill difficult or impossible.

Résumé

Les effondrements karstiques sont très répandus dans les monts Franklin, les collines Colville et la plaine Great Bear, entre la Grande rivière de l'Ours et le 67e parallèle N. Les dépressions de cette région sont considérées comme étant le résultat de la dissolution souterraine des évaporites de la formation de la rivière Saline datant du cambrien supérieur et de celle de Bear Rock datant du dévonien inférieur; elles semblent concentrées autour d'un certain nombre de «dômes», sur l'Arc Keele. Le drainage superficiel intégré est limité, voire totalement absent, dans certaines parties des zones karstiques. Des relevés hydrologiques (débit d'infiltration dans les entonnoirs; niveaux d'eau dans les dépressions inondées périodiquement; débit des sources) indiquent que l'écoulement souterrain peut atteindre 40 mm par année, soit environ 15 % des précipitations annuelles, et que des pluies aussi faibles que 6 mm par jour peuvent amorcer la recharge du réseau d'eau karstique. Les résultats des analyses au deutérium et à l'oxygène-18 indiquent que la fonte des neiges compte pour une grande partie de cette recharge; la teneur en tritium des eaux de source révèle que le temps de séjour dans le réseau d'eau karstique est relativement court.

L'inondation saisonnière des dépressions karstiques peut présenter certains problèmes pour les futurs travaux de génie dans cette région; l'effondrement des formations karstiques présente un danger géotechnique spécial, en plus des problèmes associés à la présence généralisée d'un pergélisol riche en glace. Le réseau d'eau karstique est très vulnérable à la contamination superficielle en raison de la courte distance entre les points de recharge à débit élevé et du fait que les eaux de recharge sont infiltrées. Lorsqu'un contaminant entre dans le réseau, son transport souterrain rapide rend très difficile, voire impossible, toute opération d'isolement, de récupération et de nettoyage à la suite d'un déversement accidentel.

Acknowledgments

K.U. Weyer of the Hydrology Research Division, National Hydrology Research Institute (NHRI), and O.L. Hughes of the Terrain Sciences Division, Geological Survey of Canada, alerted the author to the lack of integrated surface drainage and the existence of the large karst depression No. 110 north of Mahony Lake, respectively; S. Chatwyn, working for the Terrain Sciences Division at the time, accompanied the author during his first trip into the area in late June 1975. F.A. Michel, Department of Earth Sciences, University of Waterloo, assisted in fieldwork during the summers of 1975, 1976 and 1977.

Background information on the bedrock stratigraphy and structure of the study area was provided by D.G. Cook and J.D. Aitken, Geological Survey of Canada; J.D. Aitken accompanied the author on a field trip through the area in early August 1977 to confirm stratigraphic ages of bedrock exposures in a number of sinkholes. N.C. Meyer-Drees, Geological Survey of Canada, provided the unpublished isopach map for the Saline River Formation; A.W. Norris confirmed the Lower to Middle Devonian age for the Bear Rock Formation.

J.A. Banner, Hydrology Research Division, NHRI, designed, built and installed the time-lapse camera systems used during 1977 and 1978 and looked after the processing of the results; he also assisted in sampling and field measurements on a number of occasions. C.W. Peters, Water Survey of Canada, performed the streamflow measurements.

Isotope analyses were provided by H.R. Krouse of the Physics Department of the University of Calgary ($\delta\ ^{34}S$, δD, $\delta\ ^{18}O$) and by F.A. Michel of the Department of Earth Sciences, University of Waterloo (δD, $\delta\ ^{18}O$, T).

S.O. Ulrichsen, Okanagan Helicopters Ltd., looked after most of the transportation in the field and, on many occasions, was very helpful. On June 21, 1976, Stan was attacked by a grizzly during our sampling of a group of springs (which we have since called "Grizzly" springs) near lake No. 1 in the valley of the Hare Indian River. Although he was seriously wounded, he managed to fly us back to Norman Wells, thereby avoiding the necessity of a search and rescue operation. In September 1977, Stan used his considerable flying talents, unimpaired by the grizzly experience, to collect the "impossible" sample of water from the "lake" in the large sinkhole near Vermilion Creek.

Critical comments on the first draft of this report were provided by J.A. Vonhof, J.A. Banner and K.U. Weyer.

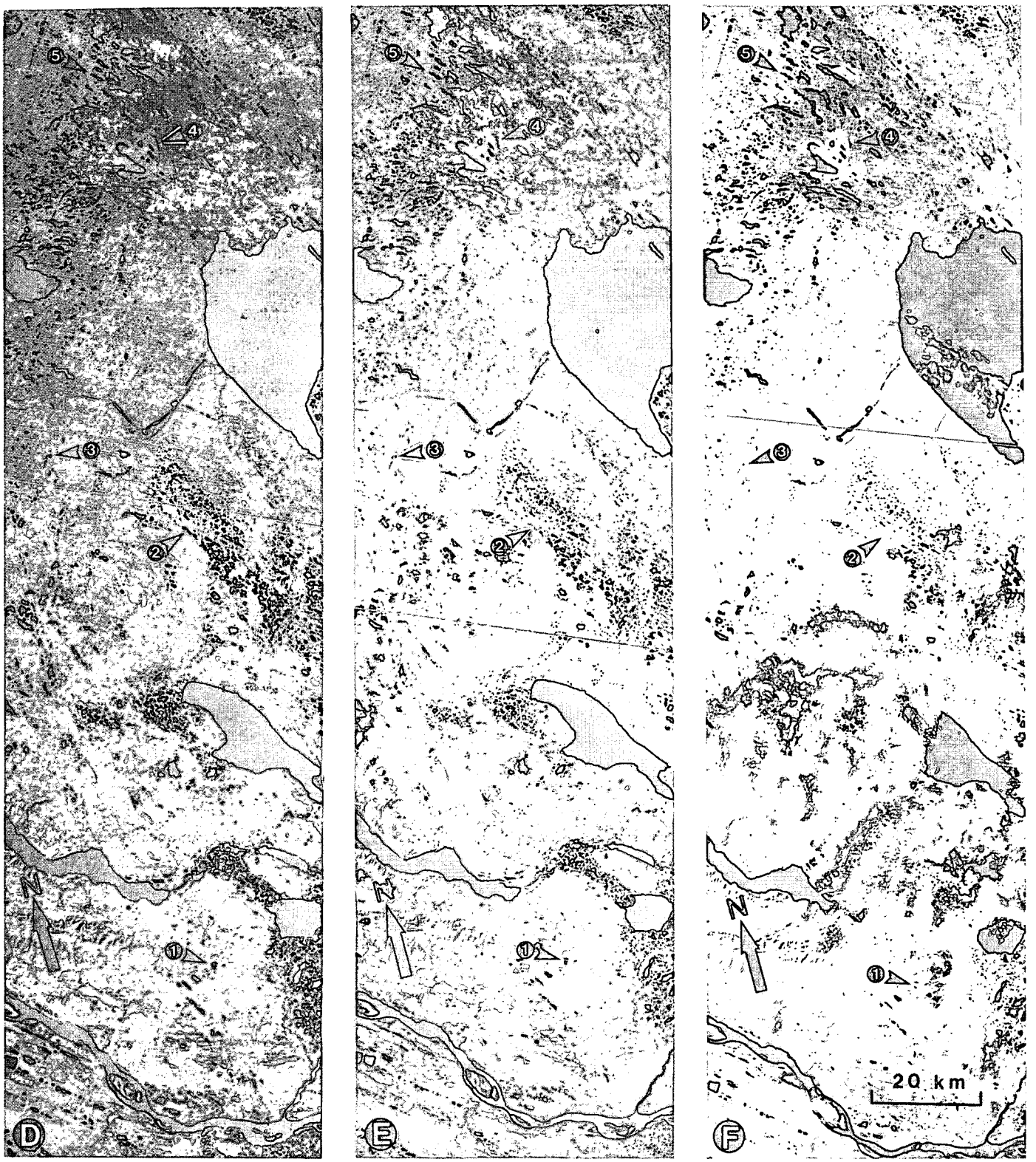
5
4
3
2
1
N
D
E
F
20 km

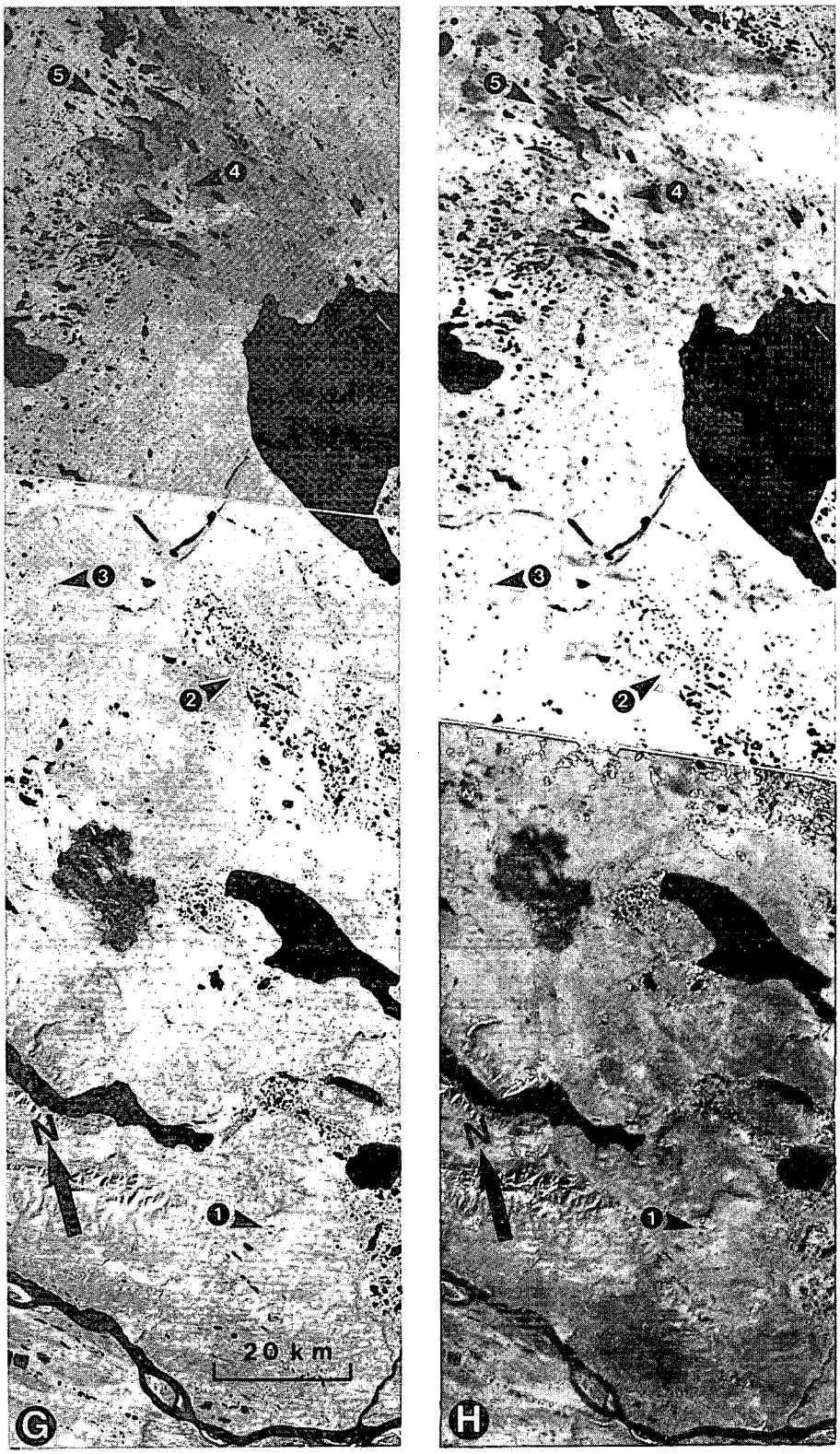
5
4
3
2
1
N
20 km
G
5
4
3
2
1
N
H

Table 1. Observations on Flooding, 1973–1977, from LANDSAT Imagery

Date	Location* 1 (Lake No. 180)	2 (Depression No. 110)	3 (Depression No. 142)	4 (Depression No. 181)
73-06-10/11	Full	S – Full	Full	Full
73-06-28/29	Full	S – Full	Partly filled	Partly filled
73-07-16	?	?	?	Partly filled
73-09-08	Empty	Empty	2 Small ponds	Partly filled
73-09-27	Empty	Empty	Empty	Small pond
74-06-06	Full	?	Small pond?	?
74-06-23	?	?	?	Small pond
74-07-11	?	S – Full	S – Full	?
74-07-29/30	Empty	S – Full	Empty	Small pond
75-06-09	Full	N, C, S – Full	Full	Full
75-06-18/19	Full	N, C, S – Full	Full	Full
75-06-27	Full	(N), C, S – Full	Full	Full
75-07-07	Full	C, S – Full	Full	Full
75-07-15/16	Partly filled	S – Full	Full	Full
75-08-20/21	Empty	Empty	2 Small ponds	Partly filled
75-08-29	Empty	Empty	2 Small ponds	Large pond
75-09-16/17	Empty	Empty	N pond only	Small pond
76-06-03/04	Full	S – Full	Small pond	Small pond
76-06-21/22	Full	S – Full	Empty	Small pond
76-07-09	Empty	S – Partly filled	Empty	Small pond
76-07-27/28	?	Empty	Empty	Small pond
77-05-29/30	Full	N, S – Full	S – Full	Full
77-06-04/05	Full	(N), S – Full	S – Partly filled	Full
77-06-16/17	?	S – Full	Nearly empty	Full
77-07-05	?	?	Empty	Full
77-07-28/29	Empty	S – Partly filled	Empty	Partly filled
77-08-09/10	Empty	S – Partly filled	Empty	Small pond
77-08-15/16	Empty	S – Partly filled	Empty	Small pond
77-08-28	?	Empty	Empty	?
77-09-03	Empty	Empty	Empty	Small pond
77-09-15	Empty	Empty	Empty	?
77-10-02/03	Empty	Empty	Empty	Small pond

* Numbers refer to Figure 20.

Note: N, C and S refer to northern, central and southern portions of depressions; parentheses indicate area only partly filled. Question marks indicate uncertainty owing to clouds; all 1974 imagery taken after July 30 was useless because of cloud cover (see rainfall data in Table 3).

WATER-LEVEL MEASUREMENTS, 1976–1978

Pressure Recording, 1976–1977

Once it had been established that the southeastern portion of depression No. 110 is likely to be filled with water (and subsequently drained) every year, the decision was made to attempt recording the water level during at least one flooding cycle. A preliminary level survey in 1975 had indicated that the maximum range in surface water level was approximately 13 m. This large range, in combination with the shape, size and terrain characteristics of the depression, made it impossible to employ standard water-level recorders. Instead, a submersible self-contained battery-operated pressure-recording system was used.

The recorders used for this purpose were Rustrak model 2162 pressure recorders (Bourdon-tube type, with 12-V DC chart drive, chart speed 1/8 in. per hour or approximately 7.6 cm per day); the pressure ranges selected were 0-15 psi (0-10.5 m H_2O) and 0-30 psi (0-21.1 m H_2O). The recorders were installed inside modified spray-painting bulk containers (Campbell Hausfeld Co., Harrison, Ohio, model PT 2300-084: maximum *internal* working pressure 60 psi; overall dimensions – height 35 cm and diameter 30 cm; inside dimensions – height 26 cm and

Figure 21. Pressure recorder installed in southeastern portion of depression No. 110, May 9, 1976 (location indicated by lowest arrow marked *R* in Fig. 17C).

diameter 23 cm). Approximately 5 kg of lead was placed in the bottom of the cans to provide sufficient submerged weight to sink the system. The pressure port of each recorder was connected by Tygon tubing to a length of small-diameter copper tubing leading to a watertight feed-through (modified Swagelock tubing fitting) installed in the lid of the container; a second length of copper tubing was connected from the feed-through to a modified NUPRO 7-μm sintered stainless-steel filter element used as a pressure inlet screen. A metal protector was mounted over the pressure inlet screen to prevent mechanical damage. The systems were calibrated with air pressure, applied in steps of 5 psi (approximately 3.5 m H_2O), against a pressure gauge of known accuracy. Figure 21 shows one of the recording systems after installation.

Three pressure-recording systems were installed in the southeastern portion of depression No. 110 on May 9, 1976, when water from snowmelt was already flowing into several swallow holes in the depression. The recorder with the pressure range of 0–30 psi was installed in the deepest swallow hole; one recorder with a range of 0–15 psi was installed on a bedrock ridge separating the first swallow hole from an adjoining one; the remaining recorder with the range 0–15 psi was installed in a shallower swallow hole to the northwest of the first one. The recorder locations are marked in Figures 17 and 18. The recorders were retrieved on August 28, 1976, and recalibrated; water-level markers installed on June 22 were surveyed to permit a check on the accuracy of the recordings. Daily water levels derived from the pressure recordings were plotted in Figure 22, together with a plot of daily precipitation and mean temperature recorded at Norman Wells, the nearest weather station. This station is located 90 km southwest of the depression on the other side of the Franklin Mountains. Data presented by Burns (1973, 1974) indicate that the Norman Wells records should be applicable to the area of the Mahony Lake dome at least in a semiquantitative way.

Figure 22 shows that the last day with a mean temperature below 0°C was April 24. Flooding in the depression started 16 days later, on May 10, although inflow into the depression began earlier, as observed on May 9. The rise in water level gradually slowed down after May 21, but was accelerated again on May 30 after a rainy period from May 26 to 29. The water level started declining after the maximum for 1975 was reached on June 5; the decline was temporarily reversed on June 20 after rain on June 18 and 19. The final decline started on July 8; the depression was dry by August 9. The maximum water level reached was 11.35 m above the level of the depression at the recorder location.

The depth of a deep swallow hole just north of the island in the southeastern portion of depression No. 110 was also measured on August 28, 1976. The rocky bottom of the hole is 19.5 m below the top of the bedrock, which is overlain by 5.9 m of unconsolidated material; the surface of the sediments around the hole is approximately 1.1 m below the apparent extreme maximum water level (deduced from the driftwood on the shore of the island). The hole was dry to the measured depth; the total range of water-level variation in the depression is thus *at least* 26.5 m.

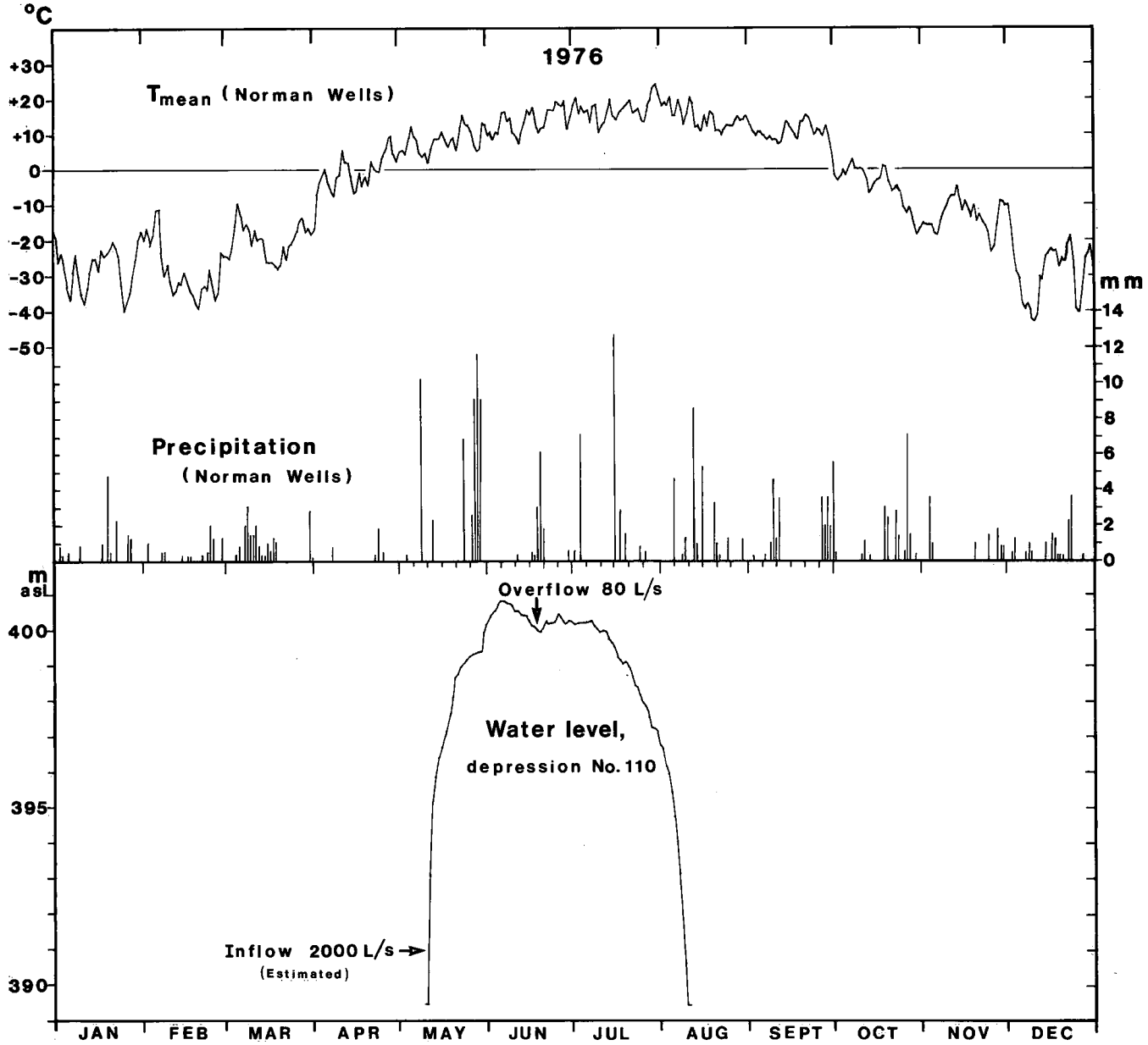

Figure 22. Daily mean temperatures and daily precipitation at Norman Wells Airport for 1976 (data from Atmospheric Environment Service), and water level in the southeastern portion of depression No. 110, recorded by pressure recorders.

Two pressure recorders (0-30 psi and 0-15 psi) were reinstalled in the deep and shallow holes in the southeastern portion of depression No. 110 on March 29, 1977. Since an appreciable amount of snow was present in the depression at the time, the recorders were lowered from the hovering helicopter onto the snow surface over the deepest point of the swallow holes using polypropylene ropes. The ropes, with wooden blocks tied to one end, were left attached to the recorders to facilitate locating them at the end of the season in case they became covered by sediment. One recorder (0-15 psi) was installed on a flat-lying rock slab in the primary sink in the southwestern portion of depression No. 142. Its location is marked "R" in Figure 15.

After the recorders were retrieved (on August 3 from No. 142; on September 24 from No. 110), it was found that gas had accumulated in the containers, presumably produced by the batteries. After venting, the recorders were re-calibrated in the field, with air pressure applied in steps of 5 psi. Water-level markers installed on June 7, June 23 and August 7 were surveyed on September 24 to permit correction of the daily water levels derived from the pressure recordings.

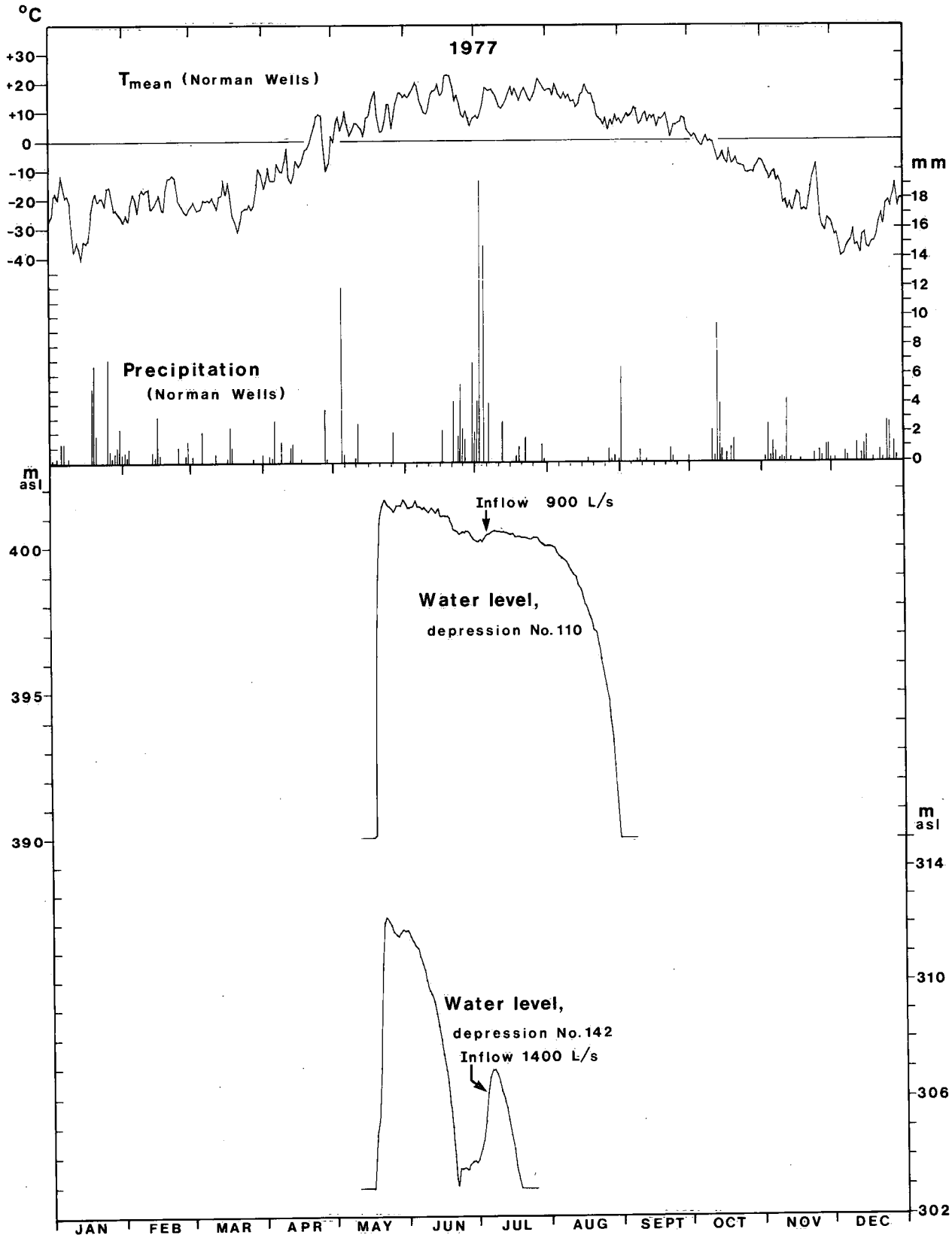

Figure 23. Daily mean temperatures and daily precipitation at Norman Wells Airport for 1977 (data from Atmospheric Environment Service), and water levels in the southeastern portion of depression No. 110 (from time-lapse photography and pressure recording) and in depression No. 142 (from pressure recording).

The daily water levels for the 1977 season determined in this way for depression No. 142 are plotted in Figure 23, which also shows daily precipitation and mean temperatures at Norman Wells. Flooding in the depression started on May 16, 15 days after the last day with a mean temperature below 0°C; the water level peaked on May 22, with a lower peak on May 29 (possibly related to rain recorded in Norman Wells on May 26). The depression was completely drained by June 21. A rainy period, starting on June 21 and culminating with 19.3 and 14.8 mm of rain on July 2 and July 4, respectively, led to renewed flooding that reached a maximum on July 6. The depression finally went dry on July 18.

The water-level graph for 1977 for depression No. 110, also shown in Figure 23, was adjusted on the basis of daily photographs obtained with the use of a recently developed system for time-lapse photography, described in the next section.

Time-Lapse Photography, 1977-1978

In early 1977, an automatic time-lapse photography system was developed by the Hydrology Research Division of Environment Canada to enable determination of the time and the rate of the growth of frost blisters that form every winter in the spring area on the east side of Bear Rock (Banner and van Everdingen, 1979; van Everdingen and Banner, 1979). Two of the seasonally flooded karst depressions were used as sites for field testing of the camera system in 1977.

On March 28, 1977, two camera systems were installed at depression No. 142, on trees about 5 m apart in the location indicated by a white arrow marked "C" in Figures 14 and 15. Both cameras were aimed at the primary sink where the pressure recorder was installed. The next day two more camera systems were installed on the island in the southeastern portion of depression No. 110, on two trees approximately 6 m apart; one of the installations is shown in Figure 24. The cameras were aimed in the direction of the deepest swallow hole; the field of view of the cameras is indicated by a print of one of the photos taken by the right-hand camera on September 13, 1977, reproduced as Figure 25. All cameras were loaded with black and white negative film and the electronic controls were set for three frames to be taken once a day at solar noon.

The cameras at both locations were tested on June 23. The two cameras at depression No. 110 were apparently operating well; since the two cameras at No. 142 were found to be jammed, they were removed. The cameras at depression No. 110 were still operating properly when tested on August 7 and again on September 24, just before they were taken out. When their films were processed, they provided a complete record of daily measurements of the water level in the southeastern portion of the depression. The total period of operation was 180 days.

The time-lapse photography taken by the cameras at depression No. 110 during 1977, and the water levels marked on June 7, June 23 and August 7 were used to adjust water levels derived from the pressure recordings to eliminate the error introduced by gas buildup in the recorder containers. The results are shown in Figure 23; the use of time-lapse photography provided additional details on snow cover and on the start of inflow into the swallow hole.

The area was snow-covered when the cameras and recorders were installed on March 29, 1977. Bare ground started appearing on April 29. The last day with a mean temperature below 0°C was May 1. Although snow fell on May 4, it was all gone on the following day. A slowly growing pond started forming in the swallow hole on May 9; the pond decreased in size between May 13 and May 17; a rapid rise in the water level took place from May 18 to May 21; the peak level was reached on May 22. The water level fluctuated after that, with a gradual decline becoming apparent by June 15. The decline in water level was reversed temporarily on two occasions, starting on June 24 and July 3, respectively, after the occurrence of rain. The final gradual decline after July 8 was accelerated significantly from August 3 onwards; the swallow hole was dry by September 1. The inflow channels continued to supply water to the depression at least until September 24, the date on which the cameras and recorders were removed.

Additional information that could be obtained from the time-lapse photography includes the occurrence of snow, rain and fog, and the relative direction and velocity of wind (from wave patterns on the karst lake).

In 1978, single time-lapse camera systems were installed in the same locations at the two depressions. This time the cameras were loaded with colour negative film and the electronic controls set for six frames to be taken once a day at solar noon. One camera was installed at depression No. 110 on May 5, and the other at depression No. 142 on May 7. Targets made of plywood (30 cm wide and 15 cm high) were installed on the sediment slope above the bedrock in depression No. 110; these targets as well as the tops of a number of the bedrock beds were surveyed to provide control for the determination of water levels from the time-lapse photography. The tops of a number of bedrock beds in the primary sink in depression No. 142, as well as several easily identifiable levels above the bedrock wall, were

Figure 24. Time-lapse camera installed on island in the southeastern portion of depression No. 110, March 29, 1977 (location indicated by arrows marked *C* on Fig. 17).

surveyed for the same purpose. This ground control, in combination with the resolution of the film, permitted determination of the water levels with an accuracy better than ±5 cm. The camera at depression No. 142 was retrieved on September 12; the one at depression No. 110, on October 10.

The water levels observed in the two depressions during 1978 are plotted in Figure 26, together with the daily precipitation and mean temperatures recorded at Norman Wells. The time-lapse photography showed that a partial snow cover was still present in both depressions when the cameras were installed. Figure 26 indicates that the last day with a mean temperature below 0°C was May 12. Both the precipitation records and the time-lapse photography indicated a light snowfall on May 17; the new snow was gone the next day. Flow in the inflow channels became visible on May 20 in depression No. 142 and on May 21 in depression No. 110.

Ponding started at the primary sink of depression No. 142 on May 24; the maximum level was reached on June 2, after which the water level declined. The decline was interrupted three times and low peaks occurred on June 10, June 26 and July 4 after significant rainstorms on June 6 and 8, June 24 and July 2. The water level dropped after that and no ponding was visible from July 14 until August 2, although inflow continued. Heavy rain on August 3, 6 and 8 led to renewed ponding from August 3 until August 11. Inflow continued after that at least until September 12, 1978, when the camera was removed.

Figure 25. Example of time-lapse photography, depression No. 110, September 13, 1977.

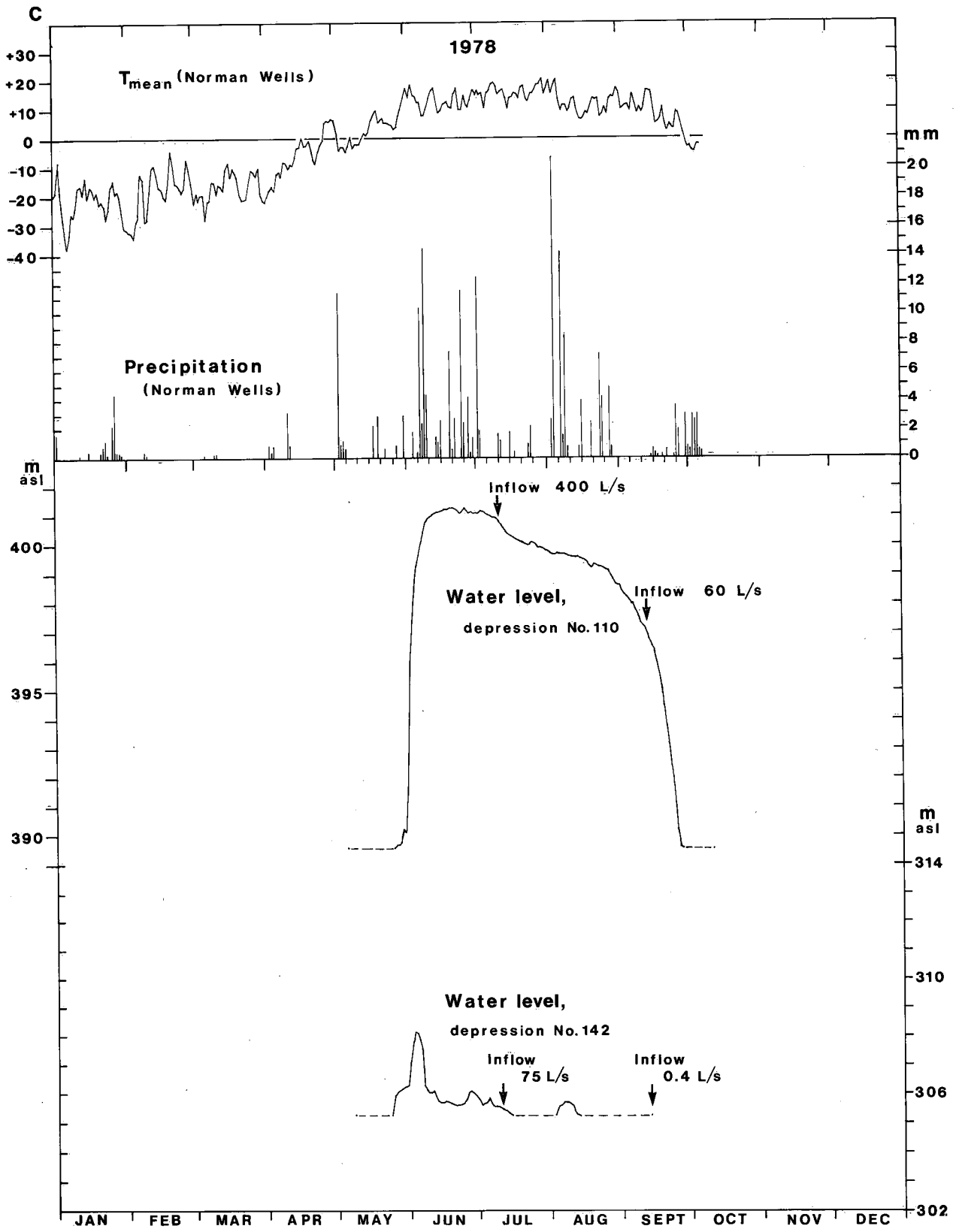

Figure 26. Daily mean temperatures and daily precipitation at Norman Wells Airport for 1978 (data from Atmospheric Environment Service), and water levels in the southeastern portion of depression No. 110 and in depression No. 142 (from time-lapse photography).

Ponding started in the instrumented swallow hole in depression No. 110 on May 26; a rapid rise after May 30, which slowed down gradually, led to the maximum water level for 1978 on June 20; two more peaks related to rain mentioned earlier are shown in Figure 26 on June 25 and on July 2 and 3. The gradual decline in water level after July 3 was interrupted three more times (July 24, August 4 and 20). The flooding ended by September 27. Inflow to the swallow hole continued at least until October 5; by that time snow covered the inflow channel.

STREAMFLOW MEASUREMENTS, 1976–1978

Streamflow measurements for this study were made by C.W. Peters of Water Survey of Canada, Norman Wells. The dates on which the measurements were made (Table 2) were to a large degree dictated by time constraints related to his normal duties. Weather conditions and the extent of flooding made measurements on these dates impossible at some places. Standard current-meter stream gauging methods were used; the accuracy of the results for individual streams will to some degree depend on the characteristics of the streambed and on the prevailing runoff conditions, but it can be expected to be better than ±10%.

The locations at which the streamflow measurements were made are listed in four subdivisions in Table 2. Each subdivision deals with a different portion of the hydrologic system in the area. The first subdivision comprises streams flowing into the southeastern portion of depression No. 110 and the overflow from the southeastern to the central portion (identified by letters in Fig. 18); the second refers to "Disappearing River", flowing into sinkhole No. 86B (Figs. 10 and 11); and the third deals with the stream flowing into the southwestern portion of depression No. 142 (Figs. 14 and 15). The first three subdivisions are thus concerned with *recharge* entering the groundwater system. The last subdivision is concerned with *discharge* from the groundwater system along the upper reaches of the Hare Indian River.

The results of the streamflow measurements listed in Table 2 indicate that the combined instantaneous inflow into the southeastern portion of depression No. 110, sinkhole No. 86B and the southwest portion of depression No. 142 could exceed 3600 L/s. When inputs into other sinkholes in this part of the area are included, the *maximum* instantaneous input into the groundwater system could likely be as high as 5000 L/s.

The apparent sequential development of sinkholes, such as that quoted for the sinkholes in group No. 86, was interpreted earlier as an indication that subsurface drainage from the northeast and north flanks of the Mahony Lake dome is directed toward the valley of the Hare Indian River. Figure 8 shows the presence of a number of springs along the left-hand side of the upper valley of the Hare Indian River; at least three of these springs (Nos. 143, 144 and 145 in Fig. 8) each produced more than 100 L/s when measured. They are all perennial; during the winter dis-

Table 2. Streamflow Measurements (L/s), 1976–1978

Location	Date			
	76-06-18	77-07-04	78-07-10	78-09-12
Depression No. 110 (Fig. 18):				
Inflow at A	–	270	370	42
Inflow at A_1	–	–	–	10
Inflow at B	–	60	20	T
Inflow at C	–	T	T	T
Inflow at D	–	340	6	5
Inflow at E	–	230	6	5
Inflow at F	–	–	–	0.6
Measured total inflow	–	900*	400	60
Overflow at Q	80	140	440	0.0
Sinkhole No. 86B: inflow	720	–	1300*	115
Depression No. 142: inflow	–	1400*	75	0.4
Hare Indian lakes (Fig. 8):				
Outflow from lake No. 1	–	–	1900	1500
Outflow from lake No. 2	–	–	3000	1900
Groundwater input to lake No. 2	–	–	1100	400

*Combined instantaneous input to groundwater system at these points could exceed 3600 L/s.
T – Indicates trickle of water only.

charge from the smaller springs freezes and forms icings below their outlets, whereas discharge from the bigger springs does not freeze before it reaches one of the two long lakes in the valley (lake No. 1 and lake No. 2 in Fig. 8 and Table 2). Only small seeps were found along the right-hand side of the valley.

Tracer tests, designed to detect the actual connections between two individual major stream sinks (No. 86B and the prime sink in No. 142) and individual springs in the valley of the Hare Indian River, were inconclusive; both adverse weather conditions and logistic limitations made continuous observation of all the spring areas in the valley impossible. It was, however, confirmed that the inflows into the karst system through the two major stream sinks are discharged into the upper reach of the valley of the Hare Indian River.

Discharge from the upper lake in the valley (lake No. 1) to the lower lake (No. 2) maintains open water in their connecting channel throughout the winter. Outflow from lake No. 2 also maintains a reach of open water throughout the winter, but the water eventually freezes to form a major icing 2.3 km downstream. The icing area is 3.5 km long and about 350 m wide at its widest point. The maximum observed thickness of the icing was 1.9 m.

The water discharged from two springs located beyond the northeast end of lake No. 1 drains via lake No. 3 and an unnamed stream into Great Bear Lake; during the winter the outflow from lake No. 3 freezes and forms an icing 600 m downstream.

The maximum measured discharge from lake No. 2 was 3.0 m^3/s, somewhat less than the combined maximum measured inflows into the karst system, as could be expected because of storage and transmissivity effects. An approximate total annual volume discharged from lake No. 2 was calculated by assuming that (1) the discharge measurement of July 10, 1978, represents the maximum discharge rate and (2) the discharge rate will decrease to approximately 63% in each subsequent period of 61 days, as indicated by comparison of the July 10 and September 12 measurements. The resulting total annual discharge would be about 33 million cubic metres. About 6 million cubic metres of this could represent precipitation that fell in the valley, minus evapotranspiration; approximately 27 million cubic metres would represent discharge from the karst system.

The area supplying subsurface drainage to the upper valley of the Hare Indian River would cover about 650 km^2, if the karst-water divides coincided with the surface water divides. The actual subsurface drainage area may be either smaller or larger, depending on the degree to which the karst-water divides deviate from the surface water divides. Information on this point is lacking.

Dividing the approximate annual karst-water discharge of 27 million cubic metres by the assumed drainage area of 650 km^2 gives an approximate depth of water of 40 mm recharged to, and discharged from, the karst-water system annually. This represents about 15% of the precipitation for the period October 1, 1977, to September 30, 1978 (285 mm). Since there is no direct runoff leaving the area and the changes in surface storage are only minor, most of the remaining 85% of the precipitation, or about 245 mm, was presumably evaporated and transpired by vegetation.

The figures for annual recharge to the karst-water system (40 mm, or about 15% of the annual precipitation) may be surprising in view of the presence of widespread permafrost, but they also indicate the effectiveness of inflow into collapse sinkholes as a recharge mechanism in the study area.

CLIMATIC AND HYDROLOGIC SUMMARIES, 1973-1978

The observations that were discussed in detail in the foregoing sections are summarized in Table 3 to permit a comparison of the significant parameters influencing the hydrology of the groundwater system in the karst on the northeastern and northern flanks of the Mahony Lake dome.

From water-level observations, Brook (1977, p. 107) believed that depressions in the Nahanni North Karst "...flood more frequently from intense frontal and/or orographic summer rainstorms than from spring snowmelt which in most years may simply add to a body of groundwater depleted by continuous, if reduced, spring flow during the winter months."

The observations for depression No. 110 for the period 1973 to 1978 (No. 2 in Table 1) indicate that flooding occurred in this depression every year. The shapes of the water-level graphs (Figs. 22, 23 and 26) indicate that snowmelt contributed a significant proportion of the annual inflow into both depressions No. 110 and No. 142.

As indicated in Table 3, comparison of the water-level graphs and the temperature curves in Figures 22, 23 and 26 revealed that flooding in depression No. 110 started 16 or 17 days after the last day with a mean temperature below 0°C in 1976, 1977 and 1978. Based on this, probable dates for the start of flooding in 1973, 1974 and 1975 have been determined and are listed in Table 3.

Table 3. Climatic and Hydrologic Summaries, 1973–1978

	1973	1974	1975	1976	1977	1978
Last date with $T_{mean} < 0°C$	May 4	May 5	May 14	April 24	May 1	May 12
Total snowfall*	128.5	103.6	155.5	100.9	110.3	82.8
Snow on ground on April 15*	91.4	81.3	144.8	48.3	61.0	76.0
Monthly precipitation*						
May	17.3	14.2	12.4	52.1	17.6	23.6
June	15.5	41.4	14.5	12.5	26.1	69.6
July	32.0	91.6	27.2	25.9	49.5	22.6
August	68.6	105.6	41.1	28.2	1.9	72.8
September	16.0	36.3	42.8	27.7	9.5	13.5
Flooding, depression No. 110†						
Date started	Before June 10 (probably May 21)	Before July 11 (probably May 22)	Before June 9 (probably May 31)	May 10	May 18	May 29
Date ended	Between July 16 and September 8	After July 30	Between July 16 and August 20	August 9	August 31	September 26
Number of days	(57–110)	(>70)	(46–80)	91	105	120
Maximum level, metres above assumed datum	–	–	>401.90	400.85	401.65	401.27

*Precipitation and snow-on-ground data are in millimetres H_2O; snowfall covers period starting October 1 of preceding year. Temperature and precipitation data for Norman Wells Airport from Monthly Records, Atmospheric Environment Service, Environment Canada. Snow-on-ground data for snow course at Norman Wells Airport from Snow Cover Data, Atmospheric Environment Service, Environment Canada.

†Data on flooding from temperature data and LANDSAT imagery (1973, 1974, 1975), water-level recording (1976, 1977), and time-lapse photography (1977, 1978).

For each year in the period 1973–1978, the snowfall during the preceding winter and the water equivalent of the snow remaining on the ground on April 15 at Norman Wells are listed in Table 3. It appears that the *maximum level* reached by the water in depression No. 110 in any year is primarily determined by the amount of snow available during the snowmelt. The maximum level for 1976 reflects the addition of inflow derived from rain during the last week of May. The maximum water level for 1978 is lower than that for 1977, although more snow was available (on April 15) in 1978 than in 1977; it is likely that a significant portion of the available snow was lost by sublimation and slow melting before the daily mean temperature finally rose above 0°C on May 13 in 1978. The slow melting did contribute to inflow into the depression, but at a rate too slow to initiate flooding.

Figures 22, 23 and 26 further show that rainfall exceeding 10 mm in one day tends to be reflected by a slowdown or a reversal in the decline of the water level in depression No. 110. Comparison of precipitation data and water levels in depression No. 142 for 1977 and 1978 (Figs. 23 and 26) shows that rainfall of as little as 6 mm in one day did cause flooding there. Relatively low-intensity rainfall can, therefore, contribute recharge to the karst-water system.

The *duration of flooding* in depression No. 110 (and elsewhere in the area) is dependent on the amount and distribution of rainfall during the summer months. In 1976, when rainfall was less than 30 mm per month after May, the depression was drained by August 9; in 1977, when 49.5 mm of rain fell in July, the depression remained flooded until August 31; and in 1978, when 69.6 and 72.8 mm of rain fell in June and in August, respectively, the depression did not drain until September 26. Inflow usually continues until freeze-up.

As stated earlier, the water level during flooding in the southeastern portion of depression No. 110 does not represent the groundwater level in the depression as a whole. It should be regarded as a local perched water level. The decline portions of the water-level graphs in Figures 22, 23 and 26 tend to confirm this; they do not show the trend usually associated with the decline of groundwater levels in homogeneous isotropic material. Their shape is more representative of the water-level decline in a funnel-shaped container, with a bottom outlet limiting the rate at which the water can drain out.

This study has shown that only modest rainfall is required to initiate recharge to the karst-water system and that a relatively high proportion of the annual precipitation enters the system as recharge. Both observations indicate the effectiveness of the high-rate recharge points provided by the collapse karst in the study area, in spite of the presence of widespread permafrost.

Hydrochemistry

BACKGROUND

Data on the geochemistry of some of the natural waters in the study area have been published earlier. Brandon (1965) presented analyses for Vermilion Creek and Bosworth Creek (NTS 96E); Hughes *et al.* (1973) listed selected data for a number of springs in the Mackenzie River valley along the Norman Range. Van Everdingen (1974) gave additional data for some of these and presented analyses for springs along Vermilion Creek as well as for the creek water from various points in the creek. Michel (1977) presented data on both the chemical composition and the abundance of several environmental isotopes for waters from more than 20 springs and spring groups in the study area. Van Everdingen and Krouse (1977a) described the sulphur-isotope geochemistry of one of these spring groups near the Hanna River (No. 112 in Fig. 6) and van Everdingen (1978a) published chemical analyses and sulphur-isotope data for the springs at Bear Rock (No. 104 in Fig. 5). Additional data and an interpretation of the results of chemical and isotope analyses were presented by van Everdingen *et al.* (1978).

In the next section a comparison will be made between the chemical composition of recharge and discharge waters, with emphasis on the karst-water system northeast and north of the Mahony Lake dome. This will be followed by a discussion of the observed abundances of the environmental isotopes D, ^{18}O and tritium in samples of precipitation, recharge and discharge and the abundances of ^{34}S in samples of discharge and mineral precipitates from icings.

MAJOR-ION COMPOSITION

The results of chemical analyses for samples of recharge are listed in Table 4a and those for samples of discharge in Table 4b. Semilog plots of the major-ion compositions are presented in Figures 27 and 28.

The water recharged into the karst lake on the top of Bear Rock (No. 153 in Fig. 5, Table 4a and Fig. 27) acquires large amounts of Ca and SO_4 through dissolution of gypsum; minor amounts of Ca, Mg and HCO_3 through dissolution of dolomite; and some Na and Cl through dissolution of halite, before being discharged from the springs at the base of Bear Rock (No. 104 in Fig. 5, Table 4b and Fig. 27). Dolomite and some gypsum are present in the Bear Rock Formation exposed on Bear Rock, whereas gypsum and halite occur in the Saline River Formation near the base of the mountain.

Inflow to the sinkhole on Mount Richard (No. 79 in Fig. 6, Table 4a and Fig. 27) is in character similar to the water recharging the Bear Rock system. Water discharged by the spring on Vermilion Creek (No. 174 in Fig. 6, Table 4b and Fig. 27) is similar to water discharged by the Bear Rock Springs, but it contains a somewhat higher proportion of Na and Cl, presumably derived from salt in the Saline River Formation. The composition of the water from the "lake" in the sinkhole west of Vermilion Creek (No. 175 in Fig. 6, Table 4b and Fig. 27) confirms that the "lake" is part of the subpermafrost groundwater flow system that discharges into Vermilion Creek.

The examples above were taken from areas where the Bear Rock Formation is exposed or present in the shallow subsurface and where the Saline River Formation, according to Figure 2, contains a significant thickness of salt. The rest of the analyses are from the area of the Mahony Lake dome, where the Bear Rock Formation is absent.

Recharge to the karst-water system in the area of the Mahony Lake dome was sampled at sinkhole No. 49 (Fig. 6); from three streams flowing into the southeastern portion of depression No. 110 and from the "Disappearing River" flowing into sinkhole No. 86B (Fig. 7); and at the primary sink in depression No. 142 (Fig. 8). The concentrations of dissolved solids were found to be low, with samples collected in the fall generally exhibiting the higher values (Table 4a and Figs. 28A to C). Most of the differences in dissolved solids concentrations appear to be due to higher concentrations of Ca and HCO_3 in samples collected in the fall as compared with those collected during or shortly after the snowmelt. As noted on Table 4a, it is likely that the relatively high values indicated for Fe (0.20–0.29 mg/L) result from interference by the brown colour of the water during colorimetric determinations.

Discharge from the karst-water system was sampled in the valley of the Hare Indian River (Fig. 8, Table 4b and Figs. 28C and D). The concentrations of dissolved solids

Table 4a. Chemical Analyses of Recharge Samples

Source	Sample No.	Date	Temperature °C	pH units	Constituents (mg/L) Ca	Mg	Na	K	HCO_3	SO_4	Cl	F	SiO_2	TDS	Fe*
Lake No. 153	76-153	76-08-30	8.5	7.7	33.2	8.0	0.3	0.4	124.3	5.5	0.5	0.07	2.0	174.5	0.18
Sinkhole No. 79	75-79	75-06-28	6.8	7.7	61.0	14.8	0.8	0.3	199.9	40.0	0.9	0.21	1.9	320.0	<0.04
Sinkhole at lake No. 49	RLH-49F	73-09-10	–	7.3	12.0	5.4	0.3	0.4	56.0	5.0	0.2	<0.05	1.0	80.4	<0.04
Depression No. 110															
Inflow at F	75-110	75-09-10	9.8	6.9	14.0	8.4	0.2	0.1	64.4	4.3	2.0	<0.05	6.1	100.5	0.91
Inflow at G	76-110	76-05-10	3.4	6.4	4.3	2.5	<0.1	0.9	9.4	6.7	2.2	–	1.5	27.7	0.21
Inflow at H	76-154	76-09-05	7.6	7.8	9.5	5.2	0.3	0.1	44.6	5.0	0.6	<0.05	4.2	69.2	0.22
Sinkhole No. 86B	75-86	75-06-30	20.4	6.6	4.2	2.9	1.0	0.2	14.3	3.6	0.8	0.05	0.7	28.0	0.29
	75-109	75-09-10	4.3	6.6	5.7	2.9	0.1	<0.1	21.8	2.6	1.2	<0.05	0.6	40.7	0.20
Depression No. 142															
Inflow from SW	76-142	76-09-05	4.2	7.7	33.9	14.3	0.6	0.3	135.3	21.0	0.7	<0.05	3.8	210.3	0.44

*High values for Fe may reflect interference by the brown colour of the water from muskeg areas.
TDS – Total dissolved solids.

Table 4b. Chemical Analyses of Samples from Springs and Spring-Fed Lakes

Source	Sample No.	Date	Temperature °C	pH units	Constituents (mg/L) Ca	Mg	Na	K	HCO_3	SO_4	Cl	F	SiO_2	TDS	Fe*
Bear Rock Spring No. 104	75-104	75-09-09	2.8	7.5	528	34.2	3.0	1.5	295	1090	2.2	0.42	4.0	1959	0.16
Sinkhole No. 175	77-175	77-09-27	5.2	7.3	300	80.0	24.0	2.8	201	905	5.3	–	4.0	1526	0.2
Spring No. 174	77-174	77-09-27	4.4	7.4	230	64.0	12.0	2.4	280	583	9.4	–	9.0	1196	0.3
"Grizzly" springs															
East spring, No. 145	76-145	76-06-21	3.3	7.0	67.0	21.6	1.4	1.0	126	136	1.5	–	–	355	0.74
Centre spring, No. 144	76-144	76-06-21	3.4	7.0	53.0	17.0	1.0	0.8	104	98	1.3	–	–	275	0.28
West spring, No. 143	76-143	76-06-21	1.5	7.0	83.5	23.2	1.4	1.0	128	176	1.7	–	–	415	0.25
Hare Indian Lakes															
Lake No. 1	RLH-51	73-09-10	–	7.9	66.6	27.5	1.8	1.1	134	167	1.3	0.24	3.7	413	<0.04
Lake No. 1, outflow	78-146	78-09-12	10.2	8.3	65.5	24.4	2.6	1.0	138	140	1.3	0.26	5.0	378	<0.04
Lake No. 2, outflow	78-147	78-09-12	10.3	8.3	69.0	25.7	3.0	1.1	146	150	1.7	0.32	5.7	403	<0.04
Spring No. 149	78-149	78-09-17	8.0	8.0	81.0	29.6	3.2	1.3	162	180	2.8	0.48	9.1	470	0.35
Spring No. 150	78-150	78-09-17	3.0	7.8	41.9	23.5	0.7	0.5	206	14.0	0.6	0.06	6.9	301	0.04

*Fe is precipitated soon after discharge and therefore does not show up in lake samples RLH-51, 78-146 and 78-147.

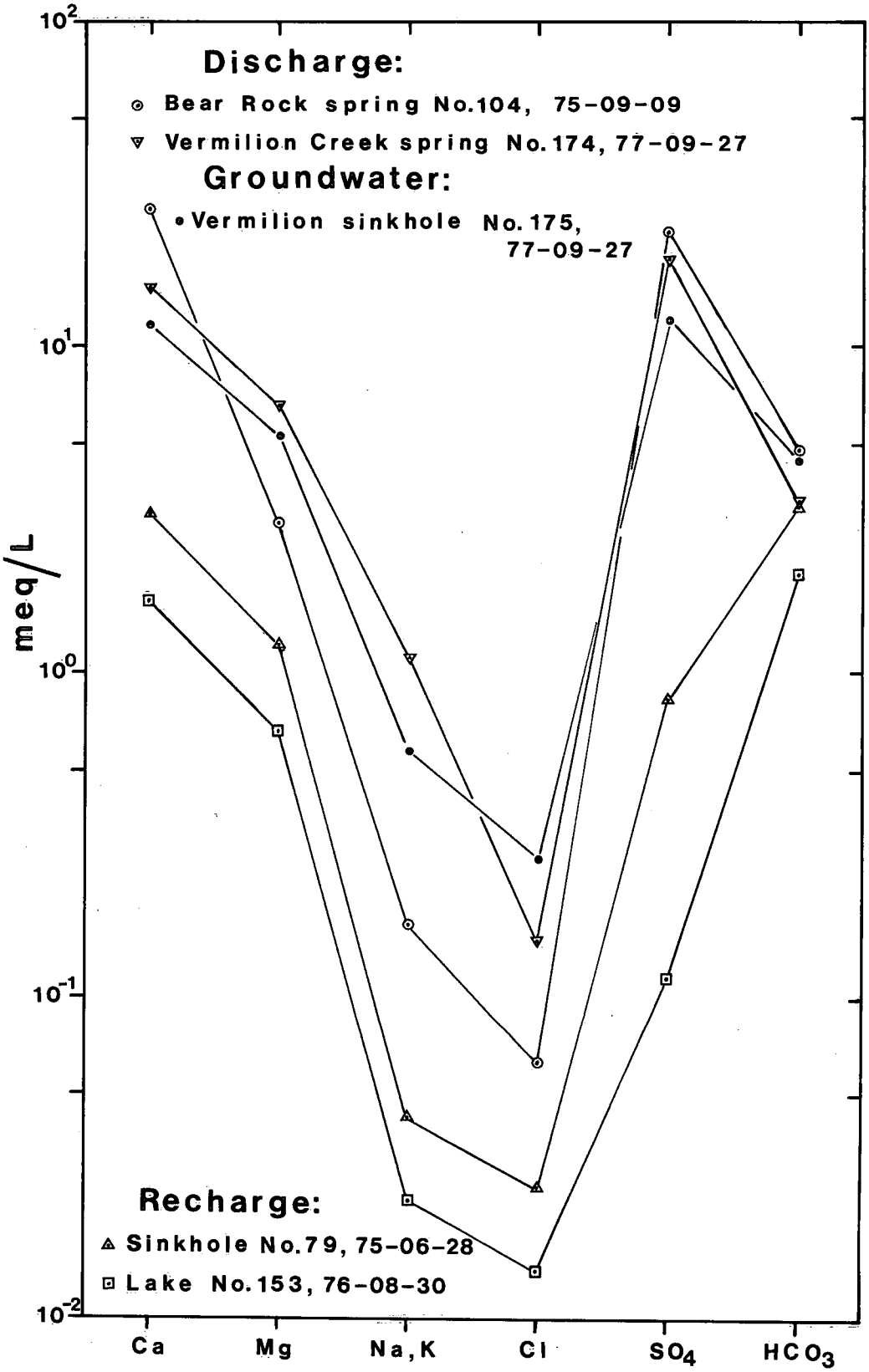

Figure 27. Semilog plots showing major-ion analyses for samples of karst recharge and discharge, from the areas of Bear Rock (NTS 96C/13), Vermilion Creek (NTS 96E) and Mount Richard (NTS 96E).

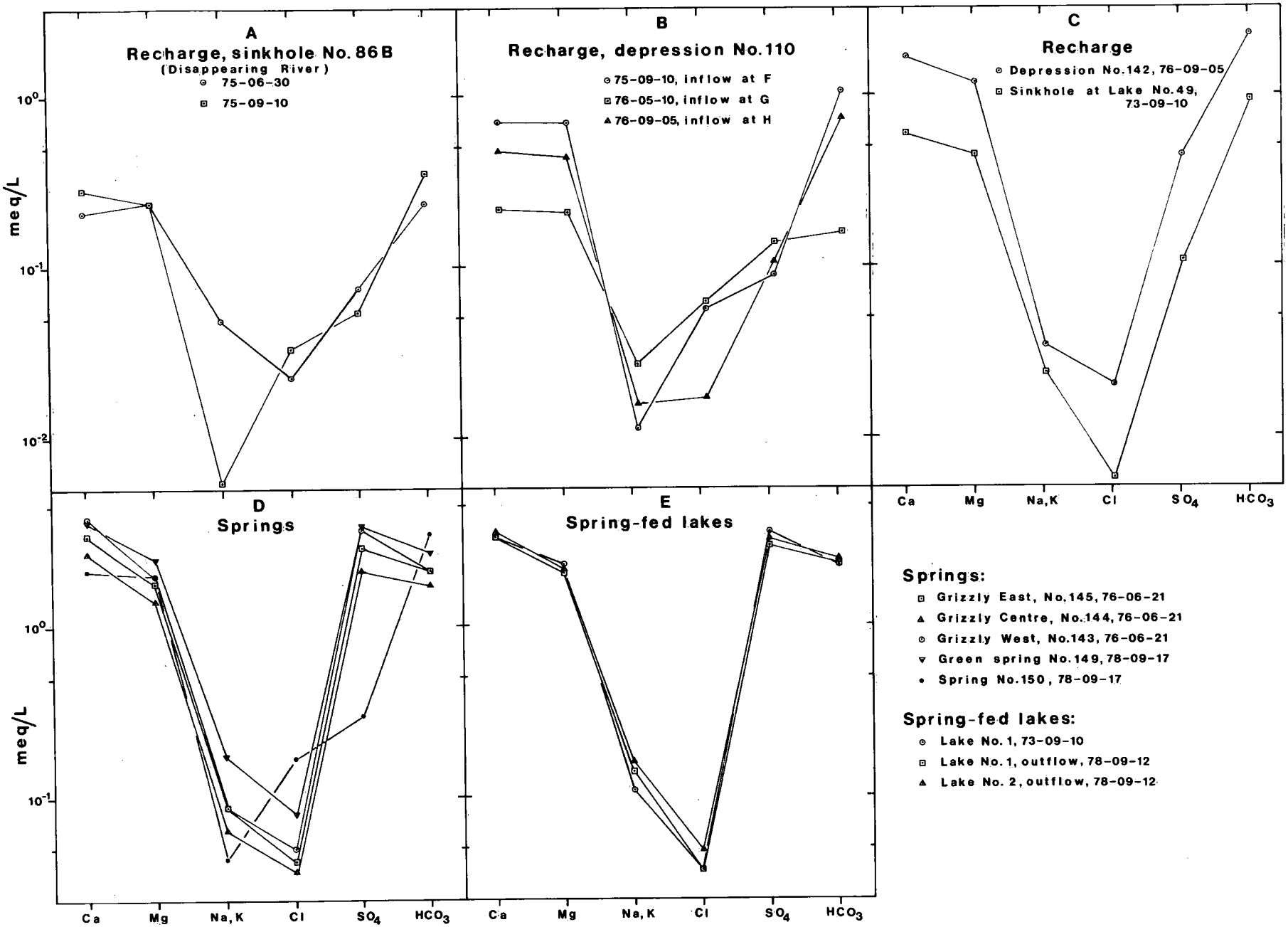

Figure 28. Semilog plots showing major-ion analyses for samples of karst recharge and discharge from the Mahony Lake-Hare Indian River area (NTS 96F and 96K). *A* – Recharge entering sinkhole No. 86B; *B* – Recharge entering depression No. 110; *C* – Recharge entering depression No. 142 and sinkhole No. 49; *D* – Discharge from "Grizzly" springs, a spring in lake No. 2 and a spring just below lake No. 2; *E* – Lake No. 1 near "Grizzly" springs and outflows from lakes Nos. 1 and 2.

are all higher than in the recharge waters. Most of the relative increases are caused by significant increases in Ca and SO_4, more modest increases in Mg and HCO_3 and minor increases in Na, K and F. No particular trend is indicated by the concentrations of Cl and SiO_2. The Fe content of the spring waters is apparently precipitated soon after discharge and therefore does not show up in the lake and lake-outflow samples.

The differences in chemical composition between the recharge and the discharge are probably caused by dissolution of dolomite from brecciated zones in the Mount Kindle and Franklin Mountain formations and by dissolution of gypsum from the upper part of the Saline River Formation. Fluorite observed in vugs in the Mount Kindle Formation could be the source of the dissolved fluoride in the discharge. The absence of significant concentrations of Na and Cl is presumed to indicate that the discharge from the springs in the valley of the Hare Indian River has not penetrated deeply enough to have come into contact with the salt beds in the lower portion of the Saline River Formation. The possibility does of course exist that groundwater moving through deeper parts of the flow system is discharged elsewhere, for example, through the bottom of Great Bear Lake.

DEUTERIUM AND OXYGEN-18 ABUNDANCES

The relative abundances of the stable, heavy hydrogen and oxygen isotopes (deuterium and ^{18}O) in samples of precipitation in the study area and in samples of the recharge and discharge of the karst-water system are listed in Tables 5a to 5c. Five of the ^{18}O values were presented earlier by Michel (1977). The isotope abundances are expressed as

$$\delta D(‰) = \frac{(D/H)_{sample} - (D/H)_{SMOW}}{(D/H)_{SMOW}} \times 1000$$

and

$$\delta\ ^{18}O(‰) = \frac{(^{18}O/^{16}O)_{sample} - (^{18}O/^{16}O)_{SMOW}}{(^{18}O/^{16}O)_{SMOW}} \times 1000$$

where SMOW indicates concentration ratios in "standard mean ocean water."

Craig (1961) has demonstrated that a linear relationship exists between the abundances of the two isotopes in precipitation, represented by the equation

$$\delta D = A\,\delta\ ^{18}O + B$$

where A represents the slope of the straight line and B, its intercept with the δD axis. Dansgaard (1964) found that there is a marked temperature-dependent seasonal variation in the δD and $\delta\ ^{18}O$ values at any given locality; during the winter months precipitation is relatively depleted with respect to the two heavy isotopes (possibly as much as 30‰ for $\delta\ ^{18}O$). A similar tendency for depletion is shown with increases in altitude ($\delta\ ^{18}O$ decreasing about 3‰ per 1000-m increase in elevation). Increases in δD and $\delta\ ^{18}O$ usually associated with decreasing latitude can be expected to be cancelled out by an opposing isotope effect associated with increasing continentality, as most storms track through the study area in a southerly to southeasterly direction.

Table 5a. $\delta\ ^{18}O$, δD and Tritium Levels in Precipitation Samples

Source	Sample No.	Date	$\delta\ ^{18}O$ (‰ SMOW)	δD (‰ SMOW)	T (tritium units)
Norman Wells Airport					
Rain	77-170	77-09-22	-24.5*	-186.5*	–
Snow	77-171	77-09-23	-20.3	-155.6	99 ± 10
Snow	77-172	77-09-23	-20.2	-157.7	100 ± 10
Snow	78-151	78-10-01	-20.0	–	–
Snow	78-152	78-10-07	-24.2	-190.4	69 ± 8
Snow	78-153	78-10-07	-22.8	-180.5	41 ± 12
Snow	78-154	78-10-10	-31.5	-244.5	27 ± 12
Snow	78-155	78-10-10	-31.9	-250.0	19 ± 8
Depression No. 110					
Snow	78-156	78-10-10	-23.8	-182.3	51 ± 12

*Determinations by Physics Department, University of Calgary; all others by Department of Earth Sciences, University of Waterloo.

Table 5b. $\delta^{18}O$, δD and Tritium Levels in Recharge Samples

Source	Sample No.	Date	$\delta^{18}O$ (‰ SMOW)	δD (‰ SMOW)	T (tritium units)
Lake No. 153	76-153	76-08-30	-19.3	-131.1*	210 ± 9
Sinkhole at lake No. 49	77-173	77-09-25	-14.7†	-133.7†	–
Sinkhole at lake No. 140	76-140	76-06-21	-21.1	-130.2*	–
Depression No. 110:					
Inflow at F	75-87	75-09-10	-21.0	-131.0*	219 ± 28
Inflow at G	76-110/1	76-05-09	-27.1	-125.1*	–
Pond	76-110/2	76-06-18	-19.1	-131.4*	–
Pond	76-110/3	76-08-28	-21.0	-130.5*	170 ± 8
Inflow at B	76-110/4	76-09-05	-20.9	–	–
Inflow at A	78-110	78-09-12	-16.4	-144.0	104 ± 8
Inflow at F	78-111	78-09-12	-20.8	-158.0	111 ± 8
Inflow at B	78-112	78-09-16	-17.1	-149.5	98 ± 8
Inflow at G	78-113	78-09-16	-20.9	-160.0	120 ± 8
Inflow at H	76-154	76-09-05	-17.4	-134.1	131 ± 10
Sinkhole No. 86B	75-86	75-06-30	-21.1	-130.2*	166 ± 20
	75-109	75-09-10	-18.2	-132.4*	169 ± 18
	77-109/1	77-08-07	-18.8†	-158.9†	–
	77-109/2	77-09-25	-17.9†	-150.8†	–
	78-109	78-09-12	-18.2	-153.0	95 ± 8
Depression No. 142	76-142	76-09-05	-20.6	-130.7*	109 ± 9
	77-142/1	77-06-23	–	-168.3†	–
	77-142/2	77-09-24	-21.8†	-159.5†	–
	78-142	78-09-12	-20.6	-159.0	108 ± 8

*Determined late in 1978; δD values are unreliable because of evaporative losses from polyethylene bottles between dates of sampling and analysis.
†Determinations by Physics Department, University of Calgary; all others by Department of Earth Sciences, University of Waterloo.

Table 5c. $\delta^{18}O$, δD, $\delta^{34}S$ and Tritium Levels in Samples from Springs and Spring-Fed Lakes

Source	Sample No.	Date	$\delta^{18}O$ (‰ SMOW)	δD (‰ SMOW)	$\delta^{34}S$* (‰)	T (tritium units)
Bear Rock Spring No. 104	75-104	75-09-09	-23.6	-179.2	+29.8	217 ± 53
Sinkhole No. 175	77-175	77-09-27	-25.0*	-174.9*	+10.1	68 ± 9
Spring No. 174	77-174	77-09-27	-23.6*	-179.6*	+13.6	78 ± 9
"Grizzly" springs						
East spring, No. 145	77-145	77-09-25	-24.8*	-185.9*	+8.9, +9.2	144 ± 10
Centre spring, No. 144	76-144	76-06-21	-22.6	-129.7†	+1.0, +1.3	114 ± 8
West spring, No. 143	76-143	76-06-21	-22.5	-129.6†	–	114 ± 9
Hare Indian Lakes						
Lake No. 1, outflow	78-146	78-09-12	-22.4	-179.6	+7.5, +7.8	64 ± 8
Lake No. 2, outflow	78-147	78-09-12	-22.6	-182.0	+10.4, +8.7	67 ± 8
Spring No. 149	78-149	78-09-17	-22.9	-179.0	–	62 ± 8
Spring No. 150	78-150	78-09-17	-22.7	-176.0	–	121 ± 8
Precipitate from icing below lake No. 2	78-148	78-09-16	–	–	+9.0, +9.6, +10.1	–

*Determinations by Physics Department, University of Calgary; all others by Department of Earth Sciences, University of Waterloo.
†Determined late in 1978; δD values are unreliable because of evaporative losses from polyethylene bottles between dates of sampling and analysis.

Precipitation that has entered the groundwater system is likely to retain its isotopic abundances unless the temperature rises above 45°C or 50°C during deep circulation of the water; in the latter case, exchanges between the water and a number of minerals in the aquifer rocks may change the isotope values in the water. In many cases, however, the δD and $\delta\ ^{18}$O can be useful in identifying the source of a particular groundwater.

The δD values for some of the samples in Tables 5b and 5c have to be considered unreliable because of evaporative losses from the polyethylene sample containers during the delay between sampling and analysis. This problem was overcome when glass containers were used later in the study.

The δD and $\delta\ ^{18}$O values for precipitation samples collected in the study area during 1977 and 1978 are listed in Table 5a and shown in graphic form in Figure 29; the δD and $\delta\ ^{18}$O values for samples of recharge and discharge are listed in Table 5b and Table 5c, respectively, and shown in Figure 30, with the exception of those marked unreliable. For comparison purposes, a solid line is drawn in Figures 29 and 30 which represents the best fit to δD and $\delta\ ^{18}$O values for precipitation between 1961 and 1967 at Fort Smith, the station closest to the study area for which such data are available.

The δD and $\delta\ ^{18}$O values for the precipitation samples from the study area (Fig. 29) show a good fit to the Fort Smith line. Also, values for samples collected at different times during a single snowstorm are in reasonable mutual agreement. One should, however, note that the values for samples collected at the same place during different snowstorms exhibit a range of variation that is large enough to hide any variations in isotope values resulting from altitude and/or latitude differences between sampling sites in the study area.

The points representing recharge to the karst-water system derived from muskeg and forest areas (Fig. 30) fall close to the Fort Smith line. On the other hand, most of

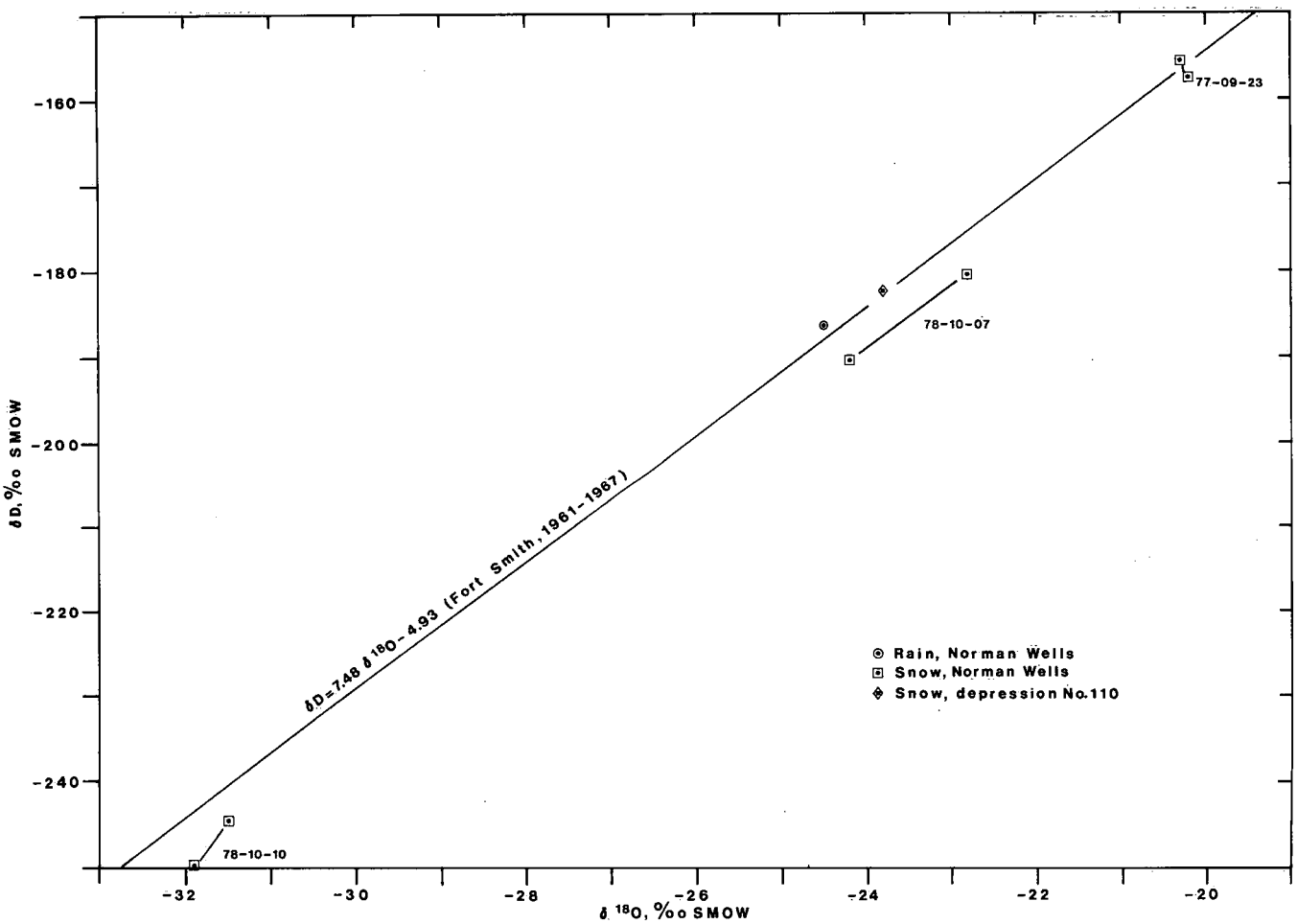

Figure 29. Plot of δD vs. $\delta\ ^{18}$O for samples of precipitation. Line representing precipitation at Fort Smith is based on data for the period 1961-1967 (IAEA Environmental Isotope Data Series).

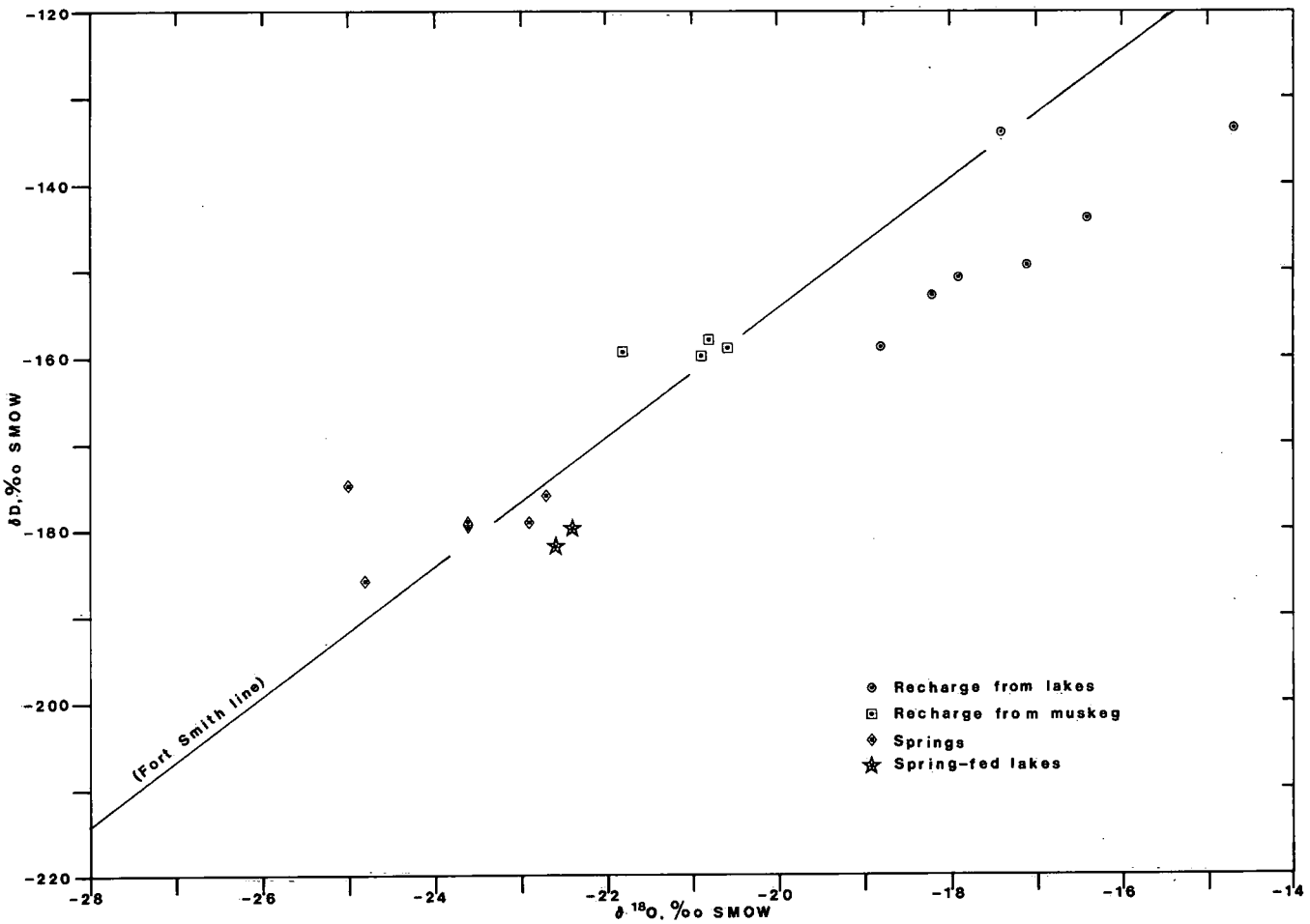

Figure 30. Plot of δD vs. δ ^{18}O for samples of karst recharge and discharge.

the points representing recharge derived from ponds and lakes show relative enrichment with respect to ^{18}O, which is interpreted as the result of isotope fractionation during evaporation. Samples of recharge were collected between mid-June and late September with one exception (Table 5b, inflow at G, May 9, 1976). They show δ ^{18}O values ranging from -16.4 to -21.8‰. The sample collected on May 9, 1976, representing snowmelt, had a δ ^{18}O value of -27.1‰; unfortunately, a reliable δD value is not available for this sample.

The δD and δ ^{18}O values for samples of discharge (Table 5c, Fig. 30) are generally more negative than those for samples of recharge; the δ ^{18}O values range from -22.4 to -25.0‰. The relatively negative δD and δ ^{18}O values for discharge from the karst system have been interpreted by van Everdingen *et al.* (1978) as an indication that the melting of snow (normally more strongly depleted with respect to the heavier isotopes than rain) provides a large proportion of the recharge. This conclusion is supported by the absence in the discharge of selective enrichment with respect to ^{18}O. Snowmelt would not be subjected to significant isotope fractionation by evaporation, because evaporation rates are generally limited by low temperatures and high relative humidity during the snowmelt period.

The δD and δ ^{18}O values in the discharge samples undoubtedly reflect the effects of mixing, in various proportions, of recharge waters with differing δD and δ ^{18}O values. The available data do not permit more detailed interpretation.

TRITIUM LEVELS

Tritium, a radioactive hydrogen isotope with a half-life of 12.35 yr, is continuously produced as a result of cosmic radiation. Concentrations of tritium in precipitation, resulting from this natural process, range from 5 to 20 T.U. (tritium units), depending on the locality and season (1 T.U. indicates $^{3}H/^{1}H = 10^{-18}$).

Man-made tritium from the testing of nuclear devices started entering the stratosphere in 1952; test series in 1954, 1958 and 1962 produced large quantities of tritium. Maximum tritium levels in atmospheric precipitation (3000+ T.U.) occurred in 1963. Brown (1970) found indications that the artificially enriched stratospheric tritium reservoir is depleting with a half-time of 1.2 yr. Because of its radioactive decay, tritium provides a potential dating tool for groundwater that it similar to ^{14}C.

Samples of precipitation, recharge and discharge were analyzed for tritium during this study to help distinguish short, fast flow systems from longer and slower ones. It was further intended to use the tritium content in water from those short, fast flow systems in which little or no mixing between old and young water occurs, to determine the probable year in which the water fell as precipitation. This could then provide an approximate measure of velocity in the flow system.

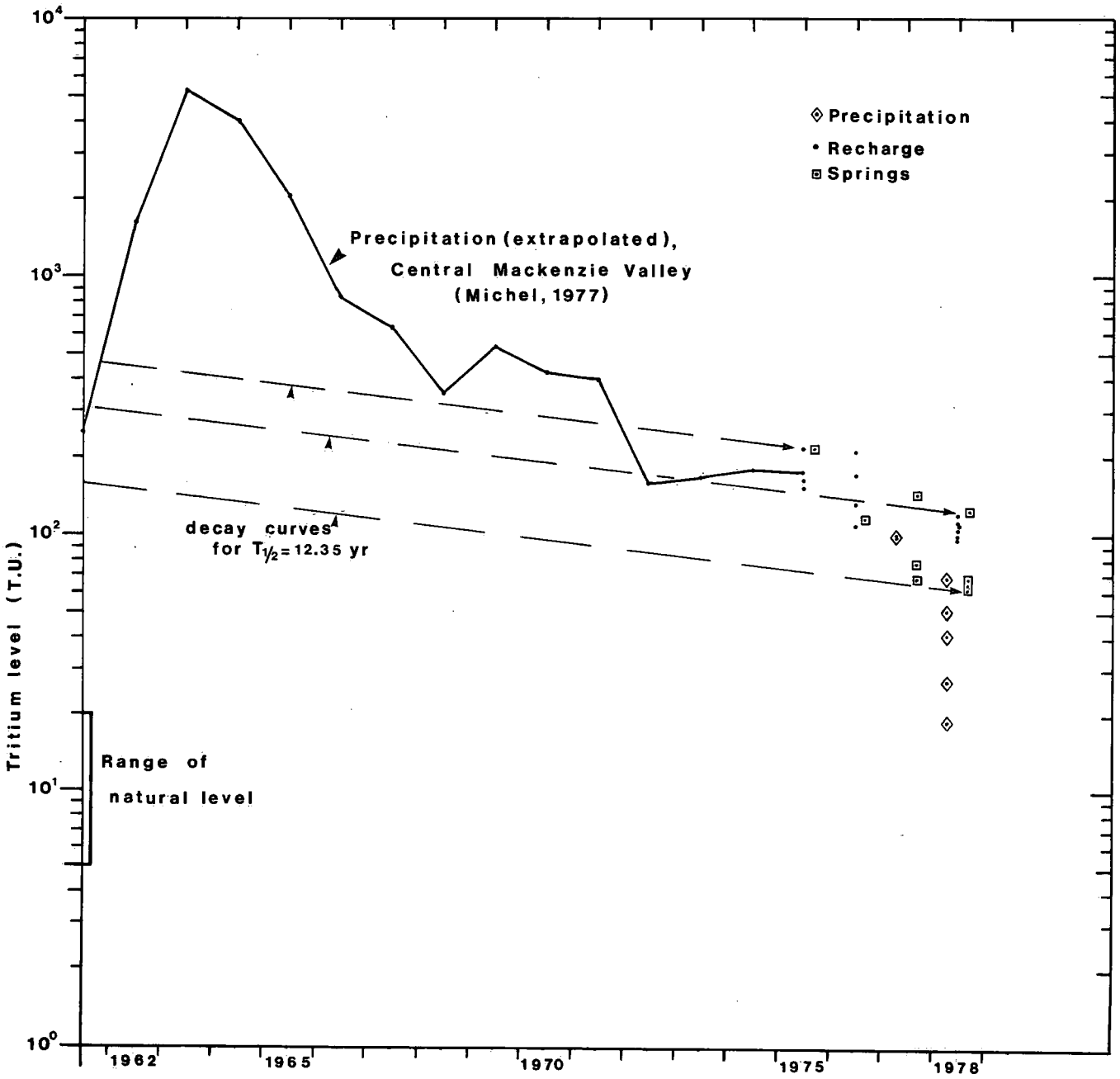

Figure 31. Tritium levels in samples of precipitation, karst recharge and karst discharge (collected between 1975 and 1978), compared with extrapolated tritium levels for precipitation in the central Mackenzie Valley for the period 1961 to 1975 (from Michel, 1977, Fig. 13).

Tritium levels in a few samples of precipitation from the study area are listed in Table 5a; those for samples of recharge, in Table 5b; and those for samples of discharge, in Table 5c. Four of the tritium values in Table 5b and two of those in Table 5c have been published earlier by Michel (1977); three additional values were published by van Everdingen *et al.* (1978).

Figure 31 presents the tritium data in graphic form. In addition, it shows a curve for extrapolated tritium levels for precipitation in the central Mackenzie Valley for the period 1961 to 1975 (after Michel, 1977, Fig. 13). The broken lines in Figure 31 indicate tritium decay curves, the slope of which represents the half-life equal to 12.35 yr. The range of natural tritium levels in precipitation is also indicated.

Tritium levels determined on *precipitation* samples show a relatively wide range, from 19 to 100 T.U. This wide range, with a maximum more than five times as large as the minimum, might be the result of isotope fractionation by the same processes that influence the D and ^{18}O abundances in precipitation. Plots of δT vs. δD and δT vs. $\delta\ ^{18}O$, using average values for the snowstorms on September 23, 1977, and on October 7 and 10, 1978 (Fig. 32), tend to support this suggestion. The relationships between δT and δD and between δT and $\delta\ ^{18}O$, however, are not linear like the relationship between δD and $\delta\ ^{18}O$, but semilogarithmic, because the natural tritium level (5–20 T.U.; assumed average 12.5 T.U.) imposes a lower limit on actual tritium levels.

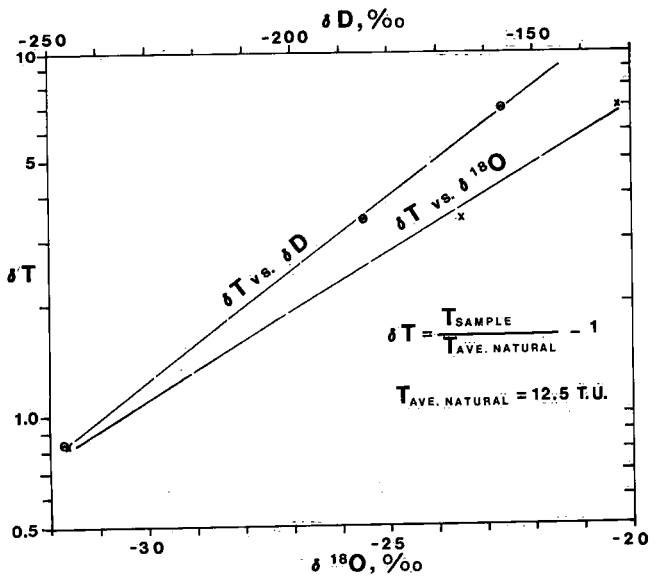

Figure 32. Plot of δT vs. δD and $\delta\ ^{18}O$ for three snowstorms at Norman Wells; values used are averages of values listed for each storm in Table 5a.

Tritium levels found in *recharge* to the karst-water systems range from 95 to 219 T.U., two to five times as high as those in local precipitation. This might indicate that, as a result of long-term storage in muskeg, ponds and lakes, the recharge at any given time is derived from precipitation that fell a number of years earlier and therefore possessed a more elevated level of man-made tritium. It is also possible that the higher tritium levels in the recharge are the result of isotope fractionation by evaporation during the summer months, similar to the enrichment observed for ^{18}O. Fractionation during evaporation could significantly affect the apparent tritium age of a water; if the fractionation efficiency approached 100%, evaporation of half the water could double the tritium content (equivalent to decreasing the apparent tritium age by 12.35 yr) within one summer.

Tritium levels in the recharge show a reduced scatter as compared with the levels in precipitation. This can be assumed to be the result of mixing.

The tritium levels in *discharge* from the karst-water systems, ranging from 68 to 217 T.U., fall within the combined ranges for precipitation and recharge waters. The tritium levels in the outflow from lake No. 1, in the outflow from lake No. 2 and in the water from spring No. 149 in lake No. 2 probably reflect mixing of spring water with precipitation that fell directly onto the two lakes.

It appears from the information contained in Figure 31 that the water discharged from the springs in the period 1975–1978 may have been derived from precipitation that has fallen at some time *after* 1971 or shortly *before* 1962. It is also possible that the spring waters represent a mixture of recent water with considerably older water (with negligible tritium levels) derived from a longer, deeper or slower flow system. In this case the tritium values in Figure 31 would be the result of dilution of the original recent components in these waters which would have possessed tritium levels higher than those now found in the samples. The recent components could then only be derived from precipitation that fell in the years between 1961 and 1972.

However, a comparison of the tritium levels for the springs outside the lakes in the valley of the Hare Indian River (Nos. 143, 144, 145, 150; average 123 T.U.) with those for recharge into the depressions Nos. 110 and 142 and into sinkhole No. 86B (average 125 T.U.) suggests that residence times in the karst-water system on the north and northeast flanks of the Mahony Lake dome are very short.

SULPHUR-34 ABUNDANCES

It is apparent from the Paleozoic stratigraphy and lithology that two major sources are available for the dis-

solved sulphates found in spring waters in the study area. One is the gypsum-bearing sequence of the Lower Devonian Bear Rock Formation, and the other is the gypsum-bearing sequence in the upper portion of the Upper Cambrian Saline River Formation.

Studies of sulphur-isotope abundances in evaporite sulphates by Holser and Kaplan (1966) indicated that Lower Devonian sulphates can be expected to have significantly lower ^{34}S abundances than Upper Cambrian sulphates. This was confirmed by sulphur-isotope analyses for samples from the Lower Devonian Bear Rock Formation and from the Upper Cambrian Saline River Formation in the study area (van Everdingen and Krouse, 1977b).

Results of sulphur-isotope analyses of sulphates in water from a number of springs in the area have been interpreted in terms of the probable source of the dissolved sulphates by van Everdingen and Krouse (1977a, for spring group No. 112, Fig. 6); van Everdingen (1978a, for springs at Bear Rock, No. 104, Fig. 5); and van Everdingen *et al.* (1978). All of these concerned springs that produce water with high dissolved solids concentrations (between 1250 and 6950 mg/L) and significant sulphate content. Most of these are located along the Mackenzie River valley. Examples presented in Tables 4b and 5c are the Bear Rock spring No. 104, which derives its sulphate from the Saline River Formation, and the Vermilion Creek spring No. 174, which derives its sulphate from the Bear Rock Formation. The rest of the data in Tables 4b and 5c are for springs in the valley of the Hare Indian River that discharge from the karst-water system of the Mahony Lake dome. Sulphur-isotope abundances have not been determined for recharge to this karst-water system, because sulphate concentrations in the recharge waters (Table 4a) are too low to permit reliable results to be obtained from water samples of reasonable size.

The sulphur-isotope values listed in Table 5c are relative sulphur-isotope abundances expressed as per mil deviations from the usual standard (Cañon Diablo meteorite troilite):

$$\delta\,^{34}S(‰) = \frac{(^{34}S/^{32}S)_{sample} - (^{34}S/^{32}S)_{standard}}{(^{34}S/^{32}S)_{standard}} \times 1000$$

Most of the $\delta\,^{34}S$ values for the waters discharging in the valley of the Hare Indian River (springs Nos. 143, 144, 145, 149 and 150; outflow from lakes Nos. 1 and 2, Fig. 8) are lower than +10‰, below the range for Bear Rock sulphates (+10 to +23.5‰) and much below the range for Saline River sulphates (+23.5 to +41‰) indicated by van Everdingen and Krouse (1977b). The Saline River Formation is the only known sulphate source in the area.

As the concentrations of dissolved sulphate in the discharge are relatively low (Table 4b), the sulphate samples on which the isotope analyses were done were small. A check on the validity of the $\delta\,^{34}S$ values was possible, however, because large quantities of $CaCO_3$ and $CaSO_4 \cdot 2H_2O$ are precipitated each winter during freezing of the discharge in the icing area downstream from lake No. 2. The $\delta\,^{34}S$ values for three large samples of this mineral precipitate, also listed in Table 5c, confirm the low values found for the discharge waters.

One explanation which can be advanced for the low $\delta\,^{34}S$ values is the possibility that the sulphates dissolved in the water are derived from evaporite $CaSO_4$ that was precipitated at a late stage when the seawater or brine reservoir had been severely depleted with respect to the heavier ^{34}S isotope as a result of earlier precipitation of sulphate. This would require isotope fractionation during precipitation, whereby the heavier isotope is preferentially incorporated in the solid phase. Variations in $\delta\,^{34}S$ in Pennsylvanian sulphate evaporites from the Canadian Arctic Archipelago have been interpreted by Davies and Krouse (1975) as being the effect of such fractionation. A less likely possibility is that a portion of the sulphur in the dissolved sulphate has gone through a complete reduction-oxidation cycle, in which bacterial reduction can be expected to produce sulphides with low or negative $\delta\,^{34}S$ values. Oxidation of these sulphides would produce sulphates with similarly low or negative $\delta\,^{34}S$ values.

Potential Geotechnical and Environmental Hazards in the Study Area

FOUNDATION HAZARDS

The occurrence of permafrost in the study area presents a number of what may be called geotechnical foundation hazards. These have been discussed in detail for parts of the area by Hughes *et al.* (1973), who indicated that the most common hazard is presented by ice-rich (and therefore potentially thaw-sensitive) fine-grained sediments in which thermokarst depressions, active-layer detachment slides or even major slumps can develop as a result of degradation of permafrost.

A water-related hazard in permafrost areas results from the commonly poorly integrated and sluggish surface drainage, which can lead to significant concentration of drainage along linear structures, with consequent hydraulic and thermal erosion. This and other water-related geotechnical hazards that can be encountered in the northern environment were discussed by van Everdingen (1979), with particular reference to pipelines.

Special geotechnical hazards will be encountered by potential engineering developments in the study area as a result of the presence of karst and especially because of the collapse nature of the karst. As noted in the section on morphology, individual karst features in the study area range in size from small subsidence sinkholes, through "semi-stupendous" collapse sinkholes to large depressions several kilometres long and several hundred metres wide.

The discussion of the processes involved in the development of these features led to the conclusion that they are formed by collapse of bedrock strata and unconsolidated deposits into solution cavities in a subjacent karst formed in soluble rocks. Indications were found that these processes are active. The potential geotechnical hazard presented by this active karst development is aggravated by the fact that it is virtually impossible to predict either the location or the timing or the magnitude of future subsidence and collapse events.

FLOODING

In Chapter 4, it was pointed out that existing topographic maps contain inaccuracies with respect to surface drainage connections; they also show some intermittent lakes as permanent lakes, and possibly even worse, they fail to identify a number of intermittent lakes or areas subject to flooding. The topographic maps for the area are based on air photographs taken in either mid-June or early July. For future developments in this and other areas with a similar karst nature, it would be advisable to have additional aerial photography done at different times of the year. Much of the necessary information on the hydrologic characteristics of such karst areas can, of course, be gathered through intermittent field observations; detailed study of available satellite imagery has also been useful for this purpose.

In the section presenting the climatic and hydrologic summaries for 1973-1978, it was concluded that the most extensive flooding of karst depressions can be expected after a winter with heavy snowfall and little melting before the main snowmelt period and that the duration of flooding primarily depends on the amount and distribution of rainfall during the summer months. It is therefore possible that the *maximum extent* of flooding in a particular location will remain unobserved during field studies. In most cases, however, it will be possible to deduce the maximum extent as well as the approximate duration of flooding, from vegetation patterns, as indicated in the section on the hydrologic significance of the karst features.

CONTAMINATION OF GROUNDWATER

Karst-water systems are extremely vulnerable to contamination from the surface because of the generally complete lack of filtering of their recharge. Conduits in many of the swallow holes in the study area were seen to absorb leaves, broken branches, clumps of grass, lumps of soil, and fish. The relatively high density of sinkholes in some parts of the area would provide almost direct access to the karst-water system for a potential contaminant only a short distance from its source. Such a contaminant could, moreover, reach distant points of discharge into surface water in a relatively short time, because the flow velocities prevailing in karst systems are usually higher than those prevailing in fractured rock and much higher than those in most porous media. The chances for containment, recovery and cleanup after an accidental spill are essentially nil.

Conclusions

Karst development in the study area is widespread. A major portion of the existing small and large karst depressions have been formed by collapse of bedrock strata and unconsolidated deposits into cavities (or into breccia "funnels" above cavities) resulting from solution of soluble rocks at depth. Two formations, the Lower Devonian Bear Rock and the Upper Cambrian Saline River formations, contain beds of hypersoluble rocks (gypsum and halite) in the study area. The intervening Cambro-Ordovician Franklin Mountain Formation and the Ordovician-Silurian Mount Kindle Formation consist of dolomites of much lower solubility.

Concentrations of collapse sinkholes and depressions were found to be centred on a number of structural domes along the Keele Arch between Great Bear River and Lac Belot. Exposures of Mount Kindle Formation found in karst depressions on the flanks of the Mahony Lake dome, as much as 75 m below the level of the Franklin Mountain Formation, have been interpreted as outliers that were preserved as a result of subsidence due to subsurface solution of evaporites from the Upper Cambrian Saline River Formation.

The present morphology of the karst depressions depends on the character of the near-surface bedrock, on the depth below surface of the soluble formation(s) and, to some extent, on the hydrology. The presence of the karst has led to disruption of drainage and to seasonal flooding of low-lying recharge areas, which have in some instances been misinterpreted in the preparation of topographic maps for the area.

The hydrologic significance of the karst depressions as points and areas of recharge is a function of the size and topography of their drainage areas and of such climatic factors as temperature regime and the amount and seasonal distribution of snow and rain. The maximum water level attained in a seasonally flooded depression in a given year is mainly a function of (1) the amount of snow remaining on the ground at the start of the snowmelt and (2) the rate at which melting proceeds. The duration of flooding in a given year is a function of (1) the maximum level reached during the snowmelt and (2) the amount and distribution of rainfall during the summer. The water levels in flooded karst depressions do not represent a regional groundwater table; they are caused by the limited inflow capacity of their swallow holes.

The inflow of surface water into swallow holes in karst depressions provides an effective mechanism for the recharge of groundwater in this area with widespread permafrost. In the well-developed collapse karst in the study area, the annual recharge (estimated at about 40 mm over the drainage area, or about 15% of the annual precipitation) is considerable. The minimum rate of rainfall required for initiation of recharge in the collapse karst (6–10 mm) is small.

Results of analyses for D and ^{18}O indicate that local precipitation is the source of recharge to the karst-water system and that snowmelt provides a large proportion of the recharge. Tritium levels in discharge from the karst-water system tend to indicate that the bulk of the water is derived from very recent precipitation.

The use of sulphur-isotope analyses has made it possible to distinguish the source (Saline River or Bear Rock Formation) of the dissolved sulphates in a number of the sulphurous spring waters in the study area; the results for the karst-water system of the Mahony Lake dome, where the Saline River Formation is the only available sulphate source, are inconclusive.

The karst-water system is extremely vulnerable to contamination from the surface because of the unfiltered nature of its recharge and the relatively close spacing of its high-rate recharge points. High flow velocities inside the system could transport a contaminant to distant discharge points in a relatively short time.

The collapse nature of the karst presents a special geotechnical hazard in the study area in addition to other, permafrost-related hazards. Field evidence indicates that the collapse process is active, but prediction of the location, timing and extent of future subsidence or collapse is not possible.

Seasonal flooding in karst depressions could become a hazard to future engineering developments, if its potential occurrence is not recognized from vegetation patterns or during study of available air photographs and satellite imagery.

References

Aitken, J.D. and D.G. Cook. 1969. Lac Belot (Geology), District of Mackenzie. Geol. Surv. Can. Preliminary Series Map 6-1969.

Aitken, J.D., R.W. Macqueen and J.L. Usher. 1973. Reconnaissance studies of Proterozoic and Cambrian stratigraphy, lower Mackenzie River area (Operation Norman), District of Mackenzie. Geol. Surv. Can. Pap. 73-9.

Banner, J.A. and R.O. van Everdingen. 1979. Automatic time-lapse camera systems. Technical Bulletin No. 112 (NHRI Paper No. 4), Inland Waters Directorate, Environment Canada, Ottawa.

Bird, J.B. 1963. Limestone terrains in southern Arctic Canada. *In* Proceedings of Permafrost International Conference, U.S. National Academy of Sciences-U.S. National Research Council, Washington, D.C., pp. 115-121.

Bostock, H.S. 1967. Physiographic Regions of Canada. Geol. Surv. Can. Map 1254A, Scale 1:5 000 000.

Brandon, L.V. 1963. Evidences of ground water flow in permafrost regions. *In* Proceedings of Permafrost International Conference, U.S. National Academy of Sciences-U.S. National Research Council, Washington, D.C., pp. 176-177.

Brandon, L.V. 1965. Groundwater hydrology and water supply in the District of Mackenzie, Yukon Territory and adjoining parts of British Columbia. Geol. Surv. Can. Pap. 64-39.

Brook, G.A. 1977. Surface and groundwater hydrology of a highly karsted sub-arctic carbonate terrain in northern Canada. *In* Karst Hydrogeology (J.S. Tolson and F.L. Doyle, eds.). Memoirs, Vol. XII, International Association of Hydrogeologists, UAH Press, Huntsville, Alabama, pp. 99-108.

Brown, R.J.E. 1978. Permafrost. *Hydrological Atlas of Canada*, Map No. 32, Scale 1:10 000 000.

Brown, R.M. 1970. Distribution of hydrogen isotopes in Canadian waters. *In* Isotopes in Hydrology, I.A.E.A. Vienna, Vol. 129, No. 1, pp. 3-21.

Burns, B.M. 1973. The climate of the Mackenzie Valley-Beaufort Sea. Atmospheric Environment Service, Environment Canada, Climatological Studies No. 24, Vol. 1.

Burns, B.M. 1974. The climate of the Mackenzie Valley-Beaufort Sea. Atmospheric Environment Service, Environment Canada, Climatological Studies No. 24, Vol. 2.

Christiansen, E.A. 1967. Collapse structures near Saskatoon, Saskatchewan, Canada. Can. J. Earth Sci. 4: 757-767.

Christiansen, E.A. 1971. Geology of the Crater Lake collapse structure in southeastern Saskatchewan. Can. J. Earth Sci. 8(12): 1505-1513.

Christiansen, E.A. and D.J. Gendzwill. 1973. The Howe Lake collapse structure. Geological Association of Canada and Mineralogical Association of Canada Annual Meetings 1973, Program and Abstracts, p. 56.

Cook, D.G. 1975. The Keele Arch – A pre-Devonian and pre-late Cretaceous paleo-upland in the northern Franklin Mountains and Colville Hills. Geol. Surv. Can. Pap. 75-1C, pp. 243-246.

Cook, D.G. and J.D. Aitken. 1971. Geology, Colville Lake map-area and part of Coppermine map-area, Northwest Territories. Geol. Surv. Can. Pap. 70-12.

Craig, H. 1961. Isotope variations in meteoric waters. Science, 133: 1702-1703.

Dansgaard, W. 1964. Stable isotopes in precipitation. Tellus, 16(4): 436-468.

Davies, G.R. and H.R. Krouse. 1975. Sulphur isotope distribution in Paleozoic sulphate evaporites, Canadian Arctic Archipelago. Geol. Surv. Can. Pap. 75-1B, pp. 221-225.

Douglas, R.J.W. and A.W. Norris. 1974. Geology, Great Slave Lake, District of Mackenzie. Geol. Surv. Can. Map 1370A, Scale 1:500 000.

Ford, D.C. and G.A. Brook. 1973. The Nahanni North Karst, Northwest Territories, Canada. Lands and People, 8: 343-349.

Ford, D.C. and J.F. Quinlan. 1973. Theme and Resource Inventory Study of the Karst Regions of Canada. Report to National Parks Service, Contract 72-32.

Gendzwill, D.J. and Z. Hajnal. 1971. Seismic investigation of the Crater Lake collapse structure in southeastern Saskatchewan. Can. J. Earth Sci. 8(12): 1514-1524.

Haimila, N.E. 1975. Possible large domal structures along a regional arch in the Northern Interior Plains. Geol. Surv. Can. Pap. 75-1C, pp. 63-68.

Holser, W.T. and I.R. Kaplan. 1966. Isotope geochemistry of sedimentary sulfates. Chem. Geol. 1: 93-135.

Holter, M.E. 1969. The Middle Devonian Prairie Evaporite of Saskatchewan. Sask. Dep. Miner. Resour. Rep. 123.

Hughes, O.L., J.J. Viellette, J. Pilon, P.T. Hanley and R.O. van Everdingen. 1973. Terrain Evaluation with Respect to Pipeline Construction, Mackenzie Transportation Corridor, Central Part, Lat. 64° to 68° N. Environmental-Social Committee, Northern Pipelines. Report No. 73-37.

Hume, G.S. 1954. The lower Mackenzie area, Northwest Territories and Yukon. Geol. Surv. Can. Mem. 273.

Jennings, J.N. 1971. Karst. Vol. 7 of *An Introduction to Systematic Geomorphology*, M.I.T. Press, Cambridge, Mass.

Michel, F.A. 1977. Hydrogeologic studies of springs in the central Mackenzie Valley, North-West Territories, Canada. M.Sc. Thesis, University of Waterloo.

Nieto-Pescetto, A.S. and A.J. Hendron, Jr. 1977. Study of sinkholes related to bedded salt production in the area of Detroit, Michigan. Solution Mining Research Institute, Inc., Flossmoor, Illinois.

Norford, B.S. and R.W. Macqueen. 1975. Lower Paleozoic Franklin Mountain and Mount Kindle Formations, District of Mackenzie: their type sections and regional development. Geol. Surv. Can. Pap. 74-34.

Ozoray, G.F. 1977. The Athabasca carbonate and evaporite buried karst. *In* Karst Hydrogeology (J.S. Tolson and F.L. Doyle, eds.). Memoirs, Volume XII, International Association of Hydrogeologists, UAH Press, Huntsville, Alabama, pp. 85-98.

Paloc, H. 1975. Glossaire d'hydrogéologie du karst. *In* Hydrogeology of Karstic Terrains (A. Burger and L. Dubertret, eds.). International Association of Hydrogeologists, Paris, pp. 151-186.

Terzaghi, R.D. 1970. Brinefield subsidence at Windsor, Ontario. Third Symposium on Salt, Northern Ohio Geological Society Inc., Cleveland, Ohio, Vol. 2, pp. 298-307.

Thornbury, W.D. 1954. *Principles of Geomorphology*. John Wiley and Sons, New York, pp. 316-353.

van Everdingen, R.O. 1974. Groundwater in permafrost regions of Canada. *In* Permafrost Hydrology, Proceedings of Workshop Seminar, 1974, Canadian National Committee, International Hydrological Decade, pp. 83-93.

van Everdingen, R.O. 1976. Use of LANDSAT imagery in studies of spring icings and seasonally flooded karst in permafrost areas. Proceedings, 1976 Workshop on Remote Sensing of Soil Moisture and Groundwater, Canadian Aeronautics and Space Institute, pp. 231A-235.

van Everdingen, R.O. 1978a. Frost mounds at Bear Rock, near Fort Norman, Northwest Territories, 1975-1976. Can. J. Earth Sci. 15(2): 263-276.

van Everdingen, R.O. 1978b. Karst in permafrost terrain near Great Bear Lake. Poster Session, Third International Conference on Permafrost, National Research Council of Canada, Programme, p. 61.

van Everdingen, R.O. 1979. Potential interactions between pipelines and terrain in a northern environment. Technical Bulletin No. 114 (NHRI Paper No. 8), Inland Waters Directorate, Environment Canada, Ottawa.

van Everdingen, R.O. and J.A. Banner. 1979. Use of long-term automatic time-lapse photography to measure the growth of frost blisters. Can. J. Earth Sci. 16(8): 1632-1635.

van Everdingen, R.O. and H.R. Krouse. 1977a. Sulfur-isotope geochemistry of springs in the Franklin Mountains, N.W.T., Canada. Proceedings, Second International Symposium on Water-Rock Interaction, Institut de Géologie, Université Louis Pasteur, Strasbourg, Vol. 1, pp. 134-145.

van Everdingen, R.O. and H.R. Krouse. 1977b. Stratigraphic differentiation by sulfur isotopes between Upper Cambrian and Lower Devonian gypsum-bearing units, District of Mackenzie, N.W.T. Can. J. Earth Sci. 14(12): 2790-2796.

van Everdingen, R.O., F.A. Michel, H.R. Krouse and P. Fritz. 1978. Hydrochemical and isotope analysis of groundwater flow systems, Franklin Mountains, District of Mackenzie, Northwest Territories, Canada. Proceedings, National Hydrogeological Conference, International Association of Hydrogeologists, Canadian National Chapter (G.F. Ozoray, ed.), pp. 165-178.

Wigley, T.M.L., J.J. Drake, J.F. Quinlan and D.C. Ford. 1973. Geomorphology and geochemistry of a gypsum karst near Canal Flats, British Columbia. Can. J. Earth Sci. 10(2): 113-129.

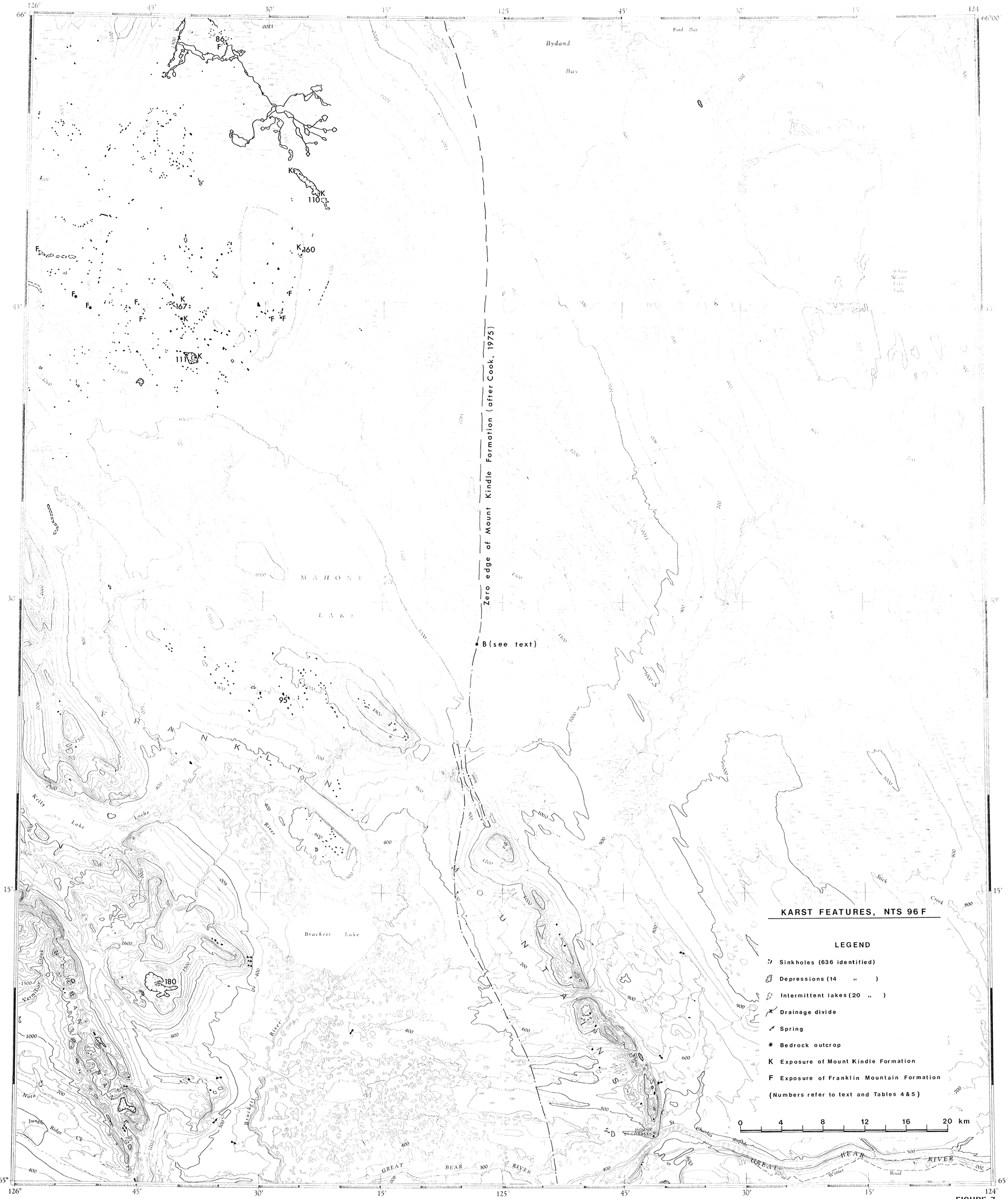
KARST FEATURES, NTS 96 F
LEGEND
Sinkholes (636 identified)
Depressions (14 ")
Intermittent lakes (20 ")
Drainage divide
Spring
Bedrock outcrop
K Exposure of Mount Kindle Formation
F Exposure of Franklin Mountain Formation
(Numbers refer to text and Tables 4&5)
0 4 8 12 16 20 km
Zero edge of Mount Kindle Formation (after Cook, 1975)
B (see text)
MAHONY LAKE
FRANKLIN MOUNTAINS
CONTACT RANGE
Bydand Bay
Ford Bay
Kelly Lake
Brackett Lake
Vermillion Creek
Nata
Jungle Rube Ck.
Stick Creek
Winter Road
GREAT BEAR RIVER
MOUNT ST. CHARLES
St Charles
126°
45′
30′
15′
125
124
66°00′
65°

FIGURE 7

KARST FEATURES, NTS 96K

LEGEND

- Sinkholes (418 identified)
- Depressions (1 ,,)
- Intermittent lakes (12 ,,)
- Drainage divide
- Spring
- Icing area

(Numbers refer to text and Tables 4 & 5)

0 4 8 12 16 20 km

LAC DES BOIS

TUNAGO LAKE

SMITH ARM (GREAT BEAR LAKE)

GOOD HOPE BAY

BYDAND BAY

Tatchini Lake

Anderson R.

Tweed Lake

Kilekale Lake

Hare Indian Rivers

Winter Road

Crosswise Island

Ford Bay

181 182 183 142 143 144 145 149 150

126° 45′ 30′ 15′ 125° 45′ 30′ 15′ 124°

67° 66° 45′ 30′ 15′

FIGURE 8

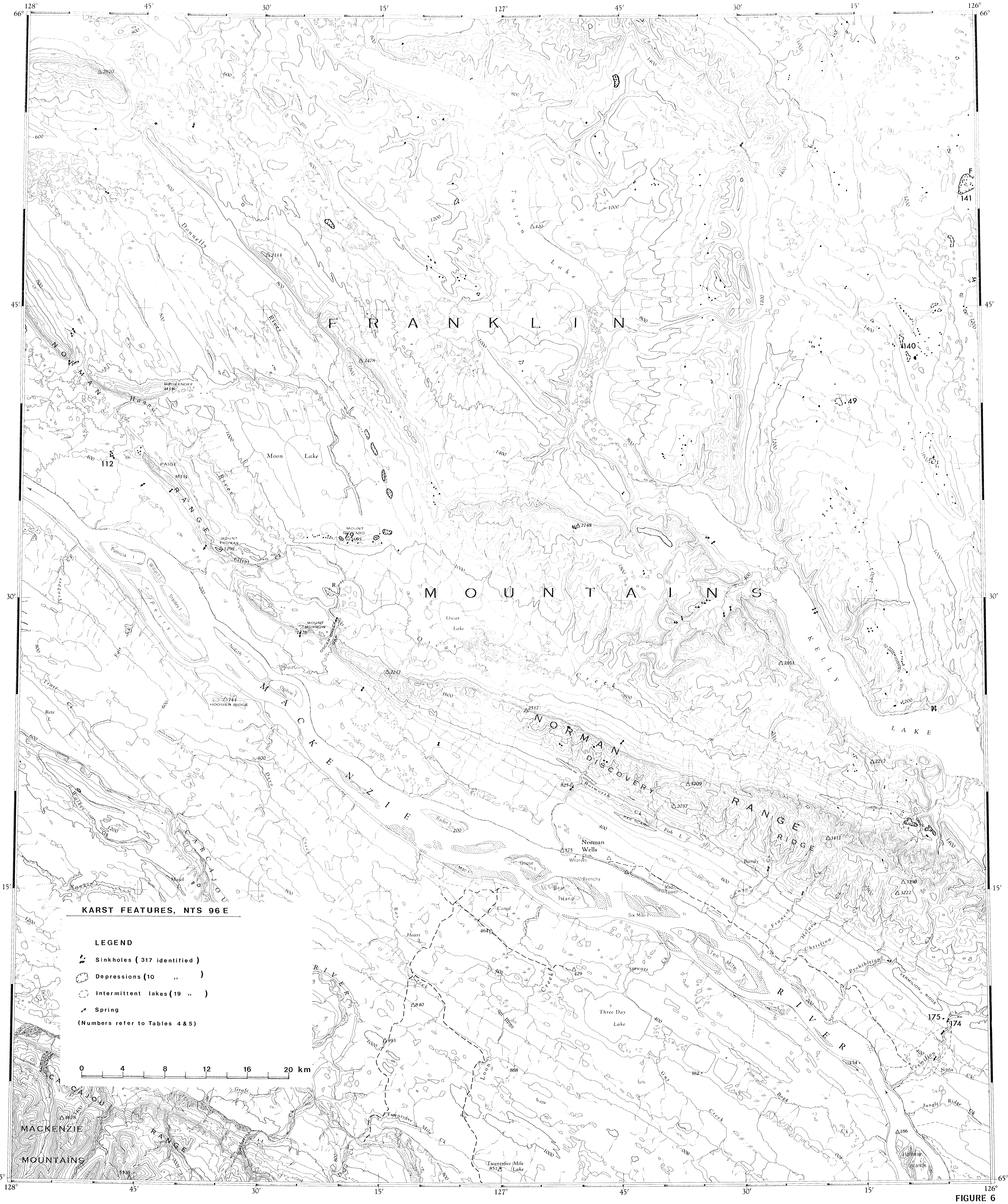
KARST FEATURES, NTS 96 E
LEGEND
Sinkholes (317 identified)
Depressions (10 ,,)
Intermittent lakes (19 ,,)
Spring
(Numbers refer to Tables 4&5)
0 4 8 12 16 20 km
128°
127°
126°
66°
65°
45′
30′
15′
FRANKLIN
MOUNTAINS
MACKENZIE
RIVER
NORMAN
DISCOVERY
RANGE
RIDGE
KELLY
LAKE
Norman Wells
Moon Lake
Oscar Lake
Three Day Lake
Twentyfive Mile Lake
Donnelly
River
Turton
Lake
MACKENZIE
MOUNTAINS
CARCAJOU
141
140
49
112
175
174

FIGURE 6

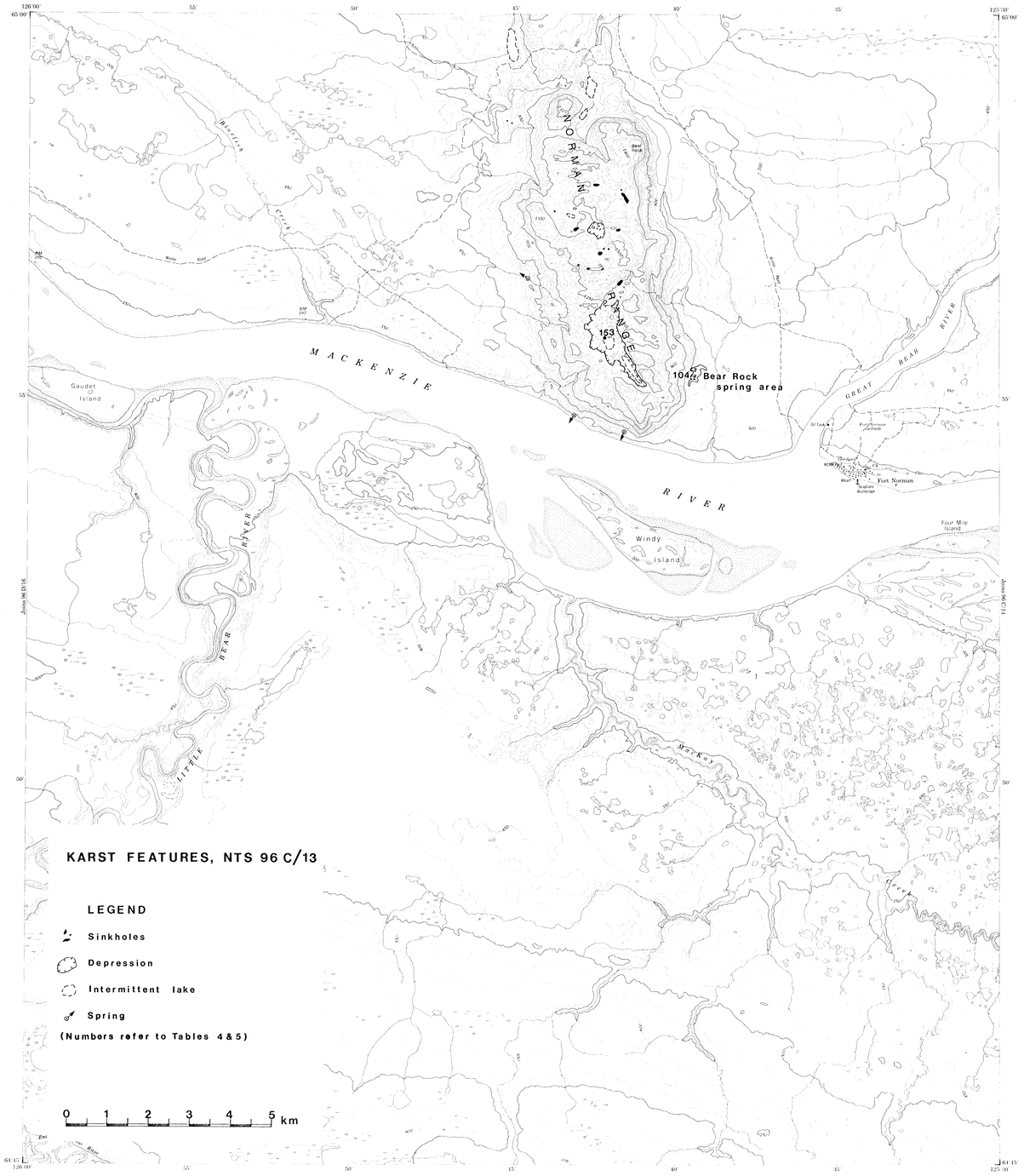
126°00'
65°00'
55'
50'
45'
40'
35'
125°30'
65°00'
NORMAN
RANGE
153
Bear Rock
spring area
104
MACKENZIE
RIVER
GREAT BEAR RIVER
Gaudet Island
Fort Norman
Windy Island
Four Mile Island
LITTLE BEAR RIVER
Mackay
Creek
Jones 96 D/16
Jones 96 C/14
64°45'
126°00'
125°30'
61°15'
KARST FEATURES, NTS 96 C/13
LEGEND
Sinkholes
Depression
Intermittent lake
Spring
(Numbers refer to Tables 4 & 5)
0 1 2 3 4 5 km

FIGURE 5

2 MAPS GREATER THAN 11" X 17"
DOUBLE SIDED